Politecnico di Milano

SCHOOL OF INDUSTRIAL AND INFORMATION ENGINEERING
Master of Science – Nuclear Engineering

Multiphysics Modelling Approach for the Analysis of Xenon Removal via Helium Bubbling in the Molten Salt Fast Reactor

Supervisor
Prof. Stefano LORENZI

Co-Supervisor
Prof. Antonio CAMMI
Ing. Andrea DI RONCO

Candidate
Federico CARUGGI – 914867

Academic Year 2019 – 2020

Sommario

I reattori a sali fusi (MSR) sono una famiglia di sistemi nucleari sotto sviluppo nell'ambito del Generation IV International Forum (GIF-IV), caratterizzati da una miscela di sali fusi che ha il ruolo sia di combustibile che di termovettore. Date le caratteristiche dei reattori con combustibile circolante, nuovi strumenti di simulazione devono essere appositamente sviluppati e testati.

In questa tesi, un modello multifisico sviluppato in OpenFOAM viene dotato di nuove funzionalità utili per l'analisi del Molten Salt Fast Reactor (MSFR), un sistema MSR sviluppato nell'ambito dei progetti europei EVOL, SAMOFAR e SAMOSAFER. Il principale obiettivo è la modellazione dei prodotti di fissione gassosi (GFP) all'interno del reattore e le loro interazioni con un sistema di iniezione di bolle di elio, che ha lo scopo di rimuovere sia essi che i prodotti metallici tramite galleggiamento. In questo modo, lo strumento multifisico può essere impiegato per fornire informazioni utili sulla capacità di estrazione del sistema di iniezione di bolle. A partire da un solutore bifase Euler-Euler capace di modellare separatamente le fasi di sale combustibile liquido e elio gassoso iniettato, viene implementato un approccio di miscela multi-componente per simulare l'evoluazione delle specie di GFP in ogni fase, considerando i meccanismi di produzione, decadimento, consumo, trasporto intra-fase, scambio di massa inter-fase e estrazione. Una verifica analitica dei modelli implementati - in particolare quello per lo scambio di massa - è condotta, insieme ad un confronto critico delle assunzioni modellistiche guidato dagli studi sperimentali condotti nel campo dei reattori a sali fusi presso l'Oak Ridge National Laboratory (ORNL).

Il modello sviluppato è quindi utilizzato per studiare l'efficienza della rimozioen dei GFP da parte del sistema di iniezione di bolle, in casi test 2D e 3D del MSFR. Come principale quantità d'interesse, viene derivato un tempo di dimezzamento che descrive l'efficienza delle bolle sul trattamento dei GFP, calcolandolo per differenti condizioni di flusso di elio. Questo lavoro costituisce un nuovo sviluppo nell'analisi multifisica del concetto del MSFR, con l'introduzione e la prova di nuove capacità di modellazione. La previsione corretta del comportamento dei prodotti di fissione gassosi e delle loro interazioni con il sistema di iniezione di bolle rappresentano aspetti chiave nella definizione del termine di sorgente radioattiva e nell'analisi del ciclo di combustibile di questo sistema nucleare innovativo.

Abstract

Molten Salt Reactors (MSRs) are a family of nuclear systems under development in the framework of the Generation IV International Forum, featuring a mixture of molten salts with the role of both fuel and coolant. Given the characteristics of circulating-fuel reactors, new simulation tools need to be developed and tested.

In this thesis, a multiphysics solver developed in OpenFOAM is provided with new functionalities useful for the analysis of the Molten Salt Fast Reactor (MSFR), a MSR system developed in the frame of the European projects EVOL, SAMOFAR and SAMOSAFER. The main objective is the modelling of Gaseous Fission Products (GFPs) inside the reactor and their interactions with a helium bubbling system aimed at removing both GFP and fission product in metallic form through flotation. In this way, the multiphysics tool can be employed to study the extraction capabilities of the bubbling system. Starting from an Euler-Euler two-phase solver able to model separately the liquid fuel salt and injected helium phases, a multi-component mixture approach is implemented to model the evolution of GFP species within each phase, considering production, decay, consumption, intra-phase transport, inter-phase mass transfer and extraction mechanisms. An analytical verification of the implemented models - in particular the one for mass transfer - is also performed along with a critical comparison of the modelling assumptions driven by the the experimental studies conducted in the field of MSRs at the Oak Ridge National Laboratory (ORNL).

The developed model is then employed to study the efficiency of GFP removal by means of the bubbling system in both 2D and 3D MSFR test cases. As main figure of merit, an halving time describing the efficiency of the gas bubbles on the treatment of gaseous fission products is derived and obtained for different helium flow injection conditions. This work constitutes a further development in the multiphysics analysis of the MSFR concept, with the introduction and testing of new modelling capabilities. The correct prediction of the behavior of gaseous fission products, and their interactions with the helium bubbling system represent a key aspect in the definition of the radioactive source term and in the analysis of the fuel cycle of this innovative nuclear system.

Estratto Esteso

Introduzione

I reattori a sali fusi sono una famiglia di sistemi nucleari di quarta generazione che presentano varie innovazioni progettuali rispetto a quelli più convenzionali in funzione ad oggi. Si tratta di reattori basati sull'utilizzo di un combustibile fluido in circolazione, che agisce allo stesso tempo anche come liquido di raffreddamento per il sistema. Questa caratteristica peculiare comporta dei vantaggi rispetto all'impiego di combustibile solido, principalmente dal punto di vista economico e da quello della sicurezza:

- Semplificazione della progettazione del nocciolo, vista l'assenza di elementi di combustibile solidi
- Possibilità di raggiungere livelli di sfruttamento delle risorse maggiori, per via della trasmutazione di elementi transuranici durante il ricircolo del combustibile
- Limitazione dei rischi legati alla presenza di un grande inventario di reattività all'accensione, non necessario in questo caso
- Possibilità di operazione a pressione atmosferica, per via dell'alto punto di evaporazione del sale.

In aggiunta a questi vantaggi, un reattore a sali fusi presenta la possibilità di avere un controllo di precisione sulla composizione della miscela di combustibile. Questa caratteristica viene sfruttata con un sistema di riprocessamento continuo, che può essere sfruttato anche come strumento per un controllo di reattività. In aggiunta, l'intervento sulla composizione del combustibile fornisce la possibilità di impiegare il reattore per lo smaltimento di prodotti di fissione pesanti provenienti da altri sistemi.

Lo studio dei reattori a sali fusi ad oggi è condotto a livello numerico, anche se alcuni lavori sperimentali sono stati seguiti negli anni '50 e '60 da parte dell'Oak Ridge National Laboratory, culminati con la realizzazione del Molten Salt Reactor Experiment (MSRE), che ha raggiunto criticità nel 1965, e la progettazione del Molten Salt Breeding Reactor (MSBR), entrambi sistemi a neutroni termici. Nel tempo gli studi sono stati però poi rediretti verso altri tipi di progetti, come i Liquid Metal

Fast Reactors (LMFR), per le migliori prospettive offerte da sistemi a neutroni veloci. Oggi, tuttavia, l'interesse per i reattori a sali fusi è stato rinnovato, principalmente in vista dei vantaggi offerti già menzionati. All'interno del panorama del Generation IV International Forum (GIF-IV) le ricerche vengono condotte sia su sistemi termici che veloci. Uno dei due principali concetti considerati, che è oggetto dell'analisi di questa tesi, è il Molten Salt Fast Reactor (MSFR), un progetto proposto dal Centre Nationale de la Recherche Scientifique (CNRS, Grenoble, Francia).

Il MSFR è caratterizzato da uno spettro neutronico intermedio-veloce, con assenza di moderatore. Il reattore di riferimento presenta una potenza nominale di 3 GW_{th} e un volume di sale complessivo di 18 m^3. È operato a pressione atmosferica, con una temperatura media nel core di 700 °C. Il reattore è alimentato da una miscela eutettica composta di ^{7}LiF (77.5 mol%) e fluoruri di metalli pesanti (22.5 mol%), il cui componente principale è ^{232}ThF, e per il resto contenenti ^{233}U o ^{235}U/^{238}U e altri elementi transuranici. Come detto in precedenza, il reattore è equipaggiato con un sistema di riprocessamento chimico del combustibile, che opera su circa 40 litri di fluido al giorno, in modo da ridurre il contenuto di prodotti di fissione e tenere sotto controllo la composizione chimica della miscela di sali. In aggiunta, il nocciolo è circondato da riflettori neutronici, per limitare le fughe, ed è prevista anche la presenza di un mantello di materiale fertile, per sfruttare la capacità di auto-fertilizzante (breeding). Un ultimo apparato previsto nella progettazione del MSFR, che è il principale punto focale per il lavoro di questa tesi, è un sistema di iniezione di elio. Un flusso di bolle viene inserito dal fondo del reattore e viene trasportato dal movimento della miscela verso la cima, da dove viene estratto. L'obiettivo di questo apparato è quello di facilitare la rimozione dei prodotti di fissione gassosi e metallici insolubili che vengono generati nella miscela, e che possono essere trasportati al di fuori del nocciolo dalle bolle di elio.

Come detto sopra, l'analisi del concetto del MSFR viene condotta, ad oggi, solamente per analisi numerica. Le peculiarità introdotte dalla progettazione di un reattore di questo tipo richiedono la creazione e lo sviluppo di nuovi strumenti computazionali, basati su principi differenti rispetto a quelli convenzionalmente impiegati nell'analisi dei reattori tradizionali.

Con il precedente lavoro di (Cervi, 2020), un approccio multifisico è stato sviluppato appositamente per lo studio del MSFR nell'ambiente di OpenFOAM, una libreria C++ di modellazione numerica di problemi complessi. Il solutore creato ha la capacità di simulare il comportamento del reattore per quanto riguarda la presenza delle due fasi (sali fusi e bolle di elio), considerando in particolare gli aspetti di comprimibilità. Sia gli aspetti termo-idraulici che quelli neutronici del problema fisico sono considerati, tenendo conto delle interazioni derivanti dal forte accoppiamento tra i due ambiti. Il solutore sviluppato costituisce un ambiente di simulazione ad oggi unico, ma non dispone ancora di tutte le capacità necessarie per una completa ricostruzione numerica del comportamento del MSFR. L'obiettivo di questa tesi è quello di implementare una nuova funzionalità nel codice, relativamente alla modellazione del comportamento dei prodotti di fissione gassosi nel reattore. In particolare, l'idea è quella di simulare la produzione di queste specie, il loro consumo per cattura neutronica e decadimento, e

la loro interazione con il sistema di iniezione di bolle di elio, andando ad osservare l'efficienza di questo apparato nella loro rimozione. Un singolo nuclide viene scelto in questa tesi come riferimento, Xe-135, ma le analisi condotte sono facilmente riproducibili anche per altre specie, e i risultati ottenuti sono validi per qualsiasi altro prodotto di fissione gassoso.

Il lavoro di questa tesi è inserito nel panorama del progetto europeo H2020 SAMOSAFER (https://samosafer.eu/), in attività dal 2019, come seguito delle precedenti iniziative EVOL (Brovchenko et al., 2013) e SAMOFAR (https://samofar.eu/).

Modello Multifisico del MSFR

Nel passato, l'analisi di reattori nucleari è stata condotta utilizzando principalmente tecniche di accoppiamento esterno tra più codici, pensati ognuno per risolvere una sola parte del problema. Ad oggi, questo approccio è stato sostituito dal tentativo di implementare tutte le differenti fisiche in un unico ambiente di simulazione. Questa metodologia si è rilevata più funzionale nella riproduzione del comportamento di sistemi complessi e densi di interconnessioni come il MSFR. Il reattore è stato già oggetto di studi di questo genere, inizialmente con grandi approssimazioni: approccio zero-dimensionale per la parte termo-idraulica e cinetica puntiforme per l'ambito neutronico (Cammi et al., 2011; Guerrieri et al., 2012; Cervi et al., 2018). Pur fornendo informazioni corrette sul sistema, questi modelli non possono dare risultati relativi alla distribuzione spaziale dei parametri e delle varie grandezze analizzate. Codici multifisici ad elementi finiti sono stati quindi in seguito sviluppati, con simulazioni condotte su modelli 2D semplificati, adottando la teoria della diffusione neutronica multi-gruppo per la parte neutronica e un modello mono-fase incomprimibile per la parte termo-idraulica (Fiorina et al., 2014).

Infine, per colmare le lacune rimanenti anche con un approccio di questo tipo, un ulteriore modello su scala 3D è stato sviluppato, facendo uso del software OpenFOAM. Il codice risultante permette di scegliere tra un modulo di diffusione e uno di equazioni del trasporto SP_3 per la parte neutronica, e per la parte termo-idraulica utilizza un modulo bifase per fluidi comprimibili. In aggiunta, presenta anche la soluzione di equazioni di trasporto dei precursori di neutroni ritardati e di calore di decadimento.

Per affrontare la simulazione, il solutore divide ogni step temporale in due cicli separati. Il primo prevede la soluzione delle equazioni della termo-idraulica per mezzo di una routine basata su un algoritmo standard multifase di OpenFOAM, dal nome "reactingTwoPhaseEulerFoam". Il secondo ciclo è dedicato alla parte neutronica, con possibilità di scegliere, come già detto, tra un modello di diffusione multi-gruppo, o di trasporto SP_3. Le equazioni termo-idrauliche e neutroniche sono risolte separatamente in modo iterativo, aggiornando di volta in volta i termini di interazione calcolati, e vengono performate iterazioni esterne in aggiunta per raggiungere convergenza di tutto il problema, secondo lo schema in Figura 1.

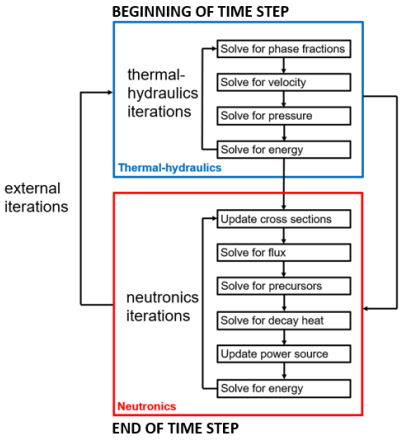

Figure 1. Schema di funzionamento del solutore (Cervi, 2020)

Il ciclo termo-idraulico è basato su un approccio della famiglia dei modelli "free-surface", per i quali la topologia dell'interfaccia tra fase liquida e gassosa è una componente esplicita della soluzione del problema. Il modello specifico, chiamato "volume-of-fluid" (VOF), si basa sull'identificazione dell'interfaccia per mezzo di funzioni indice, come la frazione in volume, ed è stato perfezionato rispetto ad altri approcci simili per evitare la diffusione dell'interfaccia. Per quanto riguarda le tecniche di calcolo delle quantità integrali, il ciclo termo-idraulico segue la formulazione "Euler-Euler", per la quale le due fasi sono considerate come continui compenetranti, piuttosto che come insiemi di singole particelle, e le equazioni impiegate per descriverli sono Euleriane, piuttosto che Lagrangiane. Questa scelta permette di ridurre considerevolmente le risorse computazionali necessarie per simulare sistemi con presenza di un numero elevato di particelle ma, d'altra parte, introduce la necessità di relazioni di chiusura per risolvere le equazioni di bilancio macroscopiche.

La parte termo-idraulica dell'algoritmo del solutore prevede quindi la soluzione dei comuni bilanci macroscopici di massa, momento ed energia, considerando una pressione comune per entrambe le fasi, e impiegando modelli empirici e correlazioni per il calcolo dei termini espliciti, come per esempio quelli di interazione interfase.

Il ciclo neutronico, come detto, si basa sulla risoluzione di equazioni multi-gruppo di diffusione o di trasporto, a seconda di una scelta dell'utente. Questo approccio prevede una procedura iterativa tra i gruppi, per via della presenza di termini espliciti di sorgente inter-gruppo. Per la risoluzione numerica delle equazioni vengono impiegate delle condizioni al contorno di tipo albedo, in modo da simulare la presenza dei riflettori neutronici esterni e del mantello di materiale fertile. Aggiuntivamente, all'interno del ciclo neutronico vengono risolte, come già menzionato, anche delle equazioni di trasporto per calcolare la distribuzione dei precursori di neutroni ritardati e quelli del calore di decadimento, seguendo una suddivisione multi-gruppo e impiegando i risultati della parte termo-idraulica del problema.

In aggiunta rispetto alla modalità predefinita tempo-dipendente, il ciclo neutronico prevede anche la possibilità di risolvere il sistema a stazionario, con un approccio agli

autovalori. In questo caso, le equazioni della neutronica sono trattate impostando le derivate temporali a zero e riscalando il numero medio di neutroni prodotti per fissione con il fattore moltiplicativo. Quest'ultimo è calcolato come rapporto tra i neutroni prodotti da fissione nell'iterazione corrente e in quella precedente.

L'accoppiamento tra i cicli termo-idraulico e neutronico è mutuale. La soluzione delle equazioni della parte neutronica fornisce le sorgenti (energia di fissione e calore di decadimento) necessarie al bilancio energetico. Viceversa, i termini delle equazioni neutroniche sono influenzati dalla soluzione termo-idraulica per mezzo di correzioni sulle sezioni d'urto neutroniche, in funzione di variazioni di temperatura, densità e frazione di vuoto del sistema.

Modellazione dello Xenon

Diverse possibilità sono state prese in considerazione per l'approccio da seguire nell'implementazione della nuova funzionalità nel codice.

In primis è stato ipotizzato l'impiego di una formulazione "one-fluid" (Haroun et al., 2010; Haroun et al., 2012), calcolando il profilo di concentrazione dello xenon in tutto il dominio con la soluzione di una singola equazione implementata nel solutore. Questo approccio è valido finché la concentrazione del soluto è sufficientemente piccola da fare sì che la sua presenza non influisca significativamente sulla termo-idraulica del solvente. Si tratta di una buona procedura per ottenere facilmente il profilo di concentrazione di una specie in un sistema composto da due fasi immiscibili, ma nel caso di studio del MSFR, dove le bolle sono disperse all'interno del combustibile liquido, non è conveniente. Inoltre, mentre nel sale la concentrazione dello xenon può essere prevista come sufficientemente bassa da non influire sul moto, ciò non è vero per le bolle di elio.

Successivamente, è stata considerata la possibilità di espandere l'ambiente del solutore in modo da trattare più di due fasi contemporaneamente, inserendo lo xenon come una terza fase, separata dal sale liquido e dalle bolle di elio. Con questa implementazione, però, vengono ignorati alcuni aspetti chiave del problema. Considerare lo xenon come una terza fase separata impedirebbe la modellazione della sua produzione all'interno del sale liquido e della relativa solubilità. Inoltre, nel momento in cui lo xenon viene estratto dalla fase liquida, il comportamento fisico corretto è la formazione di una unica fase gassosa con le bolle di elio.

L'approccio scelto è stato quindi quello di definire specie multiple per ogni fase, nello specifico sale e xenon per il liquido ed elio e xenon per il gas. Si tratta della scelta ideale per la soluzione del problema di interesse, in quanto tutti gli aspetti fisici possono essere correttamente rappresentati dalla modellazione. La produzione dello xenon può essere posta direttamente nella fase liquida, la migrazione alle bolle può essere considerata con appropriati modelli di scambio di fase, e il comportamento dei due gas quando accoppiati è quello corretto dal punto di vista fisico.

Come già detto, estensivi studi sperimentali sono stati compiuti nell'ambito dei reattori a sali fusi negli anni '50 e '60, da parte del Oak Ridge National Laboratory. Le analisi compiute in quel tempo erano relative alla progettazione di reattori termici, dove l'effetto dello xenon è di estrema importanza. È ragionevole quindi che la letteratura connessa con quegli studi contenga informazioni rilevanti in merito alla modellazione del comportamento di questo elemento. In aggiunta, nell'assenza ad oggi di un effettivo caso sperimentale da analizzare, i dati numerici derivanti dai report tecnici del MSRE e per il progetto del MSBR possono essere impiegati perlomeno per l'esecuzione di stime preliminari sul MSFR. Tra i vari documenti recuperati, in particolare, alcuni sono stati selezionati come riferimento per questa tesi, estraendone dati e informazioni necessarie all'analisi del comportamento dello xenon.

L'analisi dei report ORNL (R. Kedl et al., 1967; R. J. Kedl, 1967; Peebles, 1968; Engel et al., 1971) aiuta a cogliere i termini da considerare nell'analisi del comportamento dei prodotti di fissione gassosi, per quanto riguarda la loro produzione, il loro consumo, e la loro estrazione per mezzo delle bolle di elio. In particolare, per quanto riguarda l'implementazione del trasferimento di massa da una fase all'altra, suggeriscono di impiegare un modello di saturazione che segua la legge di Henry, fornendo anche un valore per la relativa costante. In uno dei report è proposta anche una analisi della letteratura dell'epoca per quanto riguarda le correlazioni impiegabili nella computazione del coefficiente di scambio di massa, attraverso il calcolo del numero adimensionale di Sherwood. Altro dato utile recuperabile dai documenti analizzati è il valore di diffusività dello xenon nella miscela di sali, Infine, l'analisi bibliografica del lavoro compiuto sul MSRE aiuta anche a recuperare idee per modelli analitici e test sperimentali da impiegare per una verifica dei modelli empirici considerati.

L'implementazione dell'analisi di più specie per ogni fase, in OpenFOAM, aggiunge al ciclo della termo-idraulica la soluzione di equazioni di bilancio per la massa di ogni componente, espresse in funzione di una concentrazione indipendente dal volume (per via della comprimibilità delle fasi):

$$\frac{\partial \alpha_k \rho_k Y_{i,k}}{\partial t} + \nabla \cdot (\alpha_k \rho_k \mathbf{u}_k Y_{i,k}) - \nabla \cdot \left(\frac{\alpha_k \mu_k}{\mathrm{Sc}_k} \nabla (Y_{i,k}) \right) = \frac{dm_{i,k}}{dt}$$

Per il calcolo del termine di scambio di massa tra fasi vengono impiegati due modelli distinti: uno per la concentrazione di saturazione all'interfaccia, e uno per il coefficiente di scambio (tramite il numero di Sherwood). In questo lavoro, vengono impiegati per questo, rispettivamente, la legge di Henry e la correlazione di Higbie, sviluppata per la simulazione di una risalita libera di bolle all'interno di un flusso liquido. Questo secondo approccio è stato selezionato nonostante sia sviluppato per il caso di flusso laminare, per via della mancanza di dati sperimentali a riguardo. Una volta che modelli più accurati siano disponibili, la flessibilità di OpenFOAM permette di modificare facilmente queste implementazioni.

La forma finale delle equazioni di bilancio per la massa di xenon all'interno delle due fasi, considerando anche i termini di sorgente (dipendente dal tasso di fissioni) e di consumo (decadimento e cattura neutronica), è la seguente:

$$\frac{\partial \alpha_l \rho_l Y_{Xe,l}}{\partial t} + \nabla \cdot (\alpha_l \rho_l \mathbf{u}_l Y_{Xe,l}) - \nabla \cdot \left(\frac{\alpha_l \mu_l}{\mathrm{Sc}_l} \nabla (Y_{Xe,l}) \right) = \\ = S_{Xe} - \alpha_l \rho_l \left(\lambda + \sum_n (\sigma_{c,n} \varphi_n) \right) Y_{Xe,l} + \frac{dm_{Xe,l}}{dt}$$

$$\frac{\partial \alpha_g \rho_g Y_{Xe,g}}{\partial t} + \nabla \cdot (\alpha_g \rho_g \mathbf{u}_g Y_{Xe,g}) - \nabla \cdot \left(\frac{\alpha_g \mu_g}{\mathrm{Sc}_g} \nabla (Y_{Xe,g}) \right) = -\alpha_g \rho_g \lambda Y_{Xe,g} + \frac{dm_{Xe,g}}{dt}$$

Verifica Analitica

L'implementazione al solutore della modellazione del comportamento dello xenon proposta in questa tesi si basa sull'abilità di OpenFOAM di riprodurre, tramite simulazione numerica, il sistema complesso del MSFR. Siccome una validazione sperimentale dei risultati non è disponibile ad oggi, un primo passo nel testare le capacità del modello può essere compiuto facendo un confronto con calcoli analitici. Per questo motivo, un test su una semplice geometria è stato messo a punto, in modo da avere una verifica dei calcoli compiuti dal solutore in merito allo scambio di massa di un componente tra fasi diverse.

La geometria selezionata è un dominio rettangolare 2D, rappresentante una sezione tubolare, orientata orizzontalmente per trascurare gli effetti gravitazionali. La lunghezza è scelta significativamente maggiore rispetto all'altezza, in modo da ignorare gli effetti di ingresso e uscita del liquido.

La formulazione analitica fa riferimento ad un sistema di equazioni di avvezione-dispersione (una per ogni fase), con l'aggiunta di un termine di sorgente (per la fase liquida), uno di consumo e uno di scambio di massa (nullo nel caso monofase):

$$\begin{cases} \frac{\partial \alpha_l C}{\partial t} + \nabla \cdot (\alpha_l \mathbf{u} C) - \nabla \cdot (D \nabla \alpha_l C) = S - \lambda \alpha_l C + KA(HC_g - C) \\ \frac{\partial \alpha_g C_g}{\partial t} + \nabla \cdot (\alpha_g \mathbf{u}_g C_g) - \nabla \cdot (D_g \nabla \alpha_g C_g) = -\lambda \alpha_g C_g - KA(HC_g - C) \end{cases}$$

Varie ipotesi semplificative sono state impiegate nella formulazione del problema, in modo da poter ottenere facilmente un'esatta soluzione analitica da confrontare con i dati numerici. Il flusso del fluido è considerato laminare, sviluppato da un gradiente di pressione imposto costante (e molto piccolo, in modo che la differenza di pressione non sia influente sulle proprietà del liquido). La temperatura è uniforme e costante, in assenza di sorgenti e pozzi di energia, ancora per preservare la costanza delle proprietà termofisiche del sistema. Il flusso è considerato completamente sviluppato, come anche il fenomeno del trasporto, in modo che il sistema di equazioni risulti effettivamente

mono-dimensionale. Aggiuntivamente, per la fase gassosa il fenomeno di trasporto di xenon è trascurato, in modo da semplificare ulteriormente la situazione. Le soluzioni sono formulate in funzione di alcune grandezze adimensionali definite appositamente, e vengono quindi calcolate e confrontate con i risultati numerici di OpenFOAM, sia in monofase che in bifase, per due differenti tipi di condizioni al contorno, per quanto riguarda la concentrazione dello xenon: Neumann e Dirichlet. I risultanti grafici di confronto tra la soluzione analitica e numerica delle concentrazioni di xenon, per i casi monofase e bifase, sono mostrati in Figura 2.

Analisi del Reattore

L'obiettivo di questo lavoro, come già citato, è l'analisi dell'efficienza del sistema di iniezione di bolle di elio nella rimozione dei prodotti di fissione gassosi presenti all'interno del nocciolo del MSFR. Per conseguire questo scopo, quindi, delle simulazioni su modelli che riproducano il reattore devono essere eseguite.

Come primo approccio, una geometria cilindrica semplificata viene impiegata. Si tratta di un modello 2D assial-simmetrico già impiegato nel passato progetto EVOL (Brovchenko et al., 2013), sempre nell'ambiente di OpenFOAM. Solo la parte fluida del sistema (sali e bolle di elio) viene simulata e l'effetto del sistema di iniezione/rimozione bolle, delle pompe, e dello scambiatore di calore sono simulati per mezzo di appositi termini di sorgente/pozzo nelle equazioni governative del sistema. Aggiuntivamente, una ulteriore simulazione è performata su una geometria 3D, rappresentante un quarto del reattore, in modo da verificare che i risultati ottenuti dalle analisi 2D seguano un up-scaling corretto, e possano essere riprodotti e considerati validi anche per il caso più realistico 3D.

L'efficienza del sistema di iniezione di bolle viene misurata con la computazione di un parametro caratteristico, che può essere poi utile, come già menzionato, per lo sviluppo di altri codici all'interno del panorama dello stesso progetto europeo, H2020 SAMOSAFER (https://samosafer.eu/). La modellazione dell'effetto dell'elio sulla rimozione dei prodotti di fissione è condotta, in questi altri codici, con l'introduzione di un termine di decadimento esponenziale all'interno delle equazioni di bilancio dei nuclidi opportuni. Il parametro da calcolare risulta essere quindi la relativa costante di decadimento, ottenibile come rapporto tra la portata di estrazione dello xenon e la massa complessiva del nuclide presente nel sistema allo stesso step temporale. Il valore di inventario di xenon è calcolato come output numerico delle simulazioni, per integrazione della concentrazione in ogni fase su tutto il volume relativo. L'accuratezza di computazione di questa quantità viene verificata quando il sistema raggiunge lo stazionario in monofase, per confronto con il rispettivo calcolo analitico. La portata di rimozione viene invece computata a valle delle simulazioni, dividendo la diminuzione di massa di xenon nel sistema nell'ultimo step temporale per la lunghezza dello stesso step.

Il risultato finale presentato non è esattamente la costante del modello esponenziale

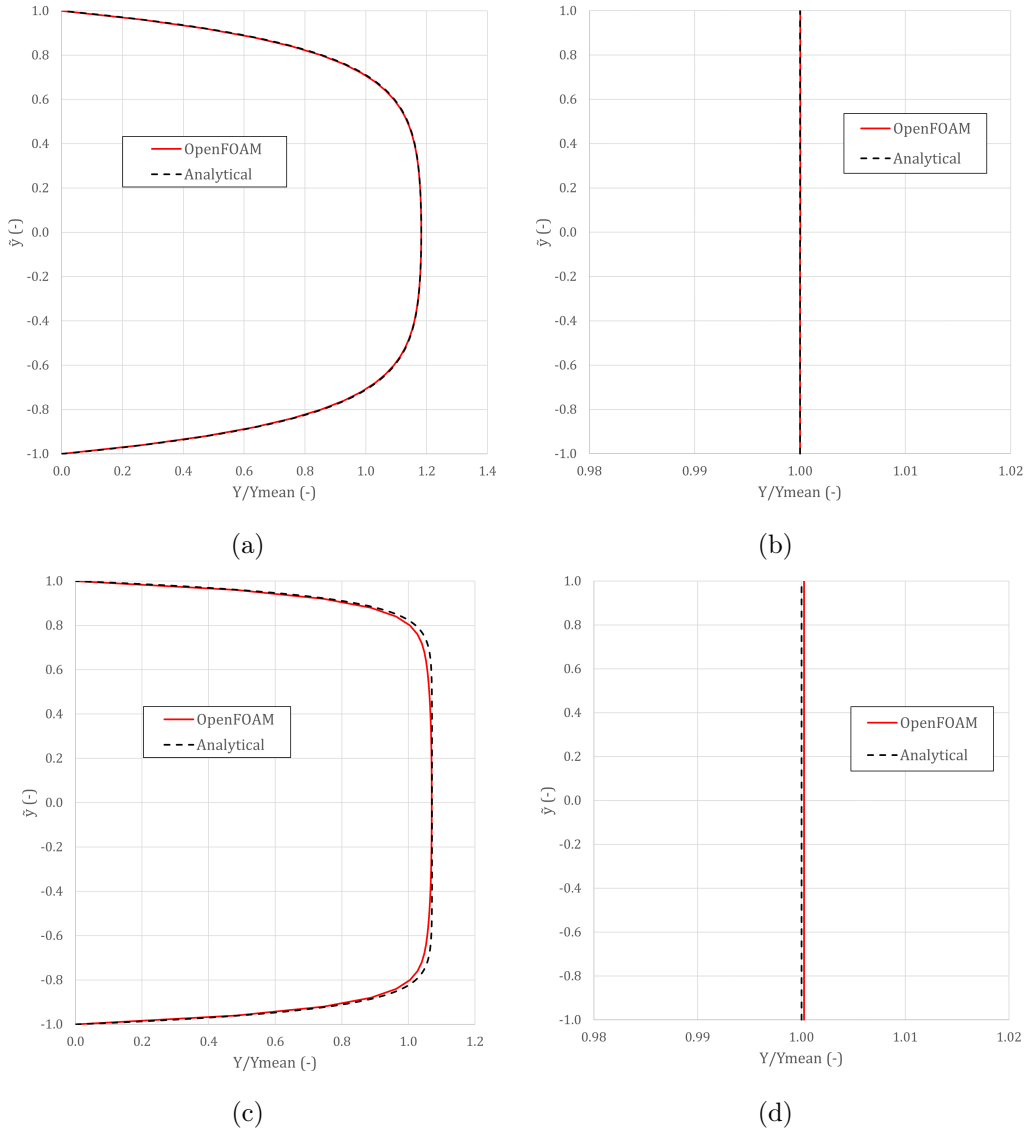

Figure 2. Profili di concentrazione di Xenon per sezioni trasversali della geometria, con confronto analitico. (a) Monofase, condizioni di Dirichlet (b) Monofase, condizioni di Neumann (c) Bifase, condizioni di Dirichlet (d) Bifase, condizioni di Neumann

di rimozione di xenon, ma piuttosto una grandezza legata ad essa: in Figura 3 è possibile, infatti, vedere l'andamento temporale del tempo di dimezzamento relativo all'effetto di estrazione di xenon per mezzo del sistema di iniezione di bolle, calcolato a partire dalla costante sopra menzionata, per la simulazione di riferimento del caso 2D. In legenda sono riportate indicazioni sulle condizioni selezionate per la modellazione dell'impianto di iniezione e rimozione di elio.

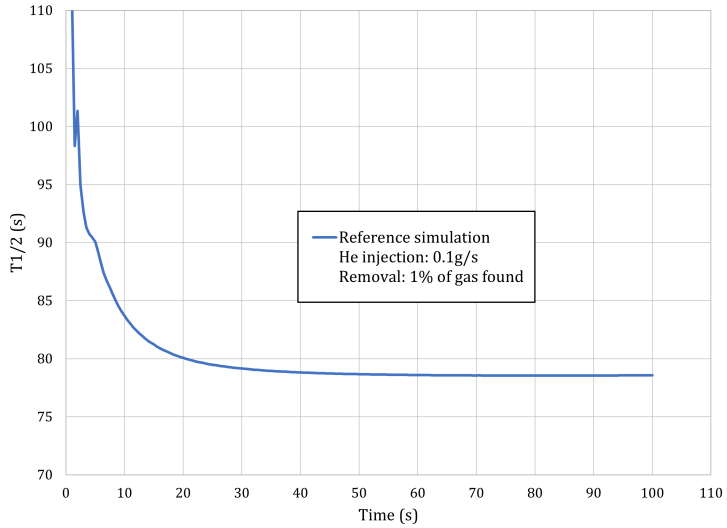

Figure 3. Andamento temporale del tempo di dimezzamento per il caso di riferimento 2D

Per verificare le assunzioni fatte nei calcoli eseguiti, vengono presentati nel testo ulteriori risultati. Prima di tutto, l'andamento nel tempo dell'inventario di xenon è mostrato, in coppia con un'interpolazione per evidenziarne l'effettivo andamento esponenziale ipotizzato. Inoltre, è presente una tabella di confronto tra i fenomeni di consumo dello xenon, in modo da evidenziare la possibilità di trascurare decadimento e cattura neutronica nel caso di analisi dell'effetto delle bolle.

Una ulteriore analisi viene poi condotta per verificare la dipendenza del tempo di dimezzamento calcolato (e quindi dell'efficienza del sistema di iniezione di bolle) da un parametro fondamentale nella definizione del problema: la portata di elio iniettata dal fondo del reattore. Il risultato ottenuto, interpretabile dalla Figura 4, è una proporzionalità inversa per quanto riguarda il tempo di dimezzamento, e quindi una linearità per quanto riguarda l'efficienza.

Considerazioni aggiuntive riguardo alla parte neutronica del problema e futuri possibili sviluppi sono riportate nel testo, prima di passare alla presentazione dei risultati del caso 3D. In questo secondo caso, il risultato di tempo di dimezzamento è riportato in Figura 5. Com'è visibile, il calcolo del parametro che esprime l'efficienza del sistema di iniezione di bolle è valido anche con questa simulazione. Come per il caso precedente, nel testo sono riportate considerazioni aggiuntive e risultati più dettagliati.

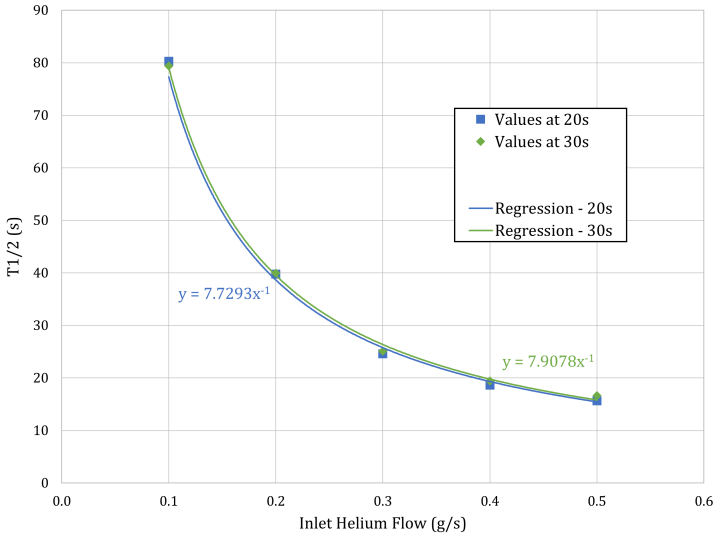

Figure 4. Valori di tempo di dimezzamento al variare della portata in ingresso di elio, con interpolazione

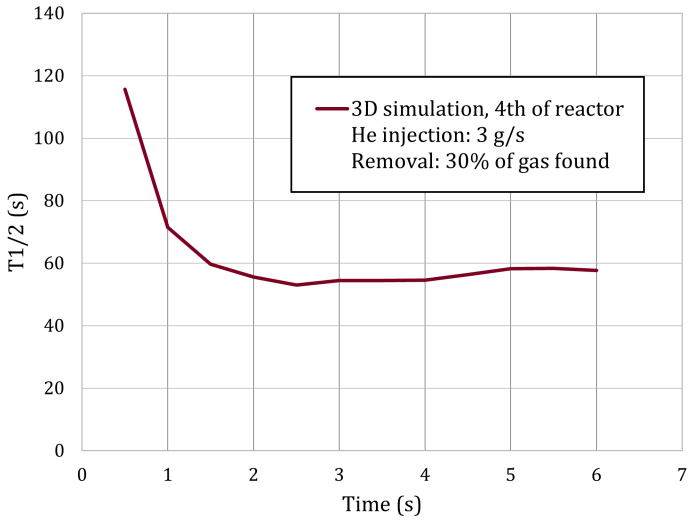

Figure 5. Andamento temporale del tempo di dimezzamento per il caso 3D

Conclusioni

Il lavoro di questa tesi contribuisce nello sviluppo di un ambiente computazionale unico per la simulazione del comportamento del MSFR. Con ulteriori migliorie e con l'aggiunta di altre funzionalità, il solutore di OpenFOAM impiegato in questo lavoro può arrivare a prevedere correttamente tutti gli aspetti che entrano in gioco nel funzionamento di un sistema complesso come quello in analisi, sia in condizioni nominali che in potenziali casi accidentali. I risultati presentati mostrano come l'approccio multifisico possa essere funzionale nella risoluzione di un problema di questo tipo, e la flessibilità di OpenFOAM dimostrata con l'implementazione della presenza di prodotti di fissione gassosi può essere sfruttata ancora per ogni altra

modifica necessaria. Come conclusione del testo, alcuni spunti di possibili obiettivi per lavori futuri sono presentati.

Contents

List of Figures

List of Tables

Chapter 1

Introduction

Molten Salt Reactors (MSRs) are a family of liquid-fueled fission reactors, identified in the frame of the Generation IV International Forum (GIF-IV) (https://www.gen-4.org/gif/) as one of the six concepts suitable for research and development. They feature a fluid molten salt mixture of thorium, uranium, and eventually transuranic elements, which acts both as fuel and coolant for the system. The employment of a fluid fuel offers some potential advantages to the concept, when compared to a more traditional solid-fueled reactor, such as

- Simplification of the core design, with the absence of solid fuel elements
- The possibility of an online reprocessing of the fuel, where the composition can be adjusted without shutting down the reactor
- Avoidance of a large initial reactivity inventory, which is not required in liquid-fueled systems
- The potential for higher burn-up and better resource utilization, since Trans-Uranic Elements (TRUs) can undergo fission or transmutation upon recirculation of the mixture
- Intrinsic safety characteristics, as the possibility of operation at atmospheric pressure, due to the high boiling point of the salt

Utilizing the salt mixture for the role of coolant as well presents some peculiar features too, among which the presence of a higher power density, the motion of the delayed neutron precursors and a strong coupling between neutronics and thermal hydraulics since fission energy is released directly into the coolant, without heat transfer delay. The analysis of the MSR design is still based on numerical modeling, even though the concept was conceived already in the Fifties. Some experimental studies were conducted throughout the 1950s and 1960s, mostly at Oak Ridge National Laboratory (ORNL), culminating in the realization of the Molten Salt Reactor Experiment (MSRE), which achieved criticality in 1965. Even if the experiment was a success, it

did not lead to the realization of the Molten Salt Breeder Reactor (MSBR), already studied in detail, and designed. This was partly because of the thermal spectrum of the MSBR, requiring intense chemical processing, and because of the presence of studies on the alternative Liquid Metal Fast Reactor (LMFR), seen as a more promising option in the Seventies. Today, the technology of the MSRs family is back under consideration for research, mainly due to the positive features already mentioned, and the efforts are focusing both on thermal and fast spectrum systems. Within the MSR System Steering Committee of the GIF-IV, in particular, two fast spectrum concepts are being analyzed: the Molten Salt Fast Reactor (MSFR), a design coming from France, and the MOlten Salt Actinide Recycler and Transmuter (MOSART), under development in the Russian Federation.

1.1 The Molten Salt Fast Reactor Concept

The Molten Salt Fast Reactor (MSFR) has been studied since 2004 at the Centre Nationale de la Recherche Scientifique (CNRS) (Grenoble, France). The concept has been consequentially developed in the frame of the Euratom Projects EVOL (Brovchenko et al., 2013) and SAMOFAR (http://samofar.eu/). Since 2019, it is under analysis in the H2020 SAMOSAFER project (https://samosafer.eu/). The MSFR is characterized by an intermediate-to-fast neutron spectrum, with the absence of in-core moderator, thus combining the advantages of extended resource utilization and waste minimization to the ones already listed of liquid-fueled reactors. The reference reactor features a nominal power of 3 GW_{th} and a total fuel salt volume of 18 m^3; it is operated at atmospheric pressure with an average in-core temperature of 700 °C. The system is composed of three circuits: the fuel circuit, the intermediate circuit, and the power conversion circuit. The main design features of the reactor are listed in Table 1.1.

The core was originally designed as a single compact cylinder with height equal to the diameter, but thermal-hydraulic studies performed in the framework of the EVOL project have shown a problem of significant stagnation close to the wall in the active zone. A toroidal shape has been consequently selected as the reference geometry, improving the results of thermal flow calculations. The fuel salt flows towards the top of the core, where it is extracted and directed to the external heat exchangers. After having transferred the heat produced by fission, the fuel is pumped back into the bottom of the reactor. A sketch of the layout of the system is shown in Figure 1.1.

The reactor is fueled with a mixture at eutectic composition of ^{7}LiF (77.5 mol%) and heavy nuclei fluorides (22.5 mol%, of which the main component is $^{232}ThF_4$). Two compositions in particular are being considered as reference for studies, one containing a single fissile nuclide, ^{233}U, and the other enriched with $^{235}U/^{238}U$ and other transuranic elements. The adoption of a closed thorium fuel cycle provides the design with an element of intrinsic sustainability, producing an actinide inventory with lower radiotoxicity with respect to other conventional solutions. The reactor is equipped with an online chemical reprocessing system, which extracts from the

Table 1.1. Reference MSFR Characteristics (Allibert et al., 2016)

Quantity	Value	Unit
Thermal Power	3000	MW_{th}
Electric Power	1300	MW_e
Core Radius	1.1275	m
Core Height	2.255	m
Fuel Salt Volume	18	m^3
Total Fuel Salt Cycle in Fuel Circuit	3.9	s
Fuel Temperature Increase in Core	100	$°C$
Mean Fuel Salt Temperature	700	$°C$
Breeding Ratio at Steady-State	1.1	-
Total Feedback Coefficient	-5	$pcm/°C$
Fuel Salt, initial composition	$LiF - ThF_4(^{233}U \text{ or } ^{enr}U)F_4$ or $LiF - ThF_4(Pu - MA)F_3$ with 77.5 mol% LiF	
Fertile Blanket Salt, initial composition	$LiF - ThF_4$ (77.5 − 22.5 mol%)	

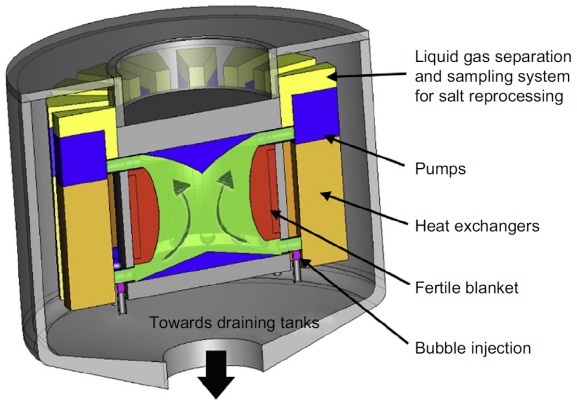

Figure 1.1. Sketch of MSFR Layout (Allibert et al., 2016)

core about 40 liters of fuel per day, in order to remove fission products from the salt mixture. The reprocessing system acts also to maintain the right proportions of elements inside the mixture for the eutectic composition. With the aim of limiting neutron leakages, improving in-core neutron economy, and protecting external core structures, thick reflectors made of nickel-based alloys are placed above and below the reactor. As further protection from remaining neutrons, the reflectors are layered with B_4C. Surrounding the core in the radial direction, a fertile blanket made of LiF-ThF_4 is present, to improve the breeding efficiency of the system. Salt draining systems are connected to the fuel circuit below the core, and they can be used both in conventional and in accidental situations. During planned shutdown operations, as short-duration maintenance, actively cooled storage tanks are employed. In case of any incident or accident resulting in excessive temperatures reached in the core, active and passive devices are employed to quickly drain the salt present inside the core to a criticality-safe tank. The design of the reactor also foresees the presence of a helium bubbling system, with injection of bubbles from the bottom and their removal from the top of the core. This is useful in order to extract both the gaseous fission products from the salt mixture, and the solid particles of precipitate produced in the fuel.

The MSFR system presents features allowing an advantage of intrinsic safety, among which are

- a largely negative feedback coefficient (for what concerns both the Doppler coefficient and the density coefficient), with a value of -5 pcm/K that counterbalance - from a safety point of view - the lower in-core delayed neutron fraction with respect to static fuel
- the production of heat directly in the coolant, which enables a quick response of the feedback coefficient
- the absence of solid materials in the core, which, in combination with a spectrum more epithermal than other fast reactors, reduces the chance of irradiation damage in the reactor internals

For more detailed information on the MSFR design, the reader is referred to (Allibert et al., 2016; Gerardin et al., 2017; Tano et al., 2017).

1.2 Motivation, Purpose and Outline of Thesis

This work is conducted in the framework of the European H2020 SAMOSAFER project (https://samosafer.eu/), which aims at the analysis of the safety aspects that a Molten Salt Reactor can offer, in view of the development of the MSFR. For this end, it is fundamental to rely on accurate modelling of the system. Most of the tools currently adopted in the field of nuclear research have been developed for the analyses of reactors of second and third generation, mainly in the framework of the Light Water

Reactors. This of systems is however substantially different with respect to the MSR design, and the related computational instruments are often tailored on the needs of conventional solid-fueled reactors, rendering them impractical for this case of study. For what concerns the models employed in the field of molten salt reactors in the Sixties, on the other hand, problems arise for the fact that they were tailored on a concept of thermal reactor, and they rely on the definition of reactor core channels for a simplified 1D approach, in contrast with what is needed for the development of the MSFR. For these reasons, new modelling tools need to be manufactured and implemented.

In previous works, a multiphysics solver was developed in the framework of OpenFOAM[1], with the purpose of improving the multiphysics modelling of the MSFR. The focus was put, in particular, on the strong coupling of neutronics and thermal-hydraulics of the system, on the effects of the presence of a gaseous phase in core (with the helium bubbling system), and on the effects of fluid compressibility. (Cervi et al., 2017; Cervi et al., 2019b; Cervi et al., 2019e)

While the previous works have set a solid basis for the multiphysics approach in the study of the MSFR environment, other aspects are still to be investigated. In particular, the helium bubbling system has been implemented considering only the consequences relative to the presence of a second phase, in a gaseous state. Both the thermal-hydraulic and the neutronic equations of the system are influenced by the presence of helium, but the solver still lacks the ability to describe the interactions of gas bubbles with Gaseous Fission Products (GFPs) and model their removal from the core, to be treated in the off-gas unit.

The ability to model the presence of GFPs in the system is fundamental in order to be able to correctly evaluate the source term in the reactor and in the reprocessing units. Fission products, in any physical state, influence directly the neutronics, due to the poisoning caused by neutron capture, but also indirectly, because of density effects. Moreover, gaseous species affect neutronics through a void feedback as well. The combination of these phenomena motivates the need of particular attention in the treatment of GFPs. The proposed helium bubbling system could be a solution for controlling their concentration, rather than having to balance the anti-reactivity effect through injection of fissile material, but there is still the need to assess its efficiency in the removal of the various species.

The purpose of this thesis is to develop a suitable framework in which the gaseous fission products are modelled and can be analyzed, for what concerns their production, their effect on the system (both on thermal-hydraulics and neutronics), their exchange between the liquid and the gaseous phase, and the efficiency of their transport out of the core through the helium bubbling system. The approach followed is depicted in Figure 1.2.

In this work, for the sake of simplicity, only Xenon-135 is considered, being one of the main gaseous fission products with a direct influence on the environment of a

[1] a description of this computational software can be found in Appendix A

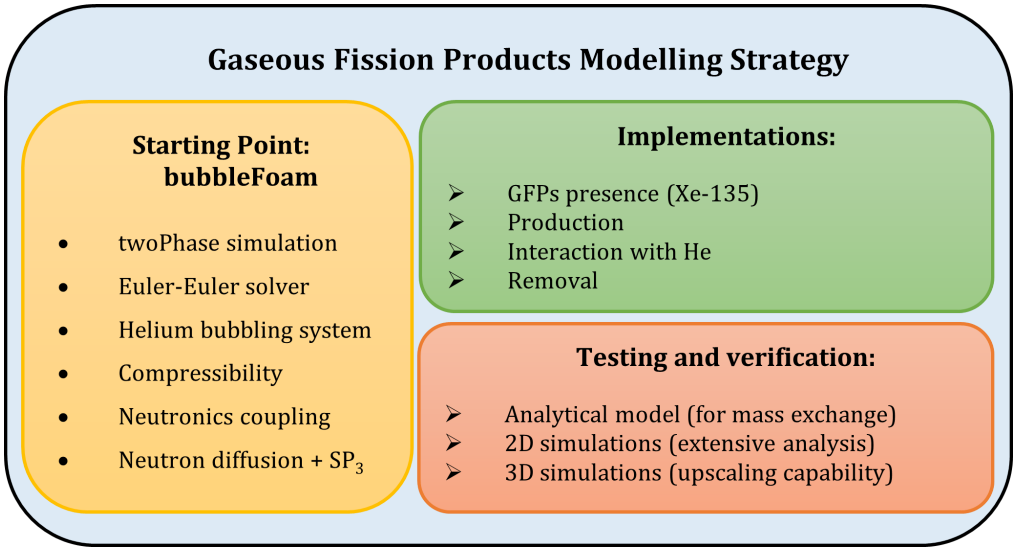

Figure 1.2. Graphical representation of the outline of this work

reactor, in its behavior as neutronic poison. The analysis conducted, however, can easily be extended to other gaseous fission products as well.

The remainder of this thesis is organized as follows. In Chapter 2, a brief report on the state-of-the-art MSFR simulation techniques is presented, together with a more detailed description of the OpenFOAM solver employed as starting point of this work. The contents of this section refer for the most part to the work of (Cervi, 2020). Additionally, preliminary test results are displayed, in order to assess the correct implementation of the solver in a more up-to-date release. (https://openfoam.org/release/6/). In Chapter 3, the development of the Xenon modelling is presented, with an overview of the possible approaches, an analysis of the experimental data found in literature, and an in-depth explanation of the mathematical basis of the code variations performed. Chapter 4 is reserved to an analytical verification of the mass transfer modelling, by comparison between an exact calculated solution and the results obtained in OpenFOAM with simulations of a simple 2D case. In Chapter 5, a complete analysis of the gaseous fission product behavior is performed on computational models resembling the reactor. Extensive tests are conducted on a simplified 2D geometry, followed by a 3D simulation of a fraction of the full-scale MSFR, in order to demonstrate the up-scaling capabilities of the proposed simulation model. Additionally, in Appendix A information about the delayed neutrons and decay heat precursors modelling are presented, and Appendix B provides data employed for the analysis of Xenon behavior from the point of view of neutronics.

Chapter 2

Multiphysics Model of the MSFR

2.1 Introduction

The employment of a liquid fuel, which has the role of coolant as well, is the most peculiar feature of the concept of Molten Salt Reactors. This choice can lead, as explained in Chapter 1, to significant advantages and improvements in the management of the fuel cycle, in safety and sustainability aspects, and in simplifications of the plant design. On the other hand, as already mentioned, the presence of liquid fuel distinguishes the MSFR from other nuclear reactor systems, for what concerns the simulation framework to be employed. Some difficulties, which are not found in more common designs, arise, and new obstacles need to be overcome, both in physical and technological constraints. One of the main features which makes the MSFR system unique in the field is a stronger coupling between neutronics and thermo-hydraulics, which needs to be considered and treated accordingly. Other key aspects that characterize the design are, for example, the drift of the neutron precursors, carried around by the moving fluid, or the absence of a channel-based structure in the core, which introduces important effects on the 3D scale, implying the need to employ CFD methods to properly consider phenomena as recirculation and inhomogeneity.

The dynamics that need to be analyzed here are complex, and the interactions among the various parts and different physics are significant, creating a strongly non-linear problem overall. New tools have to be developed in order to be able to comprehend, possibly in the same simulation framework, the effects and the consequences of all the different physics involved, together with their reciprocal influence and coupling terms.

2.2 State of the Art

In the past, the analysis of nuclear reactors has been performed employing "coupled-code" techniques, which relied on the external combination of different specialized codes for the different parts of the problem (Avramova et al., 2010). As an example, the simulations could be carried out by solving the neutronics part of the problem with a neutron transport or diffusion code and feeding the resulting output to the thermal-hydraulics code, to obtain the temperature and velocity distribution, for each time step. This approach is considered inefficient for what concerns the solution of the non-linearities arising from the coupling terms in the single time-step. Moreover, it relies on the development of suitable connections among different codes, a feature which requires precise knowledge of different codes, and that could lead to more programming errors. The implementation of all the physics in a single simulation environment in which the non-linearities are properly solved either with an iterated or fully-coupled approach, as seen in (Luzzi et al., 2012), can provide a better tool in order to model and analyze the behavior of a complex and strongly coupled system as the MSFR, for what concerns both operational and accidental conditions.

A first study on a system of this kind can be provided by zero-dimensional approach for the thermal-hydraulic modelling and point-kinetics equations for the neutronics, as it can be seen in (Cammi et al., 2011, Guerrieri et al., 2012, and Cervi et al., 2018). These analyses, however, cannot provide information on the spatial distribution of the parameters and quantities in the system that in the MSFR play a major role. In order to account for this, newer models were developed employing finite element multiphysics codes, with simulations performed on simplified 2D axial symmetric geometries. These studies adopted multi-group diffusion for neutronics and a single-phase incompressible solver for the thermal-hydraulics part (Fiorina et al., 2014). Again, these analyses can produce good results for preliminary studies, but they fail in the description of more detailed phenomena which can be observed only on a 3D scale. This issue has been addressed with the development of a 3D model of the MSFR, by (Aufiero et al., 2014a; Aufiero et al., 2014b), and its further refinement by (Cervi et al., 2017; Cervi et al., 2019b; Cervi et al., 2019c; Cervi et al., 2019e). This last model has been manufactured with the OpenFOAM toolkit, and it implements multi-group neutron diffusion as well as SP_3 transport equations for the neutronics part, together with a two-phase, compressible thermal-hydraulics model and transport equations for the delayed neutron and decay heat precursors.

The latest improvements have produced a unique simulation environment, able to couple neutron transport and two-phase compressible thermal-hydraulics, but the predicting capabilities of the framework can be extended further. In particular, the current model is not able to reproduce the evolution of the composition of the fuel mixture, with the production of fission products, which can be found in gaseous or solid form. The aim of this thesis is to address this problem in a preliminary manner, demonstrating the possibility of treatment of Gaseous Fission Products, for what concerns their production, consumption, and transport in the system. This is done with the implementation of a single nuclide, but it should pose some useful guidelines

for the further extension to multiple nuclides. Recent studies performed on the same environment of the MSFR, conducted from the point of view of neutronics and burnup (Aufiero, 2014) have considered already the effect of the hypothetical helium bubbling system on the concentration of gaseous fission products in the core, by implementation of suitable terms in the governing equations. In particular, the chosen approach was to model the helium bubbling treatment in analogy with a radioactive decay of the interested nuclides, with the definition of an appropriate halving time. The aim of this work is also to provide new simulation tools to estimate and confirm the values of the parameter employed, in view of keeping the existing links among the various studies of the same system.

2.3 The bubbleFoam Solver

For this work, a multiphysics solver called bubbleFoam has been employed. In order to solve all the equations governing the system, the algorithm divides each time step in two different cycles, as shown in Figure 2.1. The first one employs a thermal-hydraulics sub-solver, based on the pre-existing OpenFOAM solver "reactingTwoPhaseEulerFoam", in order to consider the fluid dynamics of the compressible liquid and the gaseous bubbles. The second cycle concerns the neutronics of the system and it follows one of two selectable approaches: a multi-group diffusion model, or a transport model, based on the multi-group SP_3 approximation. The two neutronics models have been developed in (Cervi et al., 2017; Cervi et al., 2019a; Cervi et al., 2019d; Cervi et al., 2019b; Cervi et al., 2019c; Cervi et al., 2019e).

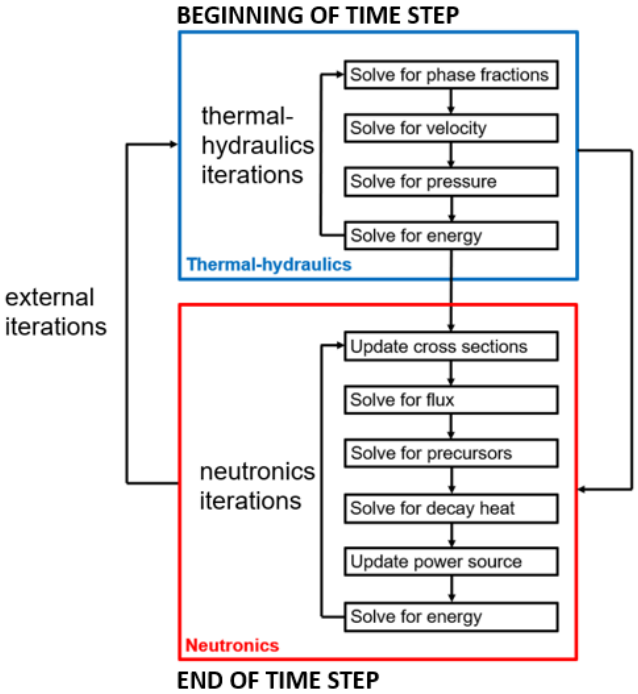

Figure 2.1. Structure of the solver and coupling (Cervi, 2020)

During the thermal-hydraulics cycle, the mass, momentum and energy equations are solved to obtain phase fractions, velocity of each phase, pressure and temperature of the system. The convergence of the solution of this part of the problem is reached performing Picard iterations, in compliance with the OpenFOAM solving approach. Then, during the neutronics cycle, the algorithm solves for the flux, the delayed neutron precursors and the decay heat. The total power source is obtained as sum of a prompt heat (calculated from the flux) and the decay heat, and it is used to solve again the energy equation. The temperature and density fields obtained from this are used to update the neutronics cross section, and Picard iterations are performed on this cycle as well until convergence. After this, integration in time of the governing equations is performed, and the solver moves on to the next time step.

The two parts of the solver have a reciprocal influence on one another. The thermal-hydraulics cycle provides the information of void fraction, fuel temperature and density useful to update the cross-section values for the flux, together with the modelling of precursor transport. Analogously, the neutronics cycle returns the power density distribution, in order to evaluate temperature and density. For this reason, external iterations can be performed between the two sub-solvers in a single time step. This is especially useful in the study of fast transient, where the reciprocal influence is greater.

2.4 Thermal-Hydraulics Sub-Solver

The analysis of two-phase flows is today the object of intensive study in the scientific community. Many methods of approach are available, and they present different levels of complexity and accuracy. A broad category of techniques is the one of "free-surface", which comprises all those approaches where the topology of the interface between liquid and gaseous phases is an explicit outcome of the problem solution (Rusche, 2002). Free-surface methodologies can be divided in three groups (Hyman, 1984):

- Surface tracking methods: a sharp interface is defined, and its motion is followed by means of marker particles or segments (Figure 2.2a)
- Moving mesh methods: the vertices of the employed mesh are displaced, keeping track of the interface themselves (Figure 2.2b)
- Volume tracking methods: the interface is not set as a sharp boundary, but rather identified by means of apposite indicator functions, such as volume fractions (Figure 2.2c)

Surface tracking and moving mesh methods have the advantageous ability of determining the exact position of the interface. This comes at the cost of the additional complexity needed to compute the relocation of markers or mesh vertices, particularly in case of large interface deformations or other big topology changes. While reducing this complexity, volume tracking methods introduce the possibility

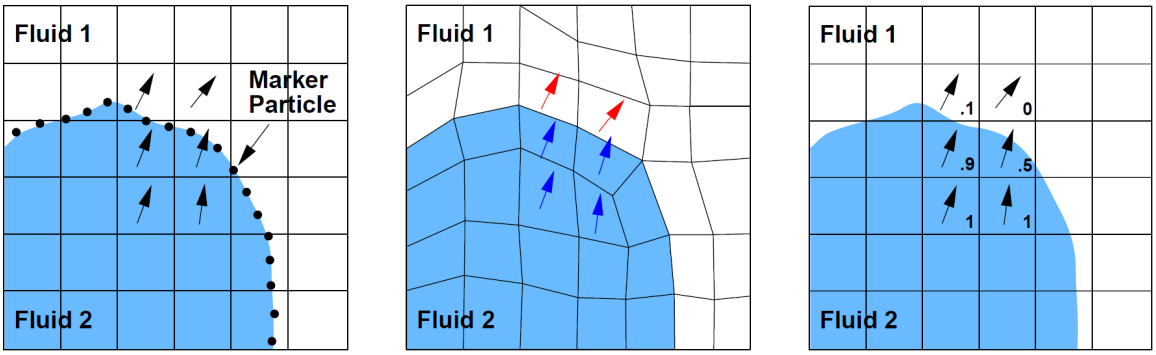

(a) (b) (c)

Figure 2.2. Free-surface techniques (Rusche, 2002). (a) Surface Tracking method with marker points (b) Moving Mesh method (c) Volume Tracking method with volume fractions

of diffusion and dispersion of the interface with its advection, possibly failing to preserve its sharpness (Rusche, 2002). To tackle this problem, in the framework of volume tracking techniques, the Volume-Of-Fluid (VOF) method has thus been introduced and is commonly employed in Computational Fluid Dynamics (CFD) analyses. This approach is based on the reconstruction of a sharp interface from the volume fraction distribution before advection and, directly solving the volume fraction balance equations, can potentially guarantee an exact mass conservation in the system (Baraldi et al., 2014).

In the study of dispersed phases, interfaces are generally characterized by a complex behavior, undergoing a lot of deformations. Keeping track of the exact position of the interface, in this case, can become unfeasible for the computational resources available today. On the other hand, for most of the practical aspects of the analyses, macroscopic properties of the flow are more important than local instances, and a suitable averaging process can be exploited. Among these, three main categories can be identified:

- Eulerian averaging: the properties of the flow are considered as functions of space and time coordinates, $\varphi(x, y, z, t)$, and the average is performed by integrating over those. Thus, the Eulerian time average can be obtained by integration of the quantity considered, for a fixed spatial position, over a finite time interval:

$$\bar{\varphi} = \frac{1}{\Delta T} \int_{\Delta T} \varphi(x, y, z, t) dt \tag{2.1}$$

  Since the operation aims at smoothing instant variations of the function, the time interval should be appropriately chosen. It should be taken large in comparison with the time scales of the local variations, but small if compared to the macroscopic time scale of the process. In the same way, Eulerian volume averaging consists in integration over a finite volume, centered around the spatial position of interest, for a fixed time instant:

$$\langle \varphi \rangle = \frac{1}{\Delta V} \sum_j \int_{\Delta V_j} \varphi(x, y, z, t) dV_j \tag{2.2}$$

The operation performed is actually the sum of the integrals over the finite volume occupied by each phase of the system (ΔV_j). Knowing this, volume integrals can be calculated also for the properties associated with a single phase, and the operation can be performed in two different approaches, namely an intrinsic phase average (Eq. (2.3)):

$$\langle \varphi_j \rangle_j = \frac{1}{\Delta V_j} \int_{\Delta V_j} \varphi_j(x, y, z, t) dV_j \tag{2.3}$$

or an extrinsic phase average (Eq. 2.4):

$$\langle \varphi_j \rangle = \frac{1}{\Delta V} \int_{\Delta V_j} \varphi_j(x, y, z, t) dV_j \tag{2.4}$$

The two expression are related by

$$\langle \varphi_j \rangle = \alpha_j \langle \varphi_j \rangle_j \tag{2.5}$$

where alpha is the phase fraction, defined as

$$\alpha_j = \frac{\Delta V_j}{\Delta V} \tag{2.6}$$

Again, the finite control volume employed for the integration should be chosen accordingly with respect to the scale of the local variations and the scale of the problem system.

- Lagrangian averaging: in the Lagrangian description, the individual particles composing the fluid are tracked and they are given personal spatial coordinates, which are themselves function of the independent time and space variables of the system: $X = X(x, y, z, t)$, $Y = Y(x, y, z, t)$, $Z = Z(x, y, z, t)$. Properties are expressed in function of the position of the single particle and time: $\varphi(X, Y, Z, t)$. Hence, time averaging can be performed for any quantity with an integral over a time interval for a fixed position of the particle considered:

$$\bar{\varphi} = \frac{1}{\Delta T} \int_{\Delta T} \varphi(X, Y, Z, t) dt \tag{2.7}$$

- Molecular averaging: the properties of the system are expressed for the particle number density $f(r, c, t)$, which is a distribution function evaluated on spatial position $r(x, y, z)$, particle velocity $c(c_x, c_y, c_z)$ and time. This formulation follows the Boltzmann equation.

For the analysis of a system where a dispersed phase flows in a continuous one, as is the case of MSFR, the combinations of approaches generally employed are Euler-Lagrange and Euler-Euler (or two-fluids).

In the Euler-Lagrange framework, the continuous phase is treated by Eulerian equations and the dispersed one follows the Lagrangian formulation (Figure 2.3a). This approach is suitable to solve the problems where the motion and the properties of

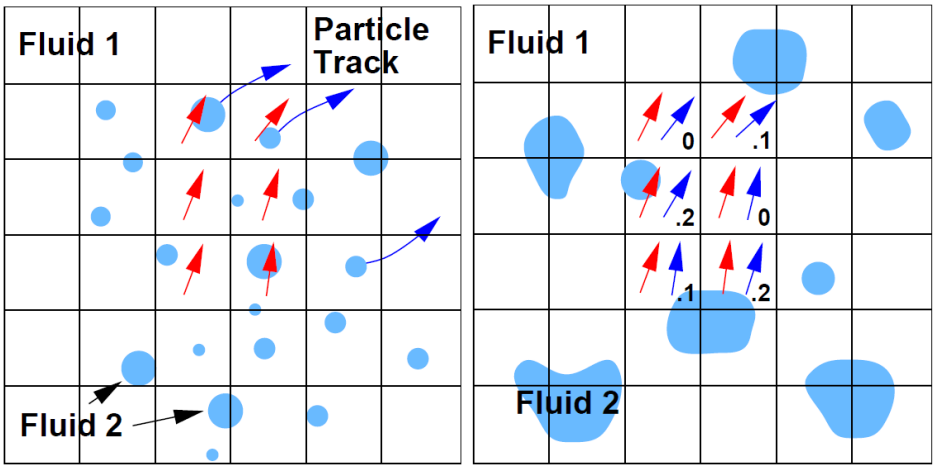

(a) (b)

Figure 2.3. Averaging modelling approaches (Rusche, 2002). (a) Euler-Lagrange method (b) Euler-Euler method

the single dispersed particles is of interest, but it requires significative computational power to keep track of each particle. Thus, the analysis can become unfeasible when the number of particles is too high (i.e., in the case of large systems or high phase fractions). In the Euler-Euler formulation, both phases are considered as continua interpenetrating each other, and they are both described by Eulerian equations (Figure 2.3b). Since the need of tracking the single dispersed particles is absent here, this approach requires much less computational burden with respect to the previous one and can be more easily applied to large-scale or large-phase-fraction systems. On the other hand, the Eulerian averaging process leads to a loss of information of some degree, and the need of closure relations arise for the macroscopic balance equations. The validity of the predictions made with this approach is hence dependent on the accuracy of the additional relations. Despite this potential limit in modelling capabilities, the Euler-Euler approach is generally the preferred one for many CFD studies, thanks to its larger range of applicability.

The MSFR system features both a large dimensional scale and a turbulent flow with a Reynolds number close to 10^6 (Gerardin et al., 2017). Additionally, for what concerns the fission products, their production is distributed in the entire core. These factors make the application of a Euler-Lagrange approach significantly difficult, if not impossible, from the computational point of view. For these reasons, the Euler-Euler approach is suggested in the MSFR analyses and is employed in this work.

2.4.1 The "reactingTwoPhaseEulerFoam" solver

Among the standard solvers present in OpenFOAM, the "reactingTwoPhaseEulerFoam" is devoted to the analysis of two-phase systems based on the Euler-Euler approach. It is employed in a vast range of fields, and it has been validated on many cases of study, as for example the simulation of bubble columns (Bhusare et al., 2017), particle and

droplet-laden flows (Reinhardt et al., 2013) and liquid-liquid flows in gravity settlers (Panda et al., 2017).

Following the Euler-Euler approach, in this solver each phase is associated to a phase fraction, defined by Eq. (2.6). In the framework of the finite volume discretization employed in OpenFOAM, α_j corresponds to the volumetric portion of cell of the computational mesh occupied by the phase j. The principal macroscopic equations of the system, i.e., mass and momentum conservation and energy balance for each phase, averaged by Eulerian approach, are defined as: (Ishii et al., 2011; Marschall, 2011)

$$\frac{\partial(\rho_j \alpha_j)}{\partial t} + \nabla \cdot (\rho_j \alpha_j \mathbf{u}_j) + S_j = 0 \tag{2.8}$$

$$\begin{aligned} \frac{\partial(\rho_j \alpha_j \mathbf{u}_j)}{\partial t} + \nabla \cdot (\rho_j \alpha_j \mathbf{u}_j \mathbf{u}_j) = \\ = \nabla \cdot \alpha_j \left[-p\mathbf{I} + (\mu + \mu_t) \left(\nabla \mathbf{u}_j + (\nabla \mathbf{u}_j)^T \right) - \frac{2}{3} \mu \mathbf{I} \, div \mathbf{u}_j \right] + M_j \end{aligned} \tag{2.9}$$

$$\begin{aligned} \frac{\partial(\rho_j \alpha_j h_j)}{\partial t} + \nabla \cdot (\rho_j \alpha_j \mathbf{u}_j h_j) + \frac{\partial(\rho_j \alpha_j k_j)}{\partial t} + \nabla \cdot (\rho_j \alpha_j \mathbf{u}_j k_j) = \\ = \alpha_j \frac{\partial p}{\partial t} + \frac{\alpha_j}{\rho_j C_{p,j}} \nabla \cdot ((K_{th} + K_{th,t}) \nabla h_j) + L \Delta T + \rho_j \alpha_j \mathbf{g} \cdot \mathbf{u}_j \end{aligned} \tag{2.10}$$

In the equations for each phase, the same value of pressure is used. This choice is valid for the cases where the dimensions of the dispersed particles are small with respect to the characteristic dimensions of the system. The explicit term M_j, present in the momentum equations, Eqs. (2.9), takes into account the momentum transfer between the two phases. Its appearance is due to non-linearity, which implies the need of closure equations. Empirical models and correlations are employed to determine the single contributions that add up to M_j, each representing a single kind of the forces acting at the interface between the phases (Lathouwers, 1999):

- Drag: force deriving from the inter-phase viscosity effects
- Virtual mass forces: forces calculated in function of the relative acceleration of the two phases, deriving from the inertia of the carrier.
- Lift: force due to the rotational part of the motion of the fluid.
- Turbulent dispersion: additional component of the drag caused by turbulent fluctuations in the dispersed phase.

Analogously, in the energy balance equation, Eq. (2.10), the term $L\Delta T$ accounts for heat transfer between the two phases. L is an inter-phase heat transfer coefficient,

evaluated by correlations, while ΔT is the calculated temperature difference between phases.

Among the main closure relations and correlations available in literature, both for momentum and heat transfer, this work follows the same choices made in a previous work (Cervi, 2020), where a sensitivity analysis is presented, verifying that the results found in these studies are not significantly dependent on the choice of correlations. For what concerns the turbulence modelling, the solver is based on the RANS approach, with the possibility of choosing among various correlations. In this work, the standard k-ϵ model was employed.

With respect to the standard version of the twoPhaseEulerFoam, the thermal-hydraulic sub-solver employed in this work presents some additional terms. Namely, the bubbleFoam solver introduces a source term in the mass conservation equation of the gaseous phase, accounting for the bubble injection/extraction process, and a source term in the energy balance equation of the liquid, representing the contribution of the volumetric power sources due to fission and decay heat, calculated by the neutronics sub-solver.

2.5 Neutronics Sub-Solver

The bubbleFoam solver allows a choice between two different approaches in the solution of the flux equations in the neutronics cycle: a multi-group neutron diffusion model (Cervi et al., 2017; Cervi et al., 2019a; Cervi et al., 2019b) and a multi-group SP_3 neutron transport model (Cervi et al., 2019a; Cervi et al., 2019c; Cervi et al., 2019e). Afterwards, the precursor balance equations and the decay heat equations are solved in the same way, independently from the choice of approach. The neutronics sub-solver is provided also with a way to calculate the multiplication factor, through a power iteration routine. A user-defined choice is given to select between the time-dependent or the steady-state eigenvalue solutions.

2.5.1 Diffusion Model

One of the most common approaches adopted with the purpose of estimating the neutron flux is the multi-group diffusion equation. It is popular in the analysis of nuclear reactor transients due to easiness of implementation, combined with the requirement of low computational time, even if these perks come at the cost of some limitations. The model is based - in its segregated form - on the solution of one equation for each energy group, in the form

$$\frac{1}{v_i}\frac{\partial \varphi_i}{\partial t} = \nabla \cdot D_{n,i}\nabla\varphi_i - \Sigma_{r,i}\varphi_i + \bar{\nu}\Sigma_{f,i}(1-\beta)\chi_{p,i}\varphi_i + S_d\chi_{d,i} + S_{n,i}(1-\beta)\chi_{p,i} + S_{s,i} \quad (2.11)$$

The solution of these equations requires an iterative procedure among the groups, because of the presence of the explicit source terms, S. They represent, respectively, the contributions of delayed neutrons, prompt neutrons coming from fissions induced by neutrons of other energy groups, and neutrons scattered from other groups:

$$S_d = \sum_k \lambda_k c_k \tag{2.12}$$

$$S_{n,i} = \sum_{j \neq i} \bar{\nu} \Sigma_{f,j} \varphi_j \tag{2.13}$$

$$S_{s,i} = \sum_{j \neq i} \Sigma_{s,j \to i} \varphi_j \tag{2.14}$$

Suitable albedo boundary conditions are applied to the neutronics problem, in order to simulate the presence of the external reflectors and of the blanket salt. This type of boundary condition is based on the definition of a ratio between the outgoing and incoming neutron currents β. The corresponding analytical expression is

$$D_{n,i} \nabla \varphi_i = -\frac{1}{2} \left(\frac{1 - \beta_i}{1 + \beta_i} \right) \varphi_i \tag{2.15}$$

2.5.2 SP3 Transport Model

The SP_N equations are a set of equations first derived by (Gelbard, 1962) as a simplified version of the spherical harmonics approximation (P_N). In these models, the angular dependence of the neutron flux is expanded into the first N spherical harmonics (Bell et al., 1970). This operation results in a complex system of $(N+1)^2$ differential equations. Replacing the 1D second order derivative in a planar formulation of the P_N model with the 3D Laplacian operator, the SP_N approach results in a system of $(N+1)/2$ equations. This operation helps in overcoming the initial complexity, maintaining an improvement in accuracy with respect to the diffusion approach. In the case of the SP_3 approximation, for each energy group two equations are solved, obtaining the first two even-order flux momenta: φ_0 and φ_2. This approach is seen as a good compromise between accuracy and computational cost for simulations, due to its simplicity and theoretically sound derivation (Brantley et al., 2000). The equations are particularly suitable for the case of the analysis of the MSFR, due to the homogeneity of the system, and they are generally advisable for systems where the flux variation near interfaces is mainly one directional (Fiorina et al., 2017).

The form in which the SP_3 equations are implemented in the solver is known as "within-group form", which is a further simplification obtained by neglecting anisotropic scattering within different energy groups. The analytical formulation is then as follows:

$$\frac{1}{v_i}\frac{\partial(\varphi_{0,i}+2\varphi_{2,i})}{\partial t} = \nabla\cdot D_{n0,i}\nabla(\varphi_{0,i}+2\varphi_{2,i}) - \Sigma_{r,i}\varphi_{0,i} + S_{n,i}(1-\beta)\chi_{p,i} + S_d\chi_{d,i} + S_{s,i} + \frac{2}{v_i}\frac{\partial\varphi_{2,i}}{\partial t} \quad (2.16)$$

$$\frac{9}{5}\frac{1}{v_i}\frac{\partial\varphi_{2,i}}{\partial t} = \nabla\cdot D_{n2,i}\nabla\varphi_{2,i} - \Sigma_{t2,i}\varphi_{2,i} + \frac{2}{5}\Sigma_{r,i}\varphi_{0,i} - \frac{2}{5}S_{n,i}(1-\beta)\chi_{p,i} - \frac{2}{5}S_d\chi_{d,i} - \frac{2}{5}S_{s,i} + \frac{2}{5}\frac{1}{v_i}\frac{\partial(\varphi_{0,i}+2\varphi_{2,i})}{\partial t} \quad (2.17)$$

where:

$$D_{n0,i} = \frac{1}{\Sigma_{tr,i}} \quad (2.18)$$

$$\Sigma_{t2,i} = \Sigma_{t,i} - \Sigma_{s2,ii} \quad (2.19)$$

$$D_{n2,i} = \frac{9}{35}\frac{1}{\Sigma_{t,i}-\Sigma_{s3,ii}} \quad (2.20)$$

The explicit source terms are defined analogously to the diffusion approach, by replacing φ with $\varphi_{0,i}$ in Eqs. (2.12), (2.13) and (2.14). Albedo boundary conditions are defined again for this approach as:

$$D_{n0,i}\nabla(\varphi_{0,i}+2\varphi_{2,i}) = -\frac{1}{2}\left(\frac{1-\beta_i}{1+\beta_i}\right)\left(\varphi_{0,i}+\frac{5}{4}\varphi_{2,i}\right) \quad (2.21)$$

$$D_{n2,i}\nabla\varphi_{2,i} = -\frac{1}{2}\left(\frac{1-\beta_i}{1+\beta_i}\right)\left(\frac{3}{20}\varphi_{0,i}-\frac{15}{20}\varphi_{2,i}\right) \quad (2.22)$$

More details about the analysis of this approach are given in (Cervi et al., 2019c).

2.5.3 Precursor Balance and Decay Heat

The delayed neutron precursors profiles are solved with a multi-group approach, as the flux. The precursor balance for the single group contains terms of diffusion and

transport in order to account for fuel motion. In case of two phase formulation, the equation reads:

$$\frac{\partial \rho_l \alpha_l c_k}{\partial t} + \nabla \cdot (\rho_l \alpha_l \mathbf{u}_l c_k) = \nabla \cdot \left(\rho_l \alpha_l \left(\frac{\nu}{Sc} + \frac{\nu_T}{Sc_T} \right) \nabla c_k \right) + \beta_k \sum_i \bar{\nu} \Sigma_{f,i} \varphi_i - \lambda_k \rho_l \alpha_l c_k \tag{2.23}$$

where Sc and Sc_T represent, respectively, the laminar and turbulent Schmidt number.

The modelling of the precursors neglects the presence of the gaseous phase, following an approximation, from the physical point of view, that they remain in the liquid phase and do not interact with gas bubbles. In particular, possible terms of mass transfer between phases are thus neglected. Additionally, the salt density is considered constant in the formulation, so that the equations can be simplified further. The corrections for the density changes and the void fraction presence are however still applied on the cross-sections. The absence of explicit source terms and cross-group interactions in the equations allows for a simple solution of each one of them, without the need for an iterative procedure.

In a similar way, decay heat is considered by solving equations modelling the behavior of the relative isotopes, subdivided into groups. The number of these "decay heat groups" is normally different from precursor or flux groups. The balance is defined in terms of the product between the concentration of the isotopes and the average heat released by that group (i.e. the unknown has units of J/kg)

$$\begin{aligned} \frac{\partial \rho_l \alpha_l d_m}{\partial t} + \nabla \cdot (\rho_l \alpha_l \mathbf{u}_l d_m) = \nabla \cdot & \left(\rho_l \alpha_l \left(\frac{\nu}{Sc} + \frac{\nu_T}{Sc_T} \right) \nabla d_m \right) \\ & + \beta_{h,l} \sum_i E_f \Sigma_{f,i} \varphi_i - \lambda_{h,l} \rho_l \alpha_l d_m \end{aligned} \tag{2.24}$$

More details about the terms appearing in the equations for precursor balance and decay heat can be found in Appendix B.

2.5.4 Power Iteration Routine

In addition to the default time-dependent mode, a power iteration routine is implemented in the neutronics sub-solver, to allow for the calculation of the multiplication factor, following the k-eigenvalue approach (Bell et al., 1970). In this steady-state mode, the neutronics equations are solved setting the time derivatives to zero and

scaling the fission source by the multiplication factor, k_{eff}

$$\nabla \cdot D_{n,i} \nabla \varphi_i - \Sigma_{r,i} \varphi_i + \frac{1}{k_{eff}} \left[\bar{\nu} \Sigma_{f,i} (1-\beta) \chi_{p,i} \varphi_i + S_{n,i} (1-\beta) \chi_{p,i} \right] + S_d \chi_{d,i} + S_{s,i} = 0 \tag{2.25}$$

$$-(\mathbf{u} \cdot \nabla) c_k + \nabla \cdot \left(\left(\frac{\nu}{Sc} + \frac{\nu_T}{Sc_T} \right) \nabla c_k \right) + \beta_k \sum_i \frac{\bar{\nu}}{k_{eff}} \Sigma_{f,i} \varphi_i - \lambda_k c_k = 0 \tag{2.26}$$

The employed value of the multiplication factor is computed as the ratio of neutron produced by fission in the current and previous iteration

$$k_{eff} = \frac{\int \sum_i \bar{\nu} \Sigma_{f,i} \varphi_i dV|_n}{\int \sum_i \bar{\nu} \Sigma_{f,i} \varphi_i dV|_{n-1}} \tag{2.27}$$

Subsequently, the neutron flux is normalized to a user-defined power level. The procedure is repeated until convergence of the value of k_{eff} to the solution.

2.6 Coupling between Sub-Solvers

The results from neutronics influence the thermal-hydraulics part of the problem through the power source term employed in the energy equation. The term is computed as sum of fission power and decay heat

$$Q = Q_f + Q_d = \left[1 - \sum_i \beta_{h,i} E_f \Sigma_{f,i} \varphi_i \right] + \left[\sum_l \lambda_{h,l} d_l \right] \tag{2.28}$$

At the same time, the neutronics equations are influenced by thermal-hydraulics through the feedback effects of temperature, density and void fraction. The macroscopic cross sections of any reaction for each energy group are updated each time-step, as

$$\Sigma_{i,j} = \left[\Sigma^o_{i,j} + B_{i,j} \log \frac{T_{fuel}}{T_{ref}} \right] \frac{\rho_{fuel}}{\rho_{ref}} (1 - \alpha_g) \tag{2.29}$$

The constant reference term is modified by an additive logarithmic term, accounting for the effect of temperature, and two multiplicative terms, one representing the effect of density and one for void fraction. Both temperature and density terms are computed by comparison of a reference value with the actual one.

The constant terms and the coefficients for the logarithmic temperature correction are provided, with a calculation of the group cross-sections, by use of the Monte Carlo code for reactor analysis and burnup calculations Serpent-2 (http://montecarlo.vtt.fi/; Leppänen et al., 2015). Coefficients are obtained through logarithmic interpolation between the values corresponding to two different temperature levels, which are chosen as representative of the problem. (Cervi et al., 2019c)

2.7 Helium Bubbling System

Together with the implementation of the neutronic sub-solver, the previous works on the bubbleFoam solver introduced the modelling of the helium bubbling system, a feature proposed in order to remove gaseous fission products from the core, transporting them to the off-gas system for treatment.

The flow of helium in the core is simulated by making use of the "fvOptions" tool in OpenFOAM, which allows for run-time definition of source and sink terms in the main equations treated by the solver. In particular, it is employed on the continuity equation, adding a constant mass source term modelling the bubble injection and a proportional removal. These additional terms are not extended over the whole domain, rather they are restricted to specific zones. Figure 2.4 shows, as an example, the location of the helium inlet and the removal region for a simplified 2D geometry of the MSFR, which will be considered later on in this work. As it can be seen, bubbles are injected from the bottom of the core, and are removed from the upper region of the hot leg, above the heat exchanger and pump sections. Currently, no detailed design information is available on this system, but the flexibility of OpenFOAM will allow to modify the implementation in the suitable way when data will be provided.

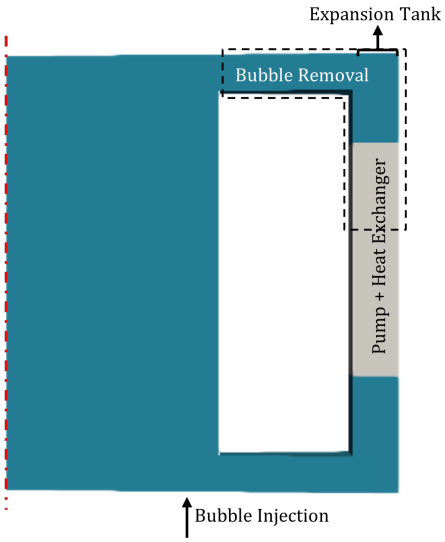

Figure 2.4. Example of implementation of bubbling system on 2D geometry

The modelling of the presence of the gaseous phase in the solver follows the equations already discussed. As stated previously, the correlations chosen in closure

models and relations for the thermal-hydraulics part of the problem are those depicted in (Cervi, 2020), where a sensitivity analysis to justify this particular choices was performed as well. The effect of the presence of bubbles on the neutronics part of the problem is considered through a suitable correction on the macroscopic cross sections, as aforementioned.

2.8 OpenFOAM Version 6

The bubbleFoam solver was developed employing OpenFOAM 4. A preliminary work for this thesis was to perform some technical changes to implement it in version 6 of the framework. A test was then performed on a simple case, in order to produce a first display of the capabilities of the solver. In Figure 2.5, an example of the profiles that can be obtained as results of the simulations is showcased. The geometry is a simplified 2D model of the MSFR system, which will be employed again in the following work, and the images show the single-phase steady-state distributions for some quantities of interest (i.e. temperature, velocity, pressure and neutron flux), obtained with the conditions of imposed power and fixed sources of momentum/energy. Additionally, the accordance of the results for the two different versions of OpenFOAM is shown, by a side-to-side comparison.

2.9 Conclusive Remarks

The development of the multiphysics OpenFOAM solver described in this chapter represented a significant step forward in the modelling and analysis of the MSFR system and of the molten salt reactors in general. The main components of focus are extensively described in the works of (Cervi et al., 2017; Cervi et al., 2019b; Cervi et al., 2019e), together with the display of various results obtained from the testing of the solver features. These studies constitute a solid basis for the implementation of new capabilities, with the aim of reaching a point where all the physical phenomenology of the MSFR can be correctly represented, both for nominal conditions and foreseeable potential accidental scenarios.

The framework of OpenFOAM grants the possibility of continuous improvement of the features already present, and its flexibility allows for the implementation of new and different models to tackle all the problems constituting the main task to be solved. Following this mindset, the work proposed in this thesis aims at the addition of the modelling of gaseous fission products in the MSFR system, for what concerns their production in the fuel, their interactions with the gaseous phase, introduced via the helium bubbling system, and their removal from the system. In the following chapters, thus, the new implemented features are presented and, subsequently, the model is tested, firstly with an analytical verification of the phenomena involved, and then with an application on the effective reactor setup.

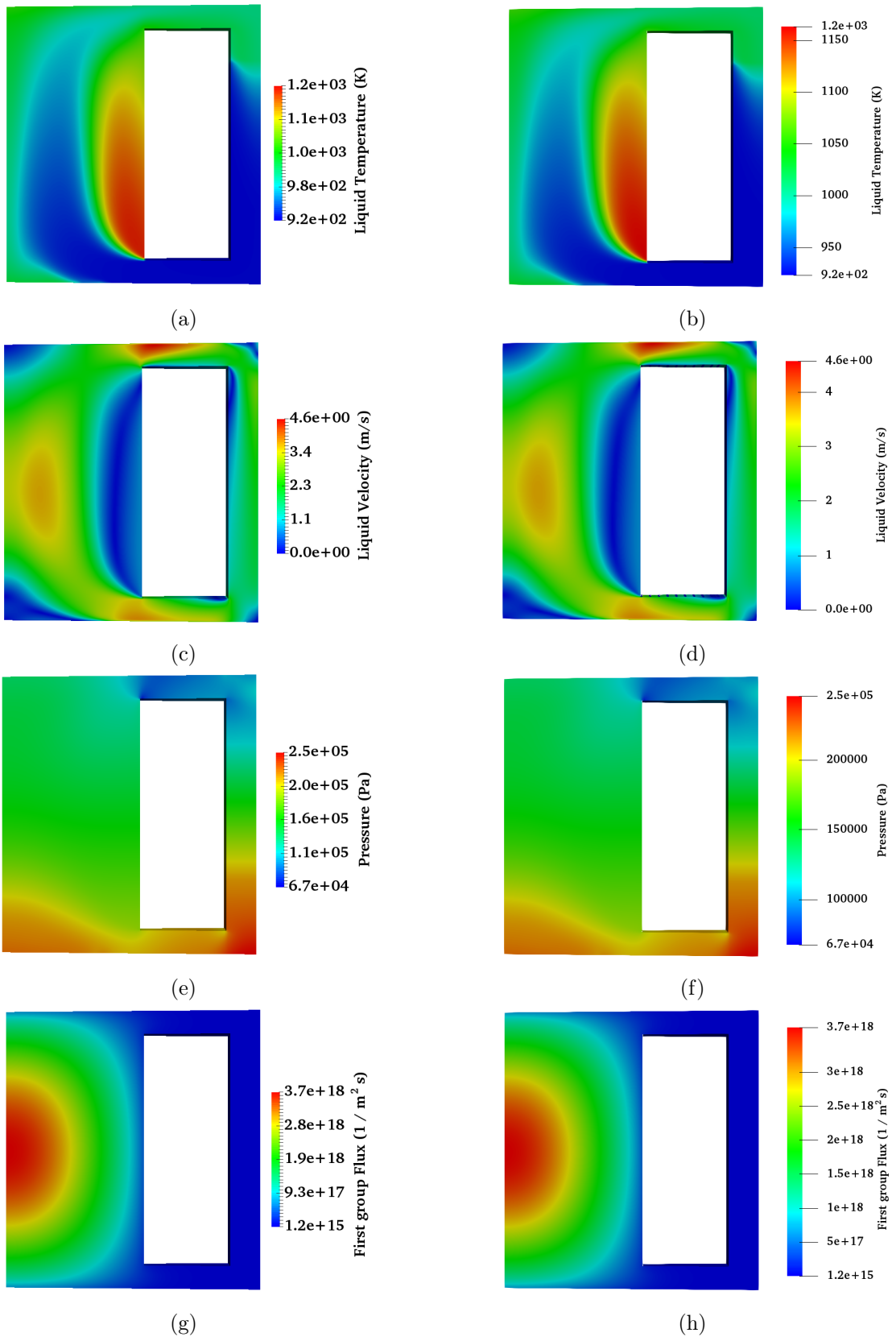

Figure 2.5. Color map plots for the comparison between OpenFOAM versions (left - OpenFOAM 4, right - OpenFOAM 6). (a)-(b) Temperature (c)-(d) Velocity (e)-(f) Pressure (g)-(h) First group Flux

Chapter 3

Xenon Modelling

For the removal of Gaseous Fission Products, the employment of a helium bubbling system, as explained above, has been proposed (Delpech et al., 2009). In previous works (Cervi et al., 2017; Cervi et al., 2019b), a model to account for the presence of this second phase in the environment of the MSFR has been developed. Nevertheless, the proposed simulation tool lacked the ability to reproduce the effects deriving from the presence of GFPs in the reactor and, most of all, their behavior in view of the transport to the off-gas system via the helium bubbles.

In this work, a closer look is taken on the problem of the GFPs, with a particular focus on the most influential one, which is Xenon. This element, or better, the single nuclide Xe-135, is taken as a reference example for the analysis of all those fission products that are generated as solute in the fuel and that can be extracted and carried to the off-gas system by the action of the helium bubbling system. In the remainder of this chapter, all the assumptions made in the development of this feature are presented and discussed, both from the physical and the coding points of view.

3.1 Modelling Approaches

In order to adapt the bubbleFoam solver to the presence of Xenon and other GFPs, three principal possibilities have been considered:

- Employment of a one-fluid formulation, as developed by (Haroun et al., 2010; Haroun et al., 2012), in order to treat Xenon concentration in the whole domain with a single equation to be implemented in the solver.
- Extension of the bubbleFoam framework to the presence of more than two phases, carrying the features already developed based on the reactingTwoPhaseEulerFoam to an equivalent formulation based on the reactingMultiphaseEulerFoam solver, and implementation of Xenon as a third phase.

- Implementation of the presence of multiple species for each phase (salt and Xenon in liquid, Xenon and helium in gaseous).

The first option is valid until the concentration of the solute is sufficiently small, so that its presence does not influence significantly the thermal-hydraulics of the carrier fluid. It represents a valid approach in order to easily obtain the profile of concentration of a specie in a system composed by two immiscible phases, considering also mass transfer at the interface and the related jump discontinuity in the profile. The method has been tested and validated by various authors (as an example, refer to (Nieves-Remacha et al., 2015; Thummala et al., 2020)), but its use has been limited to situations where the two phases are spatially separated, with a net interface dividing them (e.g. cases of laminar films or flat plates). The use of this modelling option for the study of the MSFR, where the bubbles are dispersed inside the salt, poses many challenges. In addition, while the restriction of the usage of the model to the case where the concentration of solute is small is fine considering the Xenon diluted inside the molten salt, this is not true for what concerns the gaseous phase, where Xenon could have a greater effect in modifying the thermal-hydraulics aspects of the helium flow.

The implementation of Xenon as a third separate phase is not a suitable choice for this specific work because it neglects some physical phenomena that are fundamental in the understanding of the problem. In fact, the purpose of the study is to represent and understand the effect of the helium bubbling system, extracting Xenon and other GFPs from the salt, and carrying them to the off-gas unit to be treated. Considering Xenon as a third separate phase prevents the modelling of its production inside the salt, together with the phenomenon of solubility. Moreover, from a physical point of view, once Xenon and helium are both in gaseous state, they should behave as a single phase, another aspect that would not be correctly depicted employing this kind of framework.

The definition of multiple species for each phase is the ideal solution for the task at hand. All the physics of the problem can be represented by this model: Xenon production can be placed directly in the salt, the migration to the gas bubbles can be considered with appropriate mass transfer models, and the behavior of the two gases would be the right one from the point of view of blending and other interactions. Moreover, in the framework of OpenFOAM, tools are already present in order to correctly manage some of these aspects.

3.2 Oak Ridge National Laboratory Reports

As it was cited previously, studies in the field of the Molten Salt Reactors were performed firstly starting from the Fifties, mainly at Oak Ridge National Laboratory, with some extension also in the experimental field, up to the realization of the Molten Salt Reactor Experiment and the design of the Molten Salt Breeder Reactor. The analyses performed at the time referred to the concept of a moderated reactor, a system

where the effect of Xenon as poison is of extreme relevance. It is perfectly reasonable, then, that the literature retrievable from the ORNL archives covers the argument of modelling Xenon behavior in a liquid-fueled reactor to some extent. Moreover, in the absence as of today of a real experimental case for the MSFR, numerical data from the technical reports of the MSRE and for the project of the MSBR can be employed for preliminary estimations, as the one that's object of this work. Among the various documents, in particular, only a few were selected as reference, containing the data and information necessary to the analysis of Xenon behavior. They are listed, in chronological order, in Table 3.1.

Table 3.1. Oak Ridge National Laboratory Reports Analyzed

Reference Number	Author(s)	Date	Full Title
ORNL-4069	R.J. Kedl A. Houtzeel	June 1967	Development of a Model for Computing 135-Xe Migration in the MSRE
ORNL-TM-1810	R.J. Kedl	July 1967	A Model for Computing the Migration of Very Short-Lived Noble Gases into MSRE Graphite
ORNL-TM-2245	F.N. Peebles	July 1968	Removal of Xenon-135 from Circulating Fuel Salt of the MSBR by Mass Transfer to Helium Bubbles
ORNL-TM-3464	J.R. Engel R.C. Steffy	October 1971	Xenon Behavior in the Molten Salt Reactor Experiment

In ORNL-4069 (R. Kedl et al., 1967), a first model for computing the migration of Xe-135 in the MSRE is developed. In order to obtain rate constants and other information necessary to compute the correct values, an experiment is conducted beforehand, employing Kr-85 and monitoring its behavior in the system.
The report is particularly useful to get an idea of the various terms to be considered in the modelling, especially the sources and sinks involved in the treatment. Moreover, the document reports reference values for the parameters relevant to the study, that can be taken as guidelines. In particular, a range for the value of diffusivity of Xe in the salt and the value of Henry's law constant for Xe can be found, both referred to a temperature of 1200°F (922 K).

In ORNL-TM-1810 (R. J. Kedl, 1967), the focus is put mostly on the migration of the species dissolved in the salt into the graphite surrounding the core of the MSRE. In particular, it refers to very short-lived noble gases. Hence, this report is less useful for the work of this thesis from the point of view of data gathering. Nonetheless, it presents a good example of analytical derivation of a simple case of study, an instrument which can help in preliminary modelling and testing of the simulation capabilities, just as it is done later in this work.

In ORNL-TM-2245 (Peebles, 1968), Peebles presents an extensive review of the mass transfer models that were present in literature at the time, proposing an analysis with the focus on the rate of mass transfer. The report contains correlations deriving from theoretical considerations as well as experimental results, for the main opposite cases of single bubbles rising in stationary liquids and bubbles carried along by turbulent liquid in a pipe. Particular focus is put on the distinction of two extreme cases of modelling, the ones of rigid bubble interface and perfectly mobile bubble interface.
The report helps in the understanding of the various correlations exploitable, and in the search of the more suitable ones. Even if it may appear somewhat outdated, it is still a valid review and, since it supports the theoretical analysis with experimental data, it can be still taken as reference for the works in this field. Additionally, it presents the proposal of a simple experimental setup to study the problem of mass transfer rates and the influence of hydrodynamics parameters. The setup was initially thought for replicating the MSBR environment but, with appropriate changes, it should be easily adaptable for any other kind of Molten Salt Reactor.

In ORNL-TM-3464 (Engel et al., 1971), the authors treat the comparison of the predicting models and the experimental results for what concerns the behavior of Xenon in the MSRE system, from the point of view of void fraction and Xenon poisoning (mainly in terms of deficit of reactivity during operation). This analysis aimed at defining the influence of a number of system parameters on the calculations, in order to see if the behavior observed during reactor operation could be predicted. The results were good for the steady-state conditions, but the transient changes could not be reproduced with enough accuracy.
The presented formulation considers many mechanisms influencing the behavior of Xenon, something which lie outside the aim of this thesis, but which will be recommended once a proper experimental setup is available for testing and comparison. This document is however already useful in order to confirm, through experimental validation, the suitability of the parameters cited in previous documents, which were taken as basis for the analytical derivation.

3.3 OpenFOAM Modelling

The works from Oak Ridge National Laboratory on the MSRE and the MSBR systems provide overall a good starting point for the analysis of the Molten Salt Reactor concept, and they prove themselves useful also in the studies conducted today for the MSFR. The main difference with the approach used at the time is the absence, currently, of an experimental facility to test and validate the results of the theoretical models, or from which the extrapolation of empirical models would be possible. For this reason, in order to demonstrate the capabilities of the proposed reactor design, appropriate simulation tools need to be developed and exploited. The choice of the OpenFOAM framework has been already discussed and motivated in previous chapters. In the following, the modelling approach for the treatment of Xenon as a component of the system is described in detail.

3.3.1 Multi-Component and Mass Transfer Treatment

In order to model the presence of multiple species in each phase, new equations need to be solved, to describe the concentration of the components in terms of production, transport and consumption. A general formulation for species i in phase k is

$$\frac{\partial \alpha_k C_{i,k}}{\partial t} + \nabla \cdot (\alpha_k \mathbf{u}_k C_{i,k}) - \nabla \cdot (\alpha_k D_{i,k} \nabla (C_{i,k})) = \frac{dm_{i,k}}{dt} \tag{3.1}$$

where C is the concentration expressed in kg/m^3, D represents the mass diffusion in the phase, and $\frac{dm_i}{dt}$ denotes the mass transfer of the species to or from the phase. The diffusivity coefficient of each phase, $\mathrm{D}_{i,k}$, can be calculated from the dimensionless Schmidt number, Sc, as

$$D_{i,k} = \frac{\mu_k}{\rho_k \mathrm{Sc}_k} \tag{3.2}$$

The rate of mass transfer of species i in phase k can be computed through a suitable coefficient, $K_{i,k}$:

$$\frac{dm_{i,k}}{dt} = K_{i,k} a_i (C^*_{i,k} - C_{i,k}) \tag{3.3}$$

where C^* denotes the saturation concentration at the interface, and a represents the interfacial area of exchange per unit volume (of system geometry) which is dependent on the pair of phases where the component is present. In our particular case, for a liquid-gas system, this term is computed from the bubble diameter (d_b) as

$$a_{l/g} = \frac{6 \cdot \alpha_g}{d_b} \tag{3.4}$$

At this point, in order to solve the species transport equations, there is the need to obtain the mass transfer coefficient and the saturation concentration of Eq. (3.3) for each component in each phase. This can be done exploiting, respectively, a mass transfer model and an interface composition one.

For what concerns the interface composition model, following the studies conducted by Oak Ridge National Laboratory concerning the MSRE and the MSBR, it can be seen that the most common way to tackle the problem of mass transfer is to employ a Henry-like behavior (R. Kedl et al., 1967; Peebles, 1968). The reports also propose a value of the Henry coefficient for Xenon, which can be taken as reference until more experiments are conducted. The interface composition for one phase is thus computed

from the concentration of the specie on the the other side as

$$C^*_{i,k} = H \cdot C_{i,j} \tag{3.5}$$

where H is the dimensionless Henry coefficient.

The range of validity of this modelling, which assumes an ideal dilute solution of xenon in the salt, has been questioned, and some limits have been determined (Grimes et al., 1958; Blander et al., 1959; Watson et al., 1962) but, again, in the absence of an effective experimental case to study, the approximation can be considered acceptable. Moreover, this work aims at putting a first basis for a model able to represent the behavior of GFPs in the MSFR. Once more accurate sets of data and models are available, the framework can be easily upgraded in order to give better estimations of the results.

The mass transfer model aims at computing the term K in Eq. (3.3). Since the diffusivity in each phase is already part of the solutions, this is generally done exploiting the definition of a dimensionless group, the Sherwood number, representing the ratio between convective and diffusive mass transfer

$$K_{i,k} = \frac{\mathrm{Sh} \cdot D_{i,k}}{d_b} \tag{3.6}$$

The Sherwood number is generally computed through empirical correlations, depending on the particular conditions of the flow in the case of interest. These models can be derived from both analytical and experimental studies and, for the case of gaseous bubbles in liquid flows, they generally result in an analogy with the heat transfer correlations (Dittus-Boelter-like laws, where Nu and Pr are replaced respectively by Sh and Sc):

$$\mathrm{Sh} = A \cdot \mathrm{Re}^B \mathrm{Sc}^C \tag{3.7}$$

It is worth noting that the Reynolds number employed in these formulation is the one referring to a single bubble transported by the liquid. In this formulation, the characteristic length is the diameter of the bubble (calculated, in this work, as a function of pressure), and the velocity is the difference between that of the bubble and the one of the liquid some distance away (so that the value is not influenced by the presence of the bubble itself) (Rhodes, 2008):

$$\mathrm{Re}_b = \frac{(u_g - u_l) d_b}{\nu_l} \tag{3.8}$$

Taking again the work of Oak Ridge National Laboratory as a reference, an adequate Sherwood correlation can be searched, particularly referring to the previously

cited ONRL-TM-2245 (Peebles, 1968), which contained a review of the methods available in literature. Among the various correlations examined, the one proposed by Higbie (Higbie, 1935) could be exploited for the MSFR system:

$$\mathrm{Sh} = 1.13 \cdot \mathrm{Re}^{1/2}\mathrm{Sc}^{1/2} \tag{3.9}$$

This particular formulation has been developed for the case of free-rise of bubbles in a liquid stream, which is a condition somewhat similar to the MSFR environment. The main limitation is that this approach refers to a laminar stream, while the regime of flow for the MSFR is expected to be turbulent. Being still in the absence of experimental data regarding this matter, however, the approximation can be considered acceptable.

3.3.2 Code Implementation

The treatment of multiple species in one phase in OpenFOAM is already possible in the reactingTwoPhaseEulerFoam framework, on which the bubbleFoam solver is based. The solver allows the user to choose a type of multiphase system appropriate to consider momentum, heat and mass transfer between the phases, with the aid of some standard models. A choice can be also made on the modelling of the single phases, whether they should be treated as pure, or as mixtures of multiple species.

When the phases are not declared as pure, the algorithm calls for the solution of species transport equations, based on Eq. (3.1). Since the solver is developed for the treatment of compressible flow, however, a concentration depending on the volume is not suitable. The problem is avoided in OpenFOAM by making use of a different expression, employing a species concentration dependent only on mass (with units of kg/kg),

$$Y_{i,k} = \frac{C_{i,k}}{\rho_k} \tag{3.10}$$

The formulation of the species transport equation treated by the solver is thus

$$\frac{\partial \alpha_k \rho_k Y_{i,k}}{\partial t} + \nabla \cdot (\alpha_k \rho_k \mathbf{u}_k Y_{i,k}) - \nabla \cdot \left(\frac{\alpha_k \mu_k}{\mathrm{Sc}_k} \nabla (Y_{i,k}) \right) = \frac{dm_{i,k}}{dt} \tag{3.11}$$

The algorithm builds an equation like this one for each component in each phase. In order to properly simulate the behavior of Xenon in the system, some more terms need to be supplied to reproduce the production and the transmutation of the fission products.

In this work, only the isotope 135 of Xenon is considered, since it is generally the most

as a direct fission product (with a certain yield), and as result of the decay of other fission products, I-135 and Te-135, which are precursors in its decay chain. A complete formulation of the problem would require the solution of a balance equation for each one of these nuclides but, as a first approximation, it is possible to consider only the presence of Xe, as if it was produced all by fission, with an equivalent cumulative yield. A source term is thus inserted in the transport equation, in a form of direct proportionality with the fission rate of the system

$$S_{Xe} = \sum_n (\Sigma_{f,n}\varphi_n) \cdot y_{Xe} \cdot (m_{mol}/N_{Av}) \tag{3.12}$$

where m_{mol} is the molar mass of Xe-135 and N_{Av} is the Avogadro number.

The source is implemented only in the equation relative to the liquid phase, since it is assumed that Xe is produced inside the salt, and then extracted to the gaseous phase through mass transfer.

Together with the source term, some sink terms need to be introduced in the equations as well. The ways in which Xenon leaves the system, apart from manual removal of the gaseous phase, are through neutron capture and decay. Again, for the sake of simplicity, only Xe-135 is considered and not the entire decay chain. Thus, the component is modelled as if it disappeares in both cases of capture and decay, without taking into account the products of these phenomena. Both sink terms are dependent from the quantity of Xe present in the system and need to be treated implicitly by the solver. The capture term is computed by multiplication of the flux by suitable values of a cross section (with a sum over the neutron flux groups), and the decay term is expressed by the appropriate constant, calculated from the half-life of the nuclide.

The term of neutron capture is considered only in the liquid phase, while the decay influences the concentration in the gaseous form as well.

$$\text{sinks} = -\alpha_k \rho_k \left(\lambda + \sum_n (\sigma_{c,n}\varphi_n) \right) Y_{Xe,k} \tag{3.13}$$

The capture cross sections are evaluated by means of the Monte Carlo code Serpent-2 (Leppänen et al., 2015). More details about these terms are given in Appendix C.

The final forms of the Xenon balance equations as implemented in OpenFOAM are, for liquid and gas phase respectively,

$$\begin{aligned} \frac{\partial \alpha_l \rho_l Y_{Xe,l}}{\partial t} + \nabla \cdot (\alpha_l \rho_l \mathbf{u}_l Y_{Xe,l}) - \nabla \cdot \left(\frac{\alpha_l \mu_l}{\mathrm{Sc}_l} \nabla (Y_{Xe,l}) \right) = \\ = S_{Xe} - \alpha_l \rho_l \left(\lambda + \sum_n (\sigma_{c,n}\varphi_n) \right) Y_{Xe,l} + \frac{dm_{Xe,l}}{dt} \end{aligned} \tag{3.14}$$

$$\frac{\partial \alpha_g \rho_g Y_{Xe,g}}{\partial t} + \nabla \cdot (\alpha_g \rho_g \mathbf{u}_g Y_{Xe,g}) - \nabla \cdot \left(\frac{\alpha_g \mu_g}{\mathrm{Sc}_g} \nabla (Y_{Xe,g}) \right) = -\alpha_g \rho_g \lambda Y_{Xe,g} + \frac{dm_{Xe,g}}{dt} \quad (3.15)$$

Where the mass transfer terms are implemented as previously described (taking into account the different formulation for the dimensionless concentrations), with the implementation of Henry's law to calculate the saturation concentration of Xenon at the interface, and of the Higbie correlation to compute the Sherwood number and the mass transfer coefficient.

3.4 Conclusive Remarks

The impact that gaseous fission products, and Xenon in particular, have in the framework of a liquid-fuelled nuclear reactor is not to be underestimated. In order to simulate correctly both the nominal conditions and the accidental scenarios of the lifetime of a system of this kind, it is important to know the changes that occur in the fuel mixture, and the impact that the new species produced have on their surroundings. Multiple approaches are available for choice in a CFD environment, in order to model the formation and consumption of new components in a fluid, and various have already been implemented in the OpenFOAM framework for the solution of multiple problems.

Taking into account the characteristic features of the MSFR, a way to model the presence of the gaseous fission products in the core is implemented in the previously developed multiphysics solver bubbleFoam, on the example of the reference nuclide Xe-135. A multi-component approach is chosen, rather than a one-fluid formulation or the definition of additional separate phases, in order to be able to reproduce the correct behavior of multiple gaseous species interacting in the same environment. Gathering information from the past works of the Oak Ridge national Laboratory on the MSRE and MSBR, Henry's law is employed for the calculations relative to the saturation concentration at the interface and, among the various proposed mass transfer correlations, the one proposed by Higbie is chosen to compute the dimensionless Sherwood number. As of today, the technical reports mentioned in the text constitute the main source of experimental data on the subject of molten salt reactors, and their potential contribution in modern studies should not be neglected.

In the remainder of this thesis, firstly the new features are tested against an analytical model for the mass transfer on a simple case. Subsequently, the capabilities of the solver are demonstrated on a computational case which reproduces the MSFR environment.

Chapter 4

Analytical Verification

The implementation to the bubbleFoam solver for modelling Xenon behavior proposed in this work relies on the ability of OpenFOAM to reproduce, by numerical simulation, the complex system which is the MSFR. Since an effective experimental validation of the results is not obtainable at the present, a first step in testing the capabilities of the model can be done by comparison with analytical calculations. To this aim, a simple benchmark case is defined, and the OpenFOAM results are tested against the exact analytical solution.

4.1 Geometry

The geometry chosen for the benchmark case is a two-dimensional rectangular domain, simulating a pipe section of height H and length L (Figure 4.1). The salt flow is directed towards the positive direction of the x axis, so that the left vertical segment represents the inlet and the right one the outlet, while the horizontal segments are the pipe walls.

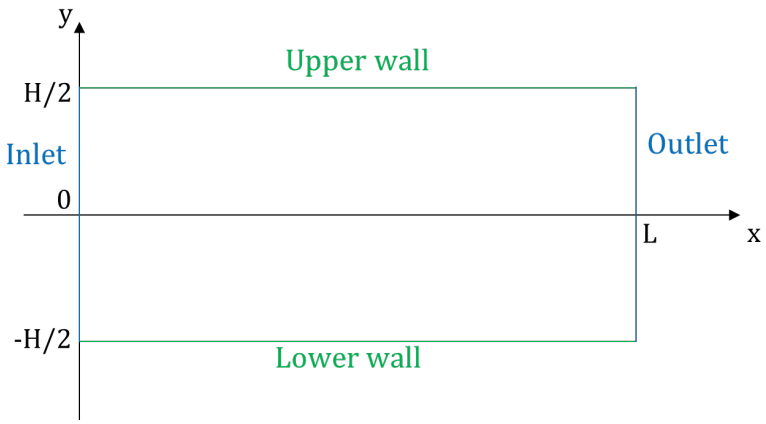

Figure 4.1. Geometry for analytical benchmark

The pipe is directed horizontally to be able to neglect the effect of gravity, simplifying the calculations. The intersection of the axes is positioned at half height of the pipe, in order to exploit the symmetry later on. The length L is significantly larger than the height H, so that inlet/outlet effects can be ignored by considering the central transverse sections.

4.2 Analytical Treatment

4.2.1 Single-Phase Case

The general formulation of the problem refers to the advection-dispersion equation with the addition of a source and a decay term (neutron capture, mentioned above, was not considered in this instance):

$$\frac{\partial C}{\partial t} + \nabla \cdot (\mathbf{u}C) - \nabla \cdot (D\nabla C) = S - \lambda C \tag{4.1}$$

which, considering a two-dimensional case at steady state, can be rewritten as:

$$\frac{\partial}{\partial x}\left(D\frac{\partial C}{\partial x}\right) + \frac{\partial}{\partial y}\left(D\frac{\partial C}{\partial y}\right) - \frac{\partial}{\partial x}\left(u_x\frac{\partial C}{\partial x}\right) - \frac{\partial}{\partial y}\left(u_y\frac{\partial C}{\partial y}\right) - \lambda C + S = 0 \tag{4.2}$$

The flow is developed from an imposed fixed pressure gradient along the longitudinal axis of the geometry, x. In order to simplify the problem, since the solver treats for compressible fluids, the pressure gradient is chosen to be low enough that pressure can be approximated as uniform throughout the domain. Additionally, no energy sources or sinks are defined, so that the temperature along the tube is uniform as well. The previous conditions grant that the thermophysical properties of the species involved remain constant for the simulation.

The flow, directed along the positive x axis, is considered to be fully developed, so that the velocity field depends only on the y coordinate. For the sake of simplicity, we consider a laminar situation, which leads to the common parabolic profile:

$$\begin{cases} u_x(x) = 0 \\ u_x(y) = \frac{3}{2}\bar{u}\left(1 - \left(\frac{y}{H/2}\right)^2\right) \end{cases} \tag{4.3}$$

In particular, the flow can be considered laminar referring both to the Reynolds number of the single bubble transported by the liquid (microscopic, useful for mass

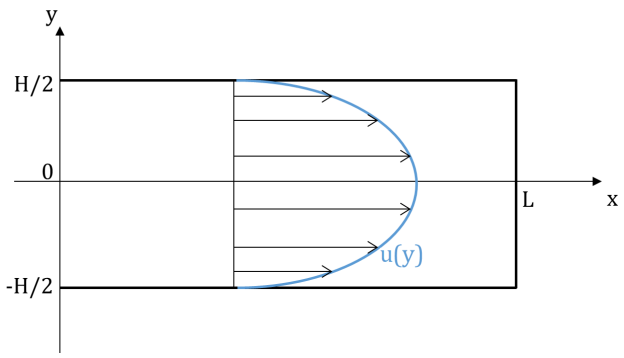

Figure 4.2. Assumed Parabolic Profile of Velocity

exchange models), defined in Eq. (3.8) and to the more commonly known tube Reynolds number (macroscopic, to examine the liquid motion):

$$\mathrm{Re}_t = \frac{\bar{u}_l D_H}{\nu} \tag{4.4}$$

where D_H is the hydraulic diameter of the tube. The hypothesis of laminar flow helps also in setting the value of the diffusivity coefficient as constant, further simplifying the resolution of the problem. Additionally, in consideration of steady state conditions, the phenomenon of transport is taken as fully developed, so that there is no variation of concentration of the specie along the longitudinal direction of the tube. This latter hypothesis removes all the remaining dependencies on the x axis in the equation, making the problem formulation effectively one-dimensional.

Considering all the assumptions above, the original equation (Eq. (4.2)) can be rewritten, in explicit Cartesian coordinates, as:

$$D\frac{\partial^2 C}{\partial y^2} - \lambda C + S = 0 \tag{4.5}$$

The problem can also be formulated more conveniently upon the definition of appropriate dimensionless quantities:

$$\tilde{y} = \frac{y}{h} \tag{4.6}$$

$$\Lambda = \frac{\lambda h^2}{D} \tag{4.7}$$

$$\tilde{S} = \frac{S h^2}{D} \tag{4.8}$$

where h corresponds to the half-height of the domain ($h = H/2$). The final

equation to be solved is thus:

$$\frac{\partial^2 C}{\partial \tilde{y}^2} - \Lambda C + \tilde{S} = 0 \tag{4.9}$$

which can be recognized as an inhomogeneous second-order Ordinary Differential Equation (ODE) problem in the form:

$$u''(t) + p(t)u'(t) + q(t)u(t) = f(t) \tag{4.10}$$

where

$$p(t) = 0 \tag{4.11}$$

$$q(t) = -\Lambda \tag{4.12}$$

$$f(t) = -\tilde{S} \tag{4.13}$$

In order to solve the problem, suitable boundary conditions need to be defined. Being the problem dependent only on the dimensionless coordinate $\tilde{y}$, conditions are just required for the upper and lower walls of the domain. The analysis is performed for both the common forms of Neumann and Dirichlet conditions:

$$Neumann \;\; C(\tilde{y}) = 0 \; ; \; \tilde{y} = \pm 1 \tag{4.14}$$

$$Dirichlet \;\; \frac{\partial C}{\partial \tilde{y}} = 0 \; ; \; \tilde{y} = \pm 1 \tag{4.15}$$

Considering the Neumann boundary conditions, the solution is readily obtainable and corresponds to a flat profile (constant value), in the form of:

$$C(\tilde{y}) = \frac{\tilde{S}}{\Lambda} \tag{4.16}$$

For what concerns the case of Dirichlet conditions, instead, the solution must be sought in the form

$$u(t) = A_1 u_1(t) + A_2 u_2(t) + u_p(t) \tag{4.17}$$

where u_1 and u_2 are the solutions of the associated homogeneous equation

$$u''(t) + p(t)u'(t) + q(t)u(t) = 0 \tag{4.18}$$

u_p is a particular solution dependent on the source term, and A_1 and A_2 are constants imposed by the boundary conditions.

The complete solution for our case, therefore, is

$$C(\tilde{y}) = \frac{\tilde{S}}{\Lambda}\left[1 - \frac{e^{\sqrt{\Lambda}\tilde{y}} + e^{-\sqrt{\Lambda}\tilde{y}}}{e^{\sqrt{\Lambda}} + e^{-\sqrt{\Lambda}}}\right] \tag{4.19}$$

It is worth noticing that, as mentioned before, in order to account for the compressibility of the liquid OpenFOAM makes use of a dimensionless concentration Y, defined as the mass of solute per unit mass of solvent (or, in other terminology, mass of component per unit mass of phase). In this analytical treatment, instead, the more common form of concentration per unit volume, C, has been used. However, the conversion between one quantity and the other is simply done through multiplication or division for the density of the liquid, which, based on the initial hypotheses of uniform temperature and pressure in the system, is a constant value.

4.2.2 Two-Phase Case

Considering the presence of the gaseous phase as well, the formulation of the problem requires an additional equation, coupled with the first one by means of a mass exchange term, which is opposite and equal for the two phases, and takes the form of a Henry-like model. Additionally, the phase fractions have to be introduced as well, which are taken as uniform and constant for this problem. The complete system then reads as:

$$\begin{cases} \frac{\partial \alpha_l C}{\partial t} + \nabla \cdot (\alpha_l \mathbf{u} C) - \nabla \cdot (D \nabla \alpha_l C) = S - \lambda \alpha_l C + KA(HC_g - C) \\ \frac{\partial \alpha_g C_g}{\partial t} + \nabla \cdot (\alpha_g \mathbf{u}_g C_g) - \nabla \cdot (D_g \nabla \alpha_g C_g) = -\lambda \alpha_g C_g - KA(HC_g - C) \end{cases} \tag{4.20}$$

where the source is defined only in the liquid phase, while the decay term is present in both equations, as it was explained in the previous Chapter.

For the sake of simplicity, an additional hypothesis is made with respect to the ones mentioned for the single-phase case: the phenomenon of transport is neglected in the gaseous phase, removing the terms of the second equation which would remain after the steady-state assumption. This allows for a simple resolution of the gas

equation, giving a direct relationship between the concentrations in the two phases:

$$C_g = \frac{KA}{\alpha_g \lambda + KAH} C \tag{4.21}$$

Upon substitution of this expression, the problem simplifies to a single equation for the liquid phase, in the form:

$$D\frac{\partial^2 C}{\partial y^2} - (\lambda + \beta)C + \frac{S}{\alpha_l} = 0 \tag{4.22}$$

where

$$\beta = -\frac{KA}{\alpha_l}\left(\frac{KAH}{\alpha_g \lambda + KAH} - 1\right) \tag{4.23}$$

From this point on, the steps for the manipulation of the equation are analogous to the ones made for the case of single phase, with the presence of the additional term deriving from mass transfer with the gas. The final form of the equation, with the appropriate dimensionless quantities reads as:

$$\frac{\partial^2 C}{\partial \tilde{y}^2} - (\Lambda + B)C + \tilde{S} = 0 \tag{4.24}$$

Where $\tilde{S}$ this time incorporates also the phase fraction, and the last dimensionless quantity, B, is defined as:

$$B = \frac{\beta h^2}{D} \tag{4.25}$$

As in the previous case, the solution is calculated for both the Neumann and the Dirichlet boundary conditions. For the former, a constant profile is obtained again, in the form of:

$$C(\tilde{y}) = \frac{\tilde{S}}{\Lambda + B} \tag{4.26}$$

For the case of Dirichlet, the solution steps are analogous to the single-phase treatment, with the added term already mentioned. The final solution is written as:

$$C(\tilde{y}) = \frac{\tilde{S}}{\Lambda + B}\left[1 - \frac{e^{\sqrt{\Lambda+B}\tilde{y}} + e^{-\sqrt{\Lambda+B}\tilde{y}}}{e^{\sqrt{\Lambda+B}} + e^{-\sqrt{\Lambda+B}}}\right] \tag{4.27}$$

4.2.3 OpenFOAM Setup

The geometry described above is easily reproducible in OpenFOAM, as a single solid element. The values of the parameters employed in the definition of the mesh are reported in Table 4.1, and the corresponding output can be seen in Figure 4.3.

Table 4.1. Mesh Parameters

Parameter	Symbol	Value	Units
Height of channel	H	0.1	m
Length of channel	L	1.0	m
Depth of channel	dz	0.01	m
Mesh elements in direction x		50	
Mesh elements in direction y		50	
Mesh elements in direction z		1	

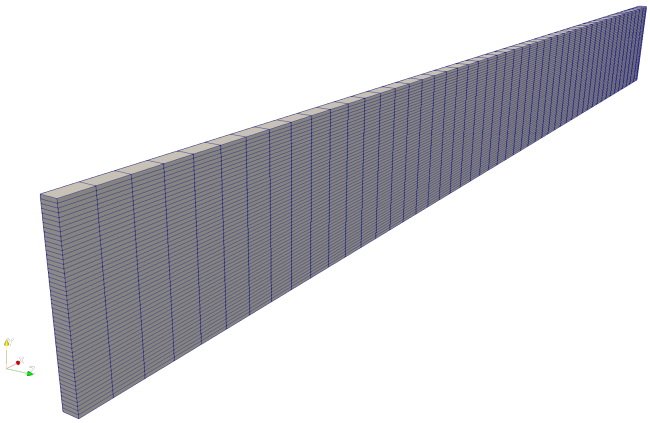

Figure 4.3. Mesh for Analytical Model

As mentioned previously, initial conditions for the system are those of uniform temperature over the whole domain and fixed pressure gradient along the x direction. Velocity is initialized with a uniform value equal to the expected average value assumed in the parabolic profile. For the single-phase simulations, the phase fraction of the salt is initialized to unity, and the one of the gas is null. Finally, the concentration of Xenon in the system is starting from zero.

The two-phase simulations are performed starting from the profiles obtained from the corresponding single-phase ones. This choice is made for a technical reason: while OpenFOAM generally allows for the use of a "steady-state" option, which puts all time derivatives in governing equations equal to zero, the treatment of two-phase flow is not compatible with this kind of simulation. The "steady-state" option is thus chosen for the single-phase case, in order to bring the solution to convergence in reasonable computational time (especially for what concerns the velocity profile), while for the two-phase case time is treated as default, starting already from a stationary situation. The only change made for correction in the initialization, thus, is to set a uniform

non-null value of gaseous fraction inside the domain. Boundary conditions for the various fields are kept as they are by default in similar OpenFOAM tutorial cases, with no-slip conditions for velocity at the walls. A closer observation is reserved for the fields of interest, which are the concentrations of Xenon in liquid and gaseous phases. For what concerns the inlet and outlet boundaries, Dirichlet conditions are applied in all cases. For the upper and the lower walls, instead, Dirichlet or Neumann conditions are imposed, depending on the actual simulation performed.

The values of the relevant thermophysical properties of the system are chosen in order to be able to satisfy different constraints of the formulation. The values of diffusivity of Xe in the salt and of the Henry coefficient are taken from the ORNL reports, as previously mentioned. A small value of viscosity is chosen for the gaseous phase, so that the diffusion terms can be neglected in the relative equation. Other useful terms are selected to obtain a significantly high amount of mass transfer, with the aim of speeding up the process. The main parameters are reported in Table 4.2.

Table 4.2. Main Parameters for the Analytical Model

Parameter	Symbol	Value	Units
Xe diffusivity in salt	D	$1.29 \cdot 10^{-9}$	m^2/s
Henry's law coefficient	H	$2.08 \cdot 10^{-4}$	-
Xe decay constant	λ	$2.1066 \cdot 10^{-5}$	$1/\mathrm{s}$
Fission rate	fR	$1 \cdot 10^{15}$	$1/\mathrm{m}^3$ s
Xe cumulative yield	y_{Xe}	0.05875	-
Xe molar mass	m_{mol}	0.135	kg/mol

The diameter of the bubbles is estimated by use of an isothermal power law, dependent on pressure:

$$d_b = d_0 \left(\frac{p_0}{p} \right)^{1/3} \tag{4.28}$$

where the reference diameter and pressure are assumed to be, respectively, $d_0 = 3\ mm$, $p_0 = 1\ atm$, in line with the later assumptions made on the reactor.

The explicit terms in the momentum balance equation, mentioned in Section 2.4.1 are treated with the following correlations (Cervi, 2020):

- For virtual mass forces, a constant coefficient correlation is chosen, with $C_{VM} = 0.5$ (Rusche, 2002)
- Lift is not considered, neither here nor in the rest of this work, following the assumption that the bubbles are sufficiently small in size to neglect the effect of vorticity on the momentum transfer between the two phases

- Turbulent dispersion is neglected as well, an easy assumption to make in this laminar case, but which will be adopted again in the reactor simulations in the following
- The drag coefficient is evaluated by use of the Schiller-Naumann correlation (Schiller et al., 1933), which depends on the bubble Reynolds number defined in Eq. (3.8):

$$C_D = \begin{cases} \frac{24(1+0.15\mathrm{Re}_b^{0.687})}{\mathrm{Re}_b} & for\ \mathrm{Re}_b < 1000 \\ 44 & for\ \mathrm{Re}_b \geq 1000 \end{cases} \tag{4.29}$$

The heat transfer between the phases is modelled following the Ranz-Marshall correlation (Ranz et al., 1952):

$$\mathrm{Nu} = 2 + 0.6\ \mathrm{Re}_b^{1/2}\mathrm{Pr}^{1/3} \tag{4.30}$$

4.2.4 Results

Results gathered from the simulations of the single-phase cases of Dirichlet and Neumann boundary conditions are reported, respectively, in Figure 4.4a and Figure 4.4b, where a color map is employed in order to display data for the whole geometry.

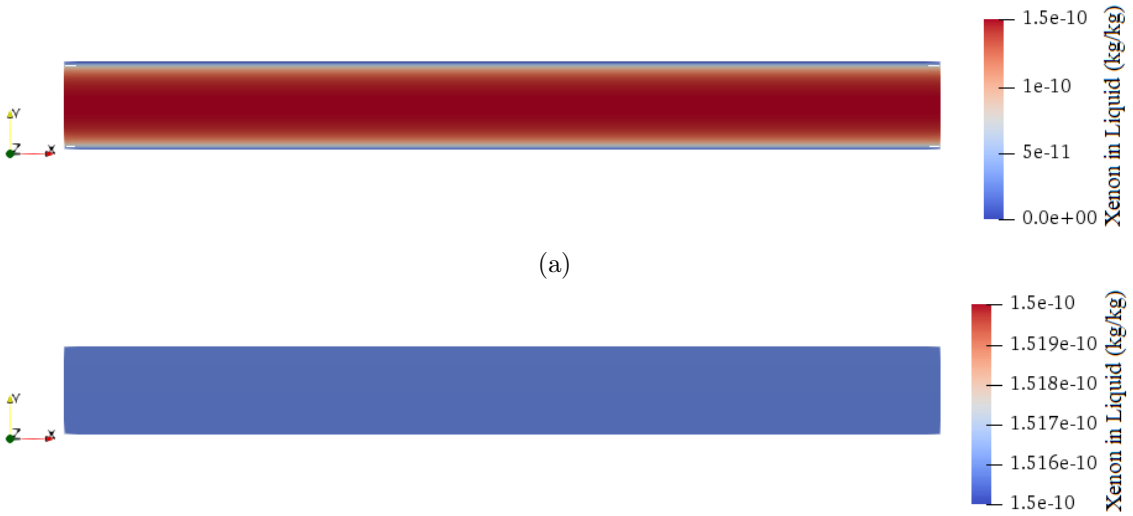

Figure 4.4. Xe concentration for single-phase simulations. (a) Dirichlet boundary conditions (b) Neumann boundary conditions

The graphs in Figure 4.5a and Figure 4.5b display the profile of Xenon concentration in the salt, for a transverse section of the geometry placed at half-length of the longitudinal axis. A comparison between values predicted from the analytical derivation and the results from the simulation is visible as well. The data presented

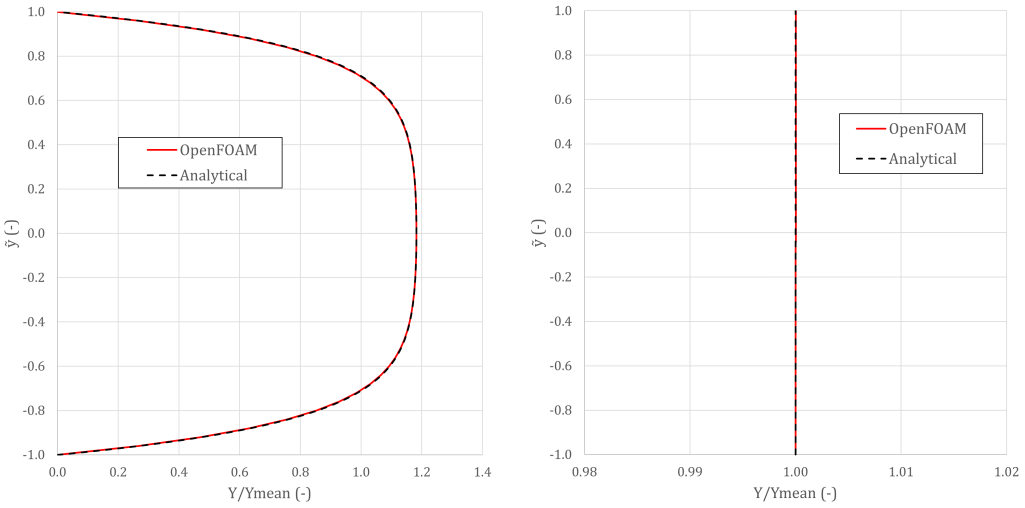

(a) (b)

Figure 4.5. Xe single-phase concentration profiles for transverse section at $x = L/2$, comparison between analytical results and OpenFOAM simulations. (a) Dirichlet boundary conditions (b) Neumann boundary conditions

show very good agreement with the predicted values obtained from the calculations. The mean relative error for the values considered is of 0.53 % with Dirichlet conditions and of 0.002 % with Neumann conditions.

For what concerns the two-phase formulation, results from preliminary simulations showed disagreement for the profiles in case of Dirichlet boundary conditions, as it can be seen from the graph in Figure 4.6a. While the value of concentration at the centerline of the domain is similar, the regions closer to the upper and lower walls display significant differences between the analytical prediction and the simulation result. This phenomenon was absent from the case of Neumann boundary conditions, where the flat profile was already achieved acceptably, as shown in Figure 4.6b.

Further analyses on this behavior showed that the cause can be referred to a different characteristic time for the Xenon dynamics in the liquid and gaseous phases. As a matter of fact, in the former (liquid phase) convergence is reached quickly but, being the mass transfer term dependent on the concentration in both phases, the steady-state value is not obtained yet. The system evolution thus goes still on for long, driven by the dynamics of the gaseous phase (in particular, the term relative to advection is slow to decrease), and the term of interaction is further corrected at each time step, until the true stationary value of all the system quantities is reached.

The final results obtained are reported, as for the single-phase cases, in form of color map plots and graphs respectively, in Figure 4.7 and Figure 4.8. It can be seen that, again, very good agreement is found between the numerical results gathered from OpenFOAM and the analytical calculations of the simplified model. The mean relative errors are, for the two-phase cases, of 1.5 % and 0.026 %, for the Dirichlet and Neumann conditions respectively.

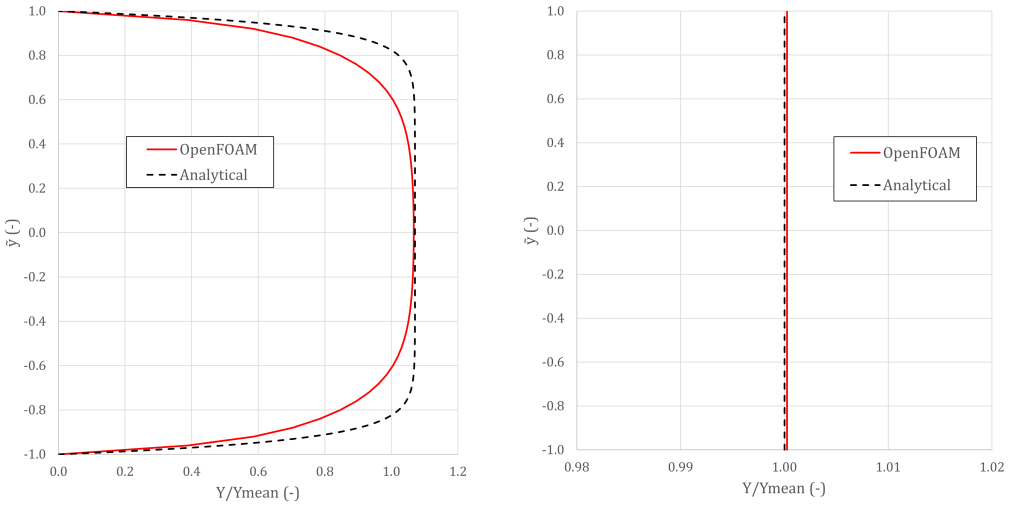

(a) (b)

Figure 4.6. Xe two-phase concentration profiles for transverse section at $x = L/2$, comparison between analytical results and OpenFOAM simulations (short simulation time). (a) Dirichlet boundary conditions (b) Neumann boundary conditions

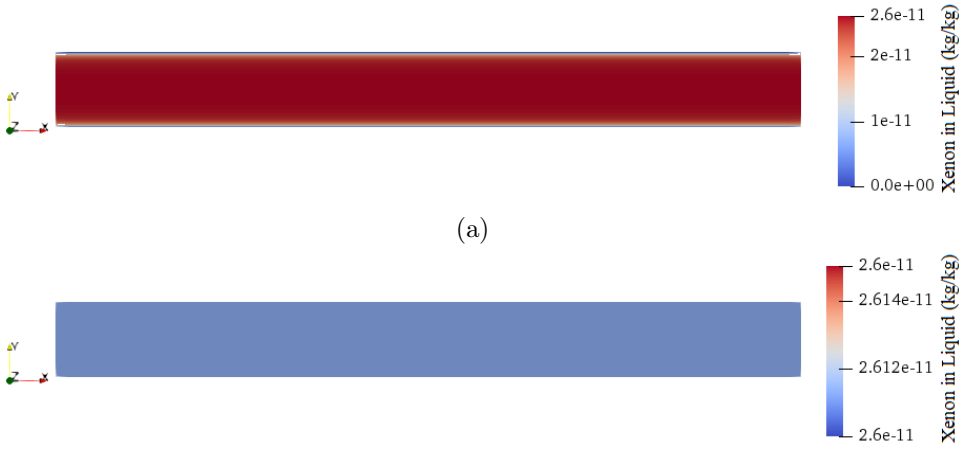

(a)

(b)

Figure 4.7. Xe concentration for two-phase simulations. (a) Dirichlet boundary conditions (b) Neumann boundary conditions

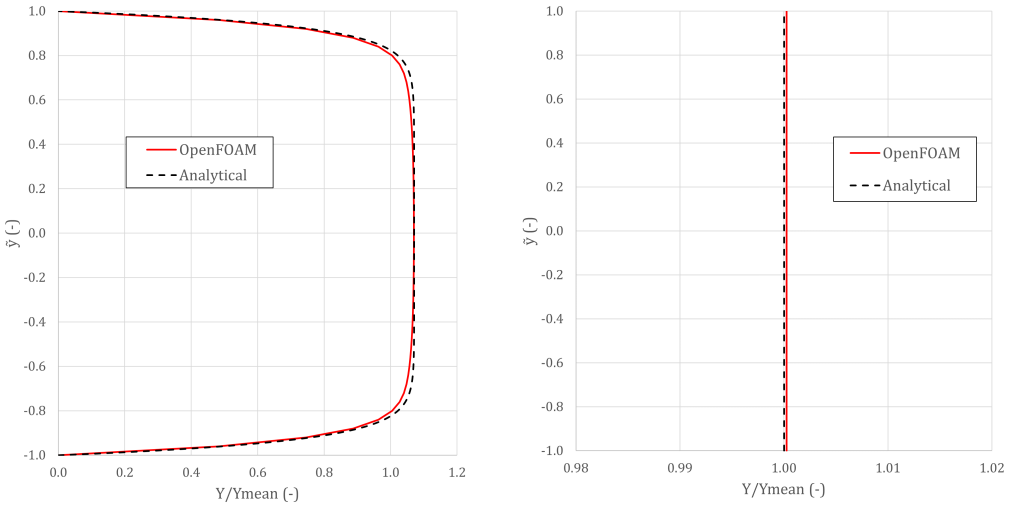

(a) (b)

Figure 4.8. Xe two-phase concentration profiles for transverse section at $x = L/2$, comparison between analytical results and OpenFOAM simulations (long simulation time). (a) Dirichlet boundary conditions (b) Neumann boundary conditions

4.3 Conclusive Remarks

In this chapter, the new functionalities introduced in this work were tested against analytical calculations, in order to verify the solver accuracy in the prediction of the mass transfer phenomenology. In a study of this kind, some simplifying assumptions have necessarily to be considered, in order to have an exact analytical solution to compare with the numerical results. In the light of these assumptions and the various hypotheses described, the results presented show that the solver is able to reproduce the correct trends for the main quantities of interest. It was pointed out that in the two-phase cases the computational time needed to have convergence of the solution was larger than expected beforehand, due to a difference between the characteristic times needed to reach the Xenon steady-state profile for the liquid and gaseous phase.

The case on which the code was tested in this chapter was kept fairly simple, due to the possible limitations of the analytical resolution. However, there are no indications suggesting that the solver should not be able to correctly reproduce a more complex situation as the one of the reactor, at least for what concerns mass transfer. In the following, therefore, new simulations are shown, displaying the results obtainable with the improved computational tools.

Chapter 5

Reactor Analysis

5.1 Introduction

In the analysis of a nuclear reactor system, the assessment of the source term is a crucial aspect since it involves both safety (i.e., reactivity and decay heat estimation) and radioprotection (i.e., activity and radiotoxicity estimation) issues. This is particularly true for MSR system in which the fission product flows with the fuel/coolant mixture. Different fission product flows are foreseen in the MSFR, i.e., from the core to the off-gas system or to the fuel treatment unit. As previously mentioned, the bubbling system covers a particular role in the MSFR, being responsible of the removal of the gaseous and metallic fission product from the core to the off gas system. Being the phenomenon strictly related to the bubble distribution in the core as well as to the mass transfer mechanism of the bubbles from the core to the helium flow, the analysis of such a system cannot be performed without a multiphysics tool capable of considering both neutronics and three dimensional thermal-hydraulics characteristics. In this Chapter, some simulations are performed with the modelling approach presented in Chapter 3, aimed at assessing the efficiency of the bubbling system through the calculation of removal rates and halving time of GFP concentration in the fuel salt. Both 2D and 3D geometries are studied with the multiphysics tool developed and the obtained results will be useful for designers in the framework of the SAMOSAFER project.

5.2 Geometry

As a first approach, a simplified cylindrical geometry is adopted, rather than a complete 3D model of the reactor. The basis for this choice is taken from the work of the previous EVOL project (Brovchenko et al., 2013). In particular, a 2D axial-symmetric model is employed, so that the cylindrical symmetry can be exploited in the solution of the problem. Only the fluid part of the system (salt and helium bubbles) is taken

into account, in order to avoid the increased computational effort that modelling the solid parts as well would require. A sketch of the geometry employed, with indications relative to the helium bubbling system, the heat exchanger and the pump location, is shown in Figure 5.1a. The latter are modelled by means of an energy sink and a momentum source, respectively, uniformly distributed in the corresponding sections. Finally, a free surface is present in the upper right corner of the hot leg, in order to allow for the expansion of the mixture. Figure 5.1b represents the computational mesh applied to the geometrical domain to perform the simulations, consisting of 22671 elements in total.

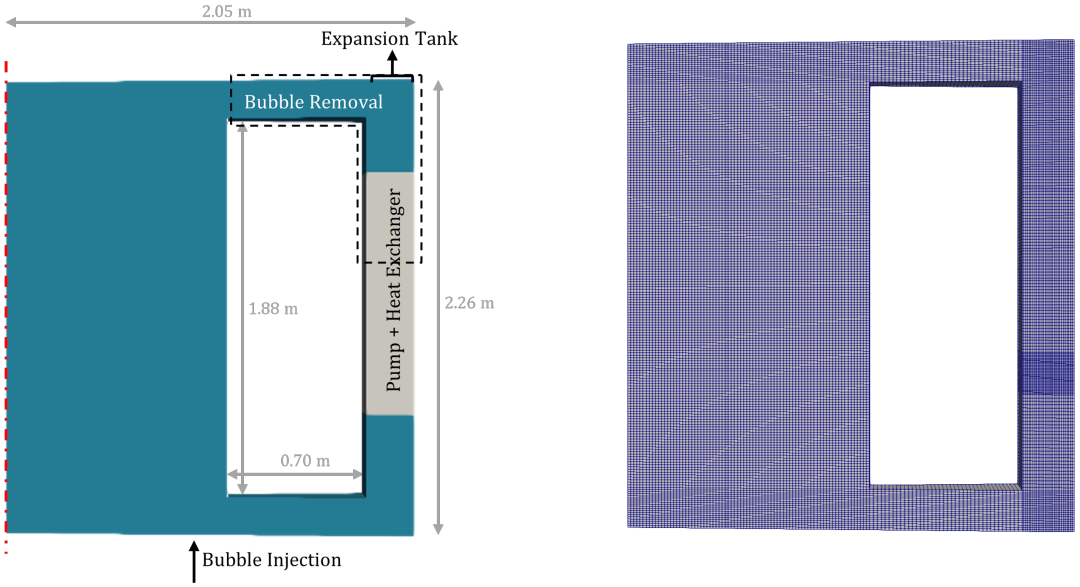

Figure 5.1. (a) Geometry and (b) Computational mesh employed for 2D simulations

The simple geometry allows conducting many tests on the behavior of the helium bubbling system and its effect on the gaseous fission products, without the need for excessive computational power. On the other hand, however, the results are not sufficient to correctly depict the complex system that is the MSFR core, and a full 3D analysis must be performed. Additional simulations are thus conducted on a 3D model of a quarter of the full scale MSFR reactor. Just as in the 2D case, only the fluid part of the system is considered. The bubbling system, the heat exchanger and the pumps are simulated as aforementioned, by definition of source/sink terms in the governing equations. Figure 5.2a displays a lateral view of the domain with the same indications of the previous example, and the 3D mesh employed, composed by 1954024 cells, is shown in Figure 5.2b. This mesh was previously analysed with a proper sensitivity study and proven suitable to be adopted for MSFR applications.

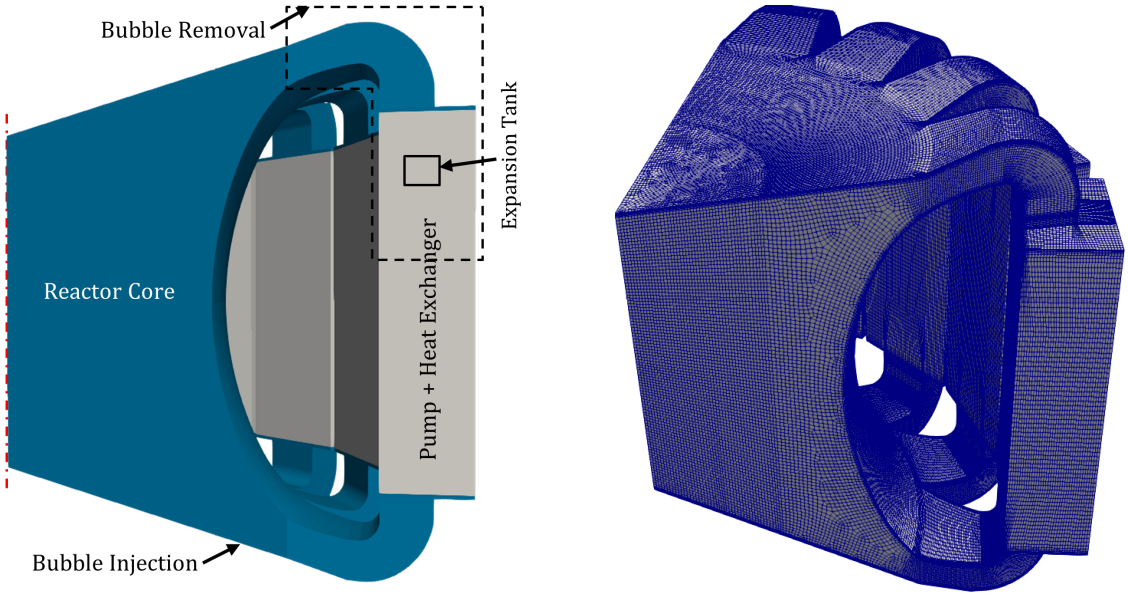

(a) (b)

Figure 5.2. (a) Geometry and (b) Computational mesh employed for 3D simulations

5.3 Efficiency of Bubbling System on Xenon

The helium bubbling system, as mentioned previously, is an apparatus envisaged in the design of the MSFR to enhance the removal of the fission products present in the core both in gaseous and metallic form. It is thus of critical importance, in the development of the reactor, to assess the effectiveness of the helium bubbles in their task. This is done in this work by defining and computing a parameter suitable to express the efficiency of the removal of GFPs, in the simulation of the behavior of the reference isotope Xenon-135, i.e. a halving time which is connected to the cycle time of the removal process. A fundamental hypothesis is made in this instance, assuming that the effect of the bubbling system on the mass balance of the gaseous fission products can be modelled in perfect analogy with a radioactive decay, upon definition of a corresponding constant parameter, γ_{bub}. From an analytical point of view, this is represented by a linear sink term in the differential equation relative to the balance of the nuclide, for which a simplified version can be written as:

$$\frac{\partial N}{\partial t} = source - reactions - \lambda_{dec} N - \gamma_{bub} N \tag{5.1}$$

This is the approach employed in the burnup analysis of MSR where is of paramount importance to take into account in the Bateman equations also the effects related to the FP removal from both the gaseous system and the fuel treatment unit to correctly predict the evolution of the salt mixture (Aufiero et al., 2013). Upon integration, the added contribution translates in an exponential trend in time, but the overall evolution of the nuclide inventory depends on the magnitude of each term in the equation. If the effect of generic reactions can be neglected, in order for the helium

bubbling to be effective the value of the parameter γ_{bub} obtained from the simulations should be considerably bigger than the decay constant of the nuclide, so that the trend in time can be driven by the effect of the gaseous bubbles and the concentration of the GFPs can be kept under control. Designers have thus assumed a value for the characteristic time around 30 seconds. Part of the aim of this work is to verify if it is possible to obtain results in the same order of magnitude with a CFD simulation considering the real bubble distribution and the phenomenon of mass exchange.

Following the approach just depicted, the necessary parameter can be directly calculated in OpenFOAM at every time-step, as the ratio between the rate of extraction of Xenon from the system via bubbling and the integrated mass inventory present in the system itself:

$$\frac{Xe_{outflow}\ (kg/s)}{Xe_{mass}\ (kg)} = \frac{\gamma_{bub} Xe_{mass}}{Xe_{mass}} = \gamma_{bub}\ (1/s) \tag{5.2}$$

The renewal time mentioned above is nothing else than the reciprocal of this coefficient. Just as in the case of exponential decay, a further multiplication by a factor of $ln(2)$ gives as a result a halving time of the system, expressing the duration of the period over which the helium bubbling system would decrease the quantity of Xenon in the system by half:

$$\tau = \frac{1}{\gamma_{bub}} \tag{5.3}$$

$$T_{1/2} = \tau \cdot ln(2) = \frac{ln(2)}{\gamma_{bub}} \tag{5.4}$$

The mass inventory of Xenon in the system is calculated as a numerical output of the simulations, by integrating the concentration on the domain. The value obtained by OpenFOAM can be verified by analytical comparison when the system reaches steady state in single-phase, without helium injection. In this condition, as a matter of fact, the quantity is dependent only on the source and sink terms, as defined in Section (3.3.2):

$$Xe_{staz} = \int_V \alpha_l \rho_l Y_{Xe,l}\ \ dV = \frac{y_{Xe} \cdot (m_{mol}/N_{Av})}{\lambda + \sum_i (\sigma_{c,i}\varphi_i)} \int_V \sum_n (\Sigma_{f,n}\varphi_n)\ \ dV \tag{5.5}$$

The removal of the gaseous phase from the system is modeled in OpenFOAM by the introduction of an implicit mass sink term in the continuity equation, through the "fvOptions" functionality. This approach allows simulating a continuous extraction of gas, distributed over a selected section of the volume, by an amount which is proportional to the quantity present in the system. In particular, for this work, the

action of the remover is confined to the hot leg of the reactor, directly beyond the outlet of the core, for what concerns the salt flow. The effect produced is sufficient to extract all the gas located in the external circuit, so that there are no bubbles re-entering the core from the cold leg through recirculation. This means that all the mass of Xenon present in the gaseous flow going out of the core is effectively removed from the system. Additionally, the Xenon exchanged from salt to helium bubbles inside the hot leg region is extracted as well. The importance of this latter amount is dependent on the chosen ratio of gaseous mass to be removed per second with the sink term. Depending on the relevance of Xenon exchange outside of the core, the rate of removal from the system can be obtained following different approaches. The easiest one, which is valid for any ratio of extraction chosen, consists in a direct calculation from the values of mass inventory in the domain, recorded for consequent time intervals, with an added term to account for the continuous production of Xenon (which is given by Eq. (3.12)):

$$Xe_{outflow}(t) = -\frac{Xe_{mass}(t) - Xe_{mass}\,(t - \Delta t)}{\Delta t} + S_{Xe} \tag{5.6}$$

This expression is valid on the assumption that both the decay and the neutron capture on Xenon give negligible contributions with respect to the manual removal. A comparison among the characteristic parameters of the phenomena is presented together with the results, in order to justify this hypothesis. With these data at hand, the renewal time can be calculated, as described above.

5.4 2D Model

The simulations were performed firstly, as already mentioned, on an axial-symmetric 2D model, with resolution of the governing equations in cylindrical coordinates. As it was the case of the analytical model, the stationary conditions are found preliminarily in the presence of the single phase only. At this point, the numerical value of Xenon inventory in the system is verified by comparison to the analytical calculation reported in Eq. (5.5) finding a good agreement (Table 5.1). The quantities of main importance in the core are displayed, in form of color map plots, in Figure 5.3. As it can be seen, the simplified geometry suffers from the presence of a stagnation zone, caused by the presence of straight walls and squared angles, where the Xenon is accumulated. This factor can be of particular influence in the removal of the gaseous fission products, if the bubbles are unable to reach the whole available core space, especially for those species for which the diffusivity in the salt is low.

The steady state conditions found are taken as starting point for the two-phase simulations. The injection and extraction of gaseous phase are modelled following the indications of Figure 5.1a. For the velocity fields, no-slip boundary conditions are employed at the reactor walls, and atmospheric pressure is imposed at the free surface of the expansion tank. A recap of the other boundary conditions employed is

Table 5.1. Xenon inventory at steady state: comparison between analytical calculation and OpenFOAM result for the 2D model

Analytical value	OpenFOAM value	Relative difference
$8.2669 \cdot 10^{-4}$ kg	$8.3197 \cdot 10^{-4}$ kg	0.639 %

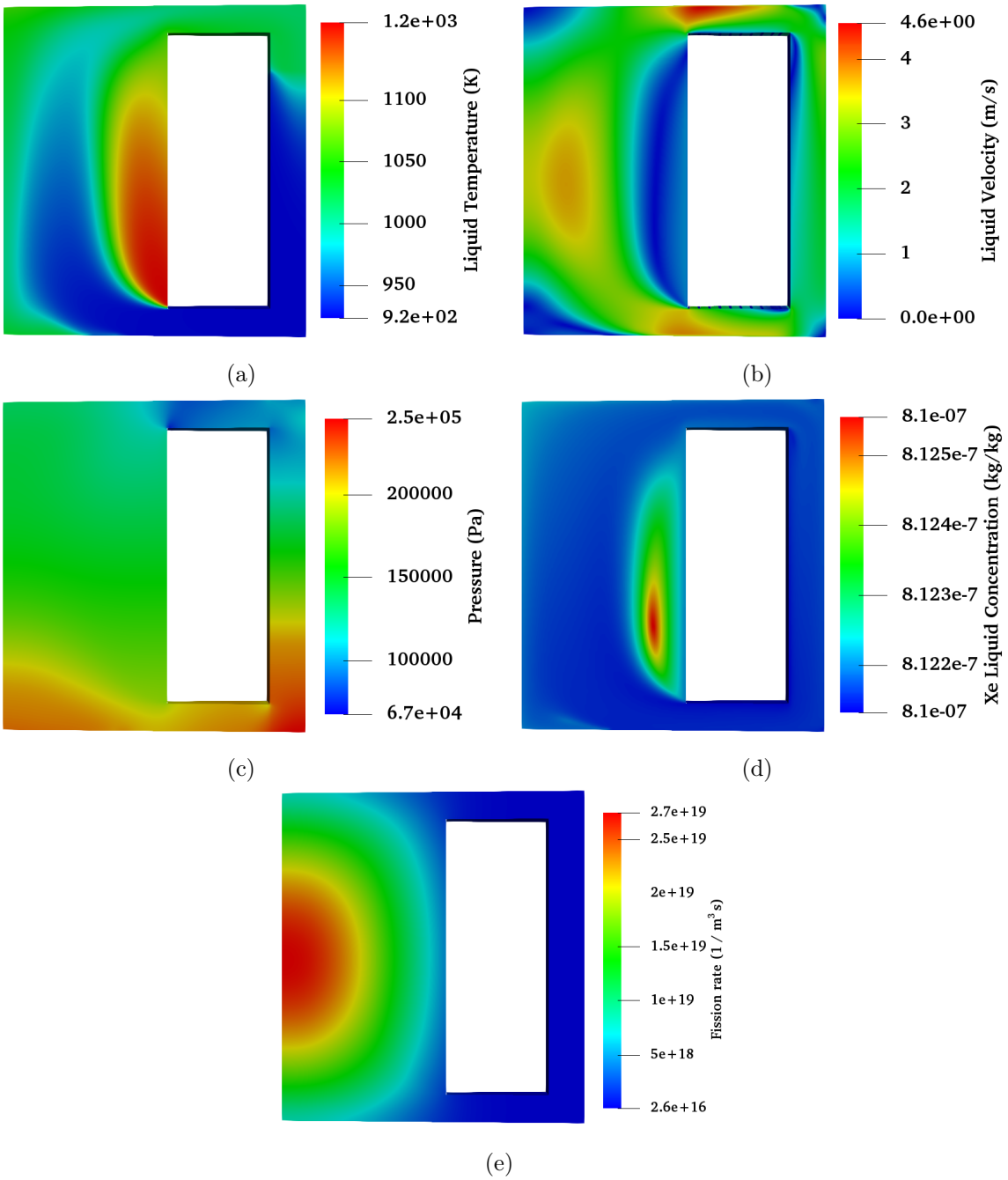

Figure 5.3. Color map plots for the profiles of the main quantities in 2D simulations. (a) Temperature (b) Velocity (c) Pressure (d) Xe concentration (e) Fission Rate

presented in Table 5.2.

Table 5.2. Boundary conditions employed in the simulations

Quantity	Boundary Conditions	
	Walls	Expansion tank
Phase fractions	Neumann	Mixed (Neumann/Dirichlet)
Decay heat precursors	Neumann	Neumann
Neutron Fluxes	Albedo	Albedo
Phase components	Neumann	Mixed (Neumann/Dirichlet)
Delayed neutron precursors	Neumann	Neumann
Pressure	Neumann	Dirichlet (1 atm)
Temperature	Neumann	Neumann
Velocity	No-slip	Mixed (Neumann/Dirichlet)

The standard k-ϵ model is employed to account for turbulence of the fuel. As in the previous chapter, the bubble diameter is evaluated by Eq. (4.28), with $d_0 = 3$ mm and $p_0 = 1$ atm. Virtual mass forces are modelled with a constant coefficient of $C_{VM} = 0.5$ and drag is accounted for employing the Schiller-Naumann correlation (Eq. (4.29)), while lift and turbulent dispersion are once again neglected. Heat transfer is considered with the Ranz-Marshall correlation (Eq. (4.30)). Mass transfer between the liquid phase and the dispersed bubbles is modelled with Henry's law, and the Sherwood number is evaluated through the Higbie correlation (Eq. (3.9)), as mentioned in Chapter 3, even though the flow in the reactor is in turbulent regime. With regard to this aspect, the mass transfer coefficient (K in Eq. (3.6)) was evaluated, in order to compare it with the value indicated in the studies performed at Oak Ridge National Laboratories on the MSRE (R. J. Kedl, 1972). The result is presented in Table 5.3.

Table 5.3. Mass Transfer Coefficient, comparison with indications from ORNL-3884

Average MTC (OpenFOAM)	MTC suggested at ORNL	Relative difference
$4.28 \cdot 10^{-4}$ m/s	$4.23 \cdot 10^{-4}$ m/s (5.00 ft/hr)	1.2%

The neutronics of the system is solved with the diffusion model, rather than the SP_3 transport, in order to reduce the computational effort required, and the power iteration routine is employed, in order to simulate stationary conditions. This means that the transient of the neutronic quantities caused by the injection of helium was neglected. Six-groups constant are generated with the Serpent-2 code, employing the cross section from JEFF-3.1.1 libraries (Santamarina et al., 2009). In Table 5.4, the energy group subdivision is reported, together with the coefficients employed for the albedo boundary conditions (β_i in Eq. (2.15)) at the reflectors and at the blanket walls.

The steady-state distribution of the gaseous phase fraction for the reference two-phase case is shown in Figure 5.4. As it can be seen, helium bubbles are injected from the bottom of the core and they are carried by the fuel to the cold leg up top, where they are progressively removed from the system. During this transit, Xenon is extracted from the liquid phase through mass transfer, and it is carried away by

Table 5.4. Ranges for energy groups and corresponding albedo coefficients for reflectors and blanket

Group	Energy Range (MeV)	Albedo coefficients (-)	
		Reflector walls	Blanket wall
1	2.23 - 20.00	0.1455	0.1249
2	$4.98{\cdot}10^{-1}$ - 2.23	0.5440	0.3849
3	$2.48{\cdot}10^{-2}$ - $4.98{\cdot}10^{-1}$	0.7771	0.6745
4	$5.53{\cdot}10^{-3}$ - $2.48{\cdot}10^{-2}$	0.7206	0.7596
5	$7.49{\cdot}10^{-4}$ - $5.53{\cdot}10^{-3}$	0.9602	0.8475
6	0 - $7.49{\cdot}10^{-4}$	1.3336	1.0951

the helium flow. The overall effect on the concentration of Xe-135 can be modelled, as aforementioned, in analogy with a radioactive decay, with the calculation of a removal constant, and a corresponding renewal time. Figure 5.5 displays the resulting distribution of Xenon concentration in the salt at the end of the reference simulation. The reduction of inventory is quite evident with respect to the results shown in Figure 5.3d, leading a decrease by a factor of 2.3 after 100 s. On the other hand, it should be pointed out that this is not the equilibrium profile for the concentration in presence of the bubbling flow, and the simulation time needed to reach the steady-state conditions is much longer.

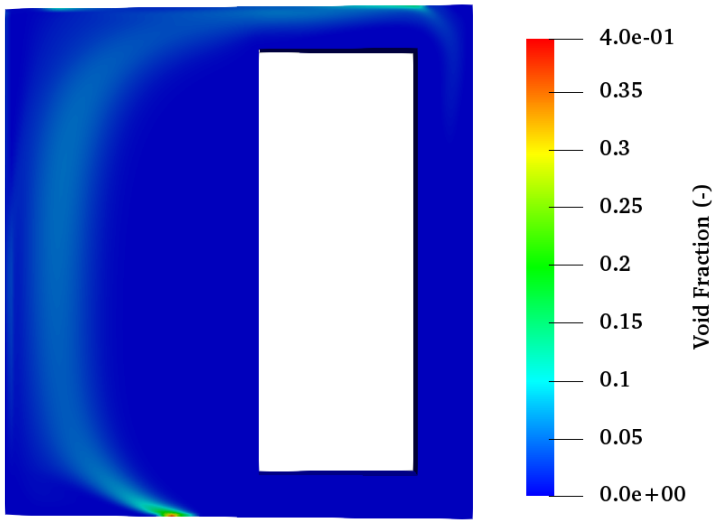

Figure 5.4. Void fraction profile for the reference case

The main figure of merit obtained from the 2D simulations is the halving time defined by Eq. (5.4). The graph in Figure 5.6 represents its behavior in time for the reference case. As it can be seen, after a first steep transient, the curve acquires a flat profile, and the parameter reaches a steady-state value which remains almost constant from there on, even if the stationary conditions are not met yet at the end of the simulation. The reference conditions chosen for the helium bubbling system modelling are portrayed in the Figure as well.

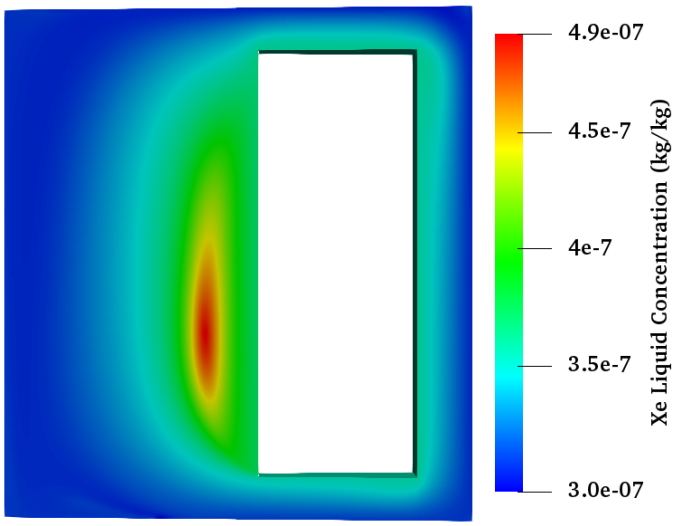

Figure 5.5. Xenon concentration profile at the end of the reference simulation

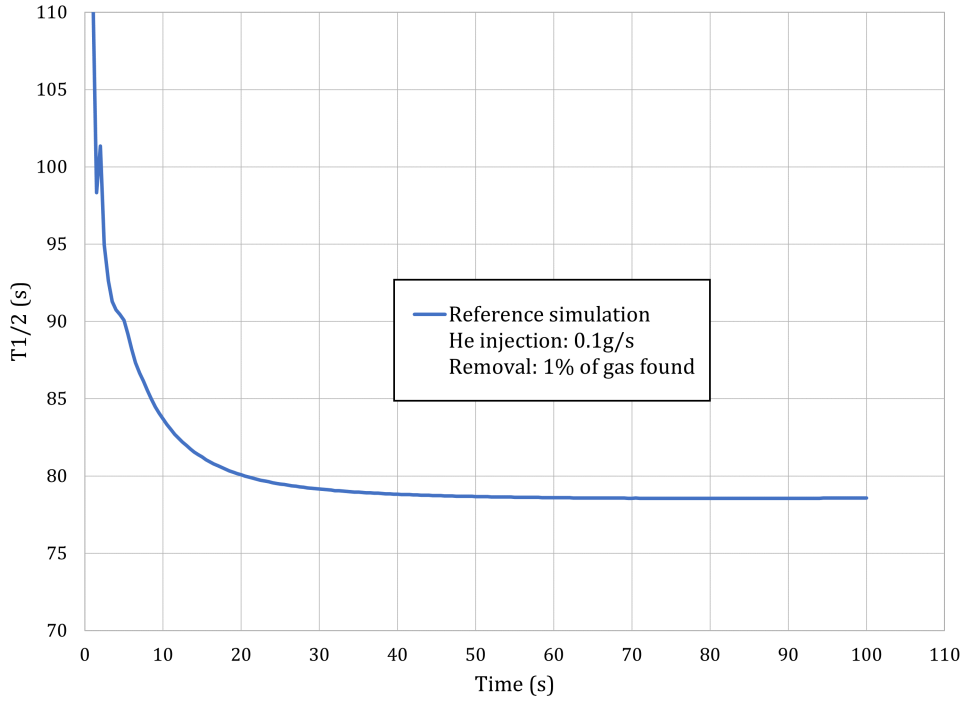

Figure 5.6. $T_{1/2}$ trend in time for the reference case

The flat profile that the curve just displayed assumes after the initial transient can be seen as a proof that the Xenon removal through helium bubbling system acts effectively in analogy with a radioactive decay, with an appropriate constant. As further confirmation of this fact, the graph in Figure 5.7 shows the Xenon inventory in the system through time. The regression of the curve puts in evidence the exponential trend, usually associated with decay. It should be pointed out that the real behavior in time is not a simple exponential, and this regression is valid only for the initial stationary, where the dynamic is driven by the effect of the remover alone. The aim

of the work is, however, to estimate the removal capability of the helium bubbling system, rather than establishing the final steady-state conditions of the reactor, and the graph displayed is meant only to confirm the validity of the hypothesis made in the modelling of the effect of bubbles on the Xenon concentration.

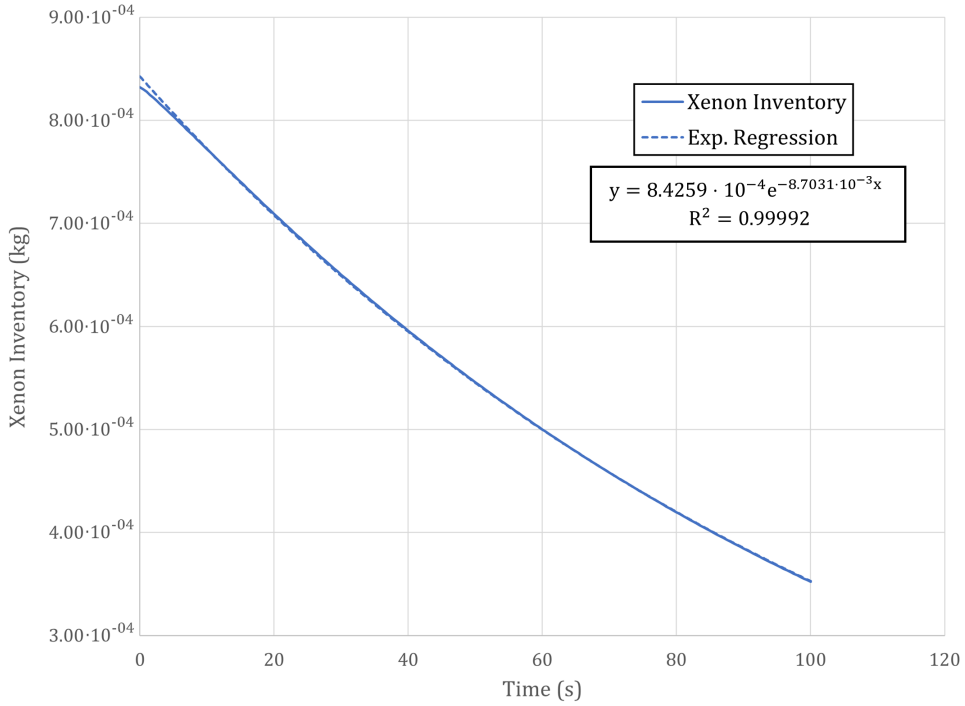

Figure 5.7. Xenon inventory trend in time for the reference case, with exponential regression

As mentioned before, the assumptions made for these previous considerations are valid if the other phenomena of consumption of Xenon are negligible with respect to the removal through the helium bubbling system. In Table 5.5, a comparison among indicative values of the respective characteristic parameters is displayed, showing the order of magnitude of impact of each phenomenon.

Table 5.5. Comparison among characteristic parameters of Xenon consumption phenomena

Helium bubbling (γ_{bub})	Decay (λ_{dec})	Neutron Capture ($\sigma_c \cdot \varphi$)
$8.7 \cdot 10^{-3}$ s^{-1} (reference case)	$2.11 \cdot 10^{-5}$ s^{-1} (half-life of 9.14 hrs)	$1.5 \cdot 10^{-9}$ s^{-1} (maximum value)

The result shown in Figure 5.6 is obviously dependent on a series of parameters chosen to perform the reference simulation. The main quantity of relevance in the definition of the problem is considered to be the mass flow of helium injected in the system. Multiple simulations were thus performed with different values for this parameter, keeping all the other conditions unaltered. The result, in terms of comparison of values for the halving time, is presented in Figure 5.8. From the graph, it can be seen that the time needed to complete the transient and reach the steady-state value is always shorter than the one seen in the reference case (with

the lowest helium inlet flow). Additionally, the $T_{1/2}$ shows an inversely proportional behavior with respect to the inlet mass flow of helium. This fact gains further confirmation by the display of Figure 5.9, where the values of halving time are plotted in function of the parameter, for two distinct moments of time in the simulations. The proportionality trend is clearly visible, and it is numerically verified by the data in Table 5.6. Additionally, the results reported here show that the aforementioned value of 30 seconds supposed by the SAMOSAFER designers for the characteristic time of the gaseous fission products removal can be effectively reached in CFD simulations under some conditions, and the order of magnitude of the quantity is the correct one for all of the values of helium inlet flow considered.

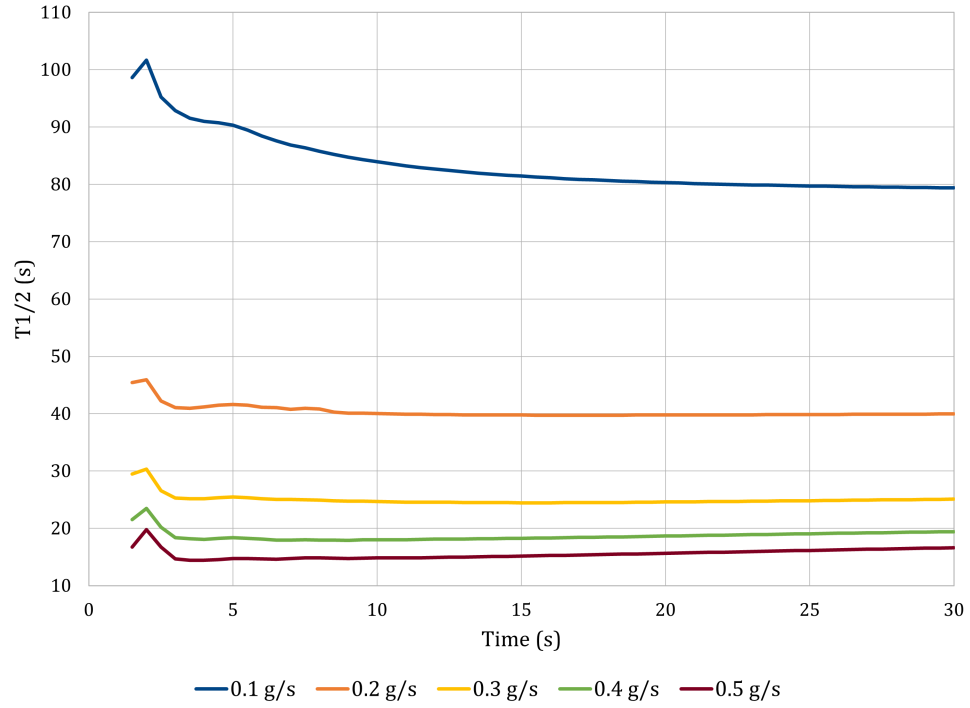

Figure 5.8. $T_{1/2}$ trends in time for different values of helium inlet flow

Table 5.6. Values of $T_{1/2}$ at different times for increasing helium inlet flow, with evidence of proportional behavior

Helium inlet flow (g/s)	$T_{1/2}$ at 20 s (s)	Ratio (-)	$T_{1/2}$ at 30 s (s)	Ratio (-)
0.1	80.0779	1.000	79.1503	1.000
0.2	39.7698	0.495	39.9570	0.503
0.3	24.5920	0.306	25.0847	0.316
0.4	18.6479	0.232	19.4328	0.245
0.5	15.6507	0.195	16.6205	0.209

The halving time and its dependence on the helium inlet flow surely represent the main results of the 2D simulations. The collected data give an indication of the efficiency of the helium bubbling system on the removal of Xenon and other gaseous fission products from the core. At this point, it would seem that the effect of increasing

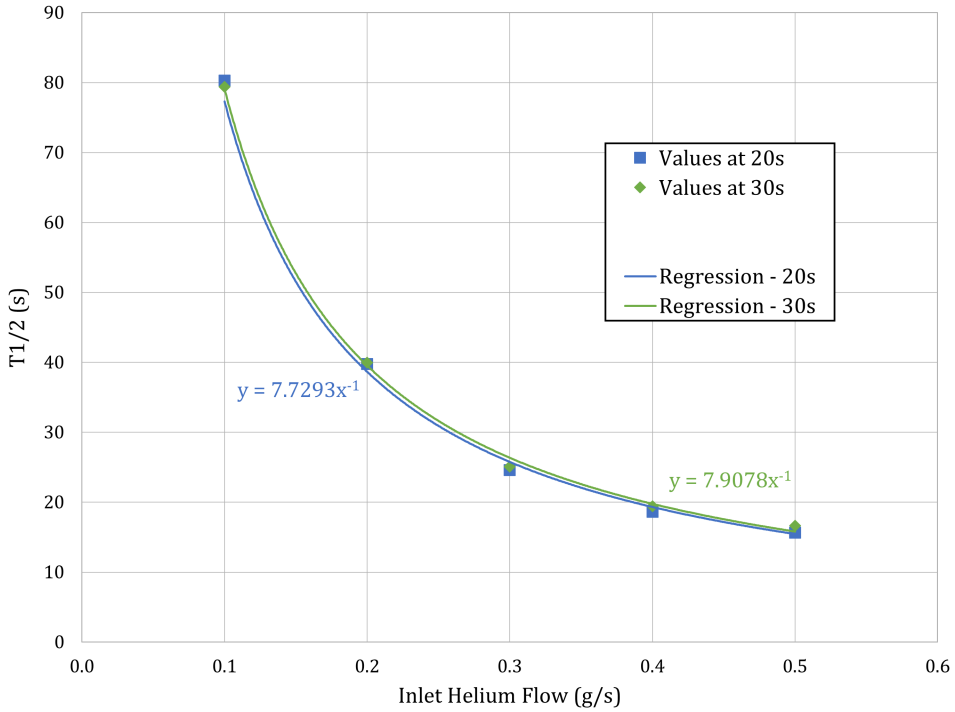

Figure 5.9. $T_{1/2}$ trend as a function of helium inlet flow, with evidence of proportionality

the helium inlet flow has no limit, and it would only be beneficial to increase the injection indefinitely. This is not true, however, because of the presence of operational limits dictated by the nature of the reactor. In order to understand this concept, some analyses must be performed on the neutronics part of the problem, so that the impact of the presence of the helium bubbles in the system can be observed. This aspect is of great importance on the development of the new reactor concept, both from the point of view of knowledge of normal operative conditions and, most importantly, on the subject of safety in accidental situations.

The presence of void in the core of a nuclear reactor has a direct effect on the reactivity of the system, through a feedback coefficient. This contribution is generally negative, in the sense that more gas implies lower reactivity. The quantity of helium injected in the system at steady state in nominal conditions, thus, needs to be monitored, to keep into account this influence in the calculations aimed at the knowledge of the reactivity inventory during normal operation. Additionally, the presence of this contribution becomes relevant in the case of an accident involving the helium bubbling injection apparatus. If the helium flow at the inlet is abruptly cut off, as a matter of fact, the system experiences a positive insertion of reactivity, which could be dangerous if not controlled properly. The entity of this insertion, together with the characteristic time of development of an accident of this kind, need to be analyzed in detail, if the helium bubbling system is to be effectively employed in the MSFR system.

In the work of (Cervi, 2020), values of the void reactivity coefficient for the MSFR were calculated, with a direct comparison between results from the OpenFOAM solver

and Monte Carlo simulations performed with the Serpent-2 code. The same figure of merit can be employed here to evaluate the effect of the presence of the helium bubbles on the reactivity of the system, through the analysis of the average in-core void fraction for different values of the inlet gaseous flow. The numerical results are reported in Table 5.7. The values in the "Reactivity deficit" column put in evidence the contribution, as a function of inlet helium flow, of the presence of the bubbles, that would translate in a positive reactivity insertion in case of the aforementioned accident. Considering that the value for the circulating delayed neutron fraction (β_{eff}) for the reactor with the composition considered in this work is of 146 pcm (Aufiero et al., 2014a), the accidental reactivity swings can be higher than one dollar for all the cases with injection higher than 0.1 g/s, which would render the safety management difficult.

Table 5.7. Values of void fraction, reactivity and calculated void feedback coefficient for different values of helium inlet flow

Helium inlet flow	Void fraction	Reactivity deficit	Feedback coefficient
0.1 g/s	0.00719	-107.99 pcm	-150.19 pcm/%
0.2 g/s	0.01645	-255.12 pcm	-155.09 pcm/%
0.3 g/s	0.03194	-569.81 pcm	-178.40 pcm/%
0.4 g/s	0.05059	-827.17 pcm	-163.50 pcm/%
0.5 g/s	0.06905	-1069.20 pcm	-154.84 pcm/%

Some last analyses were performed on the 2D model, in order to evaluate the impact of the simulation numerical parameters on the results. In particular, it was verified that the output is not dependent on further increase of the solver corrector cycles (both for thermal-hydraulics and neutronics solution). On the other hand, however, a change in the numerical schemes employed for the simulations may have a significant impact on the results. The complexity of the multiphysics problem at hand has required, for now, the need to use robust first-order schemes, in order to maintain stability throughout the simulation, since the objective is principally the estimation of integral quantities. A test with second-order schemes was performed, however, to see if the choice can be changed in future studies.

The single-phase steady-state profiles obtained for the main fields of interest, in the same conditions of the previous simulations performed, are displayed in Figure 5.10, and the void fraction profile from the two-phase simulation can be seen in Figure 5.11. As it can be seen from the pictures, the profiles for the single-phase quantities are characterized by little differences with respect to the ones obtained with first-order schemes, which could be seen as a confirmation of the validity of the previous results. For what concerns the void fraction profile, instead, a significant reduction in diffusion can be noted, in combination with higher maximum concentrations of gaseous phase as well. This can lead to different results from the point of view of Xenon extraction as well, and a deeper analysis on this aspect could be object of future studies.

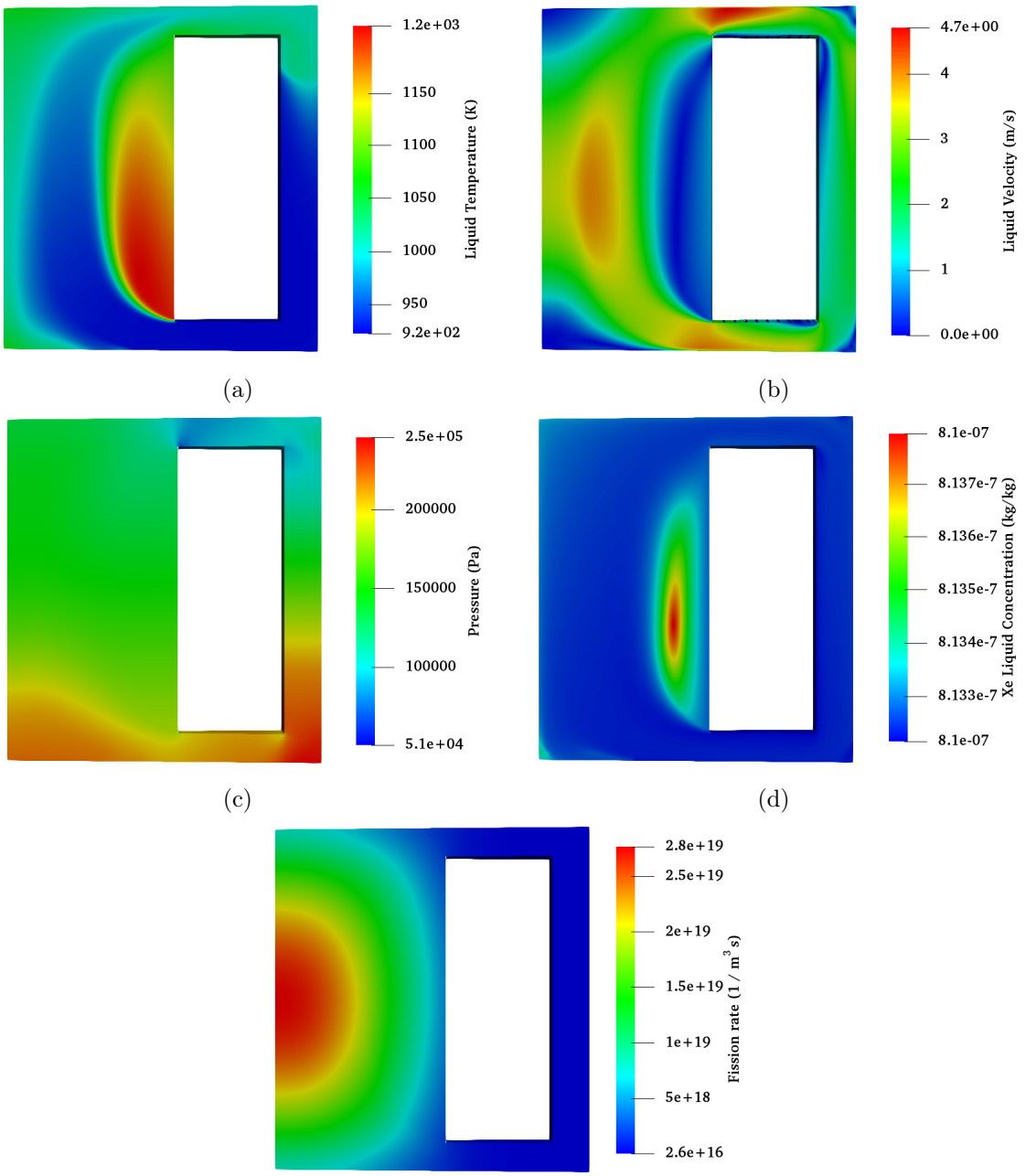

Figure 5.10. Color map plots for the single-phase steady-state conditions found with second-order schemes. (a) Temperature (b) Velocity (c) Pressure (d) Xenon concentration (e) Fission rate

5.5 3D Model

After the collection of extensive results from the simulations of the simplified 2D model, a test on a complete 3D model was performed, in order to verify the up-scaling capabilities of the new features implemented in the code and to get some preliminary results on the helium bubbling efficiency in the present configuration, represented as a

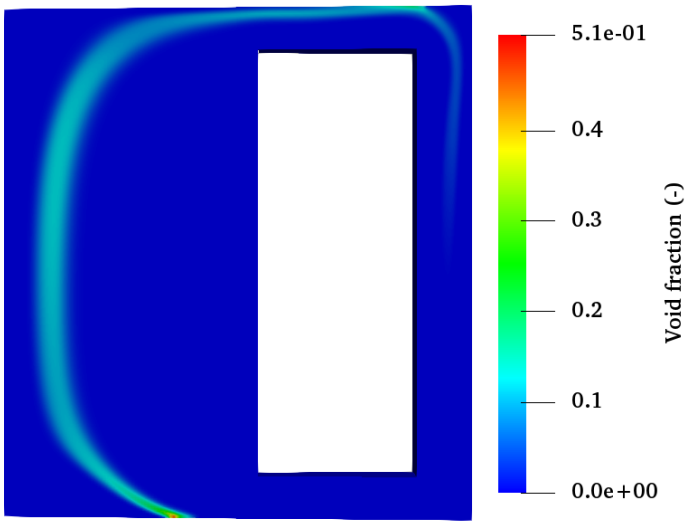

Figure 5.11. Void fraction profile for the simulation performed with second-order schemes

quarter of the full-scale MSFR system Cervi, 2020. The initial conditions employed are the same used for the 2D simulations. The main profiles of interest for the single-phase steady-state conditions are displayed in Figure 5.12, for internal vertical sections of a single reactor leg.

As it can be seen, the pressure profile is similar to the one obtained with the 2D model, as is the case of the fission rate, while the other ones present some differences. In particular, the refined curved design of the 3D geometry prevents the formation of the previously mentioned stagnation zone, modifying the temperature and velocity profiles in particular. As already stated, this factor can be also of importance in the removal of Xenon, since in this case the helium bubbles are facilitated in reaching the whole space of the core.

In this case too, the value of Xenon inventory at stationary computed by OpenFOAM is compared with the analytical result from Eq. (5.5), and good agreement is found, as reported in Table 5.8.

Table 5.8. Xenon inventory at steady state: comparison between analytical calculation and OpenFOAM result for the quarter of the reactor

Analytical value	OpenFOAM value	Relative difference
$1.4953 \cdot 10^{-2}\ kg$	$1.5068 \cdot 10^{-2}\ kg$	0.767 %

Again, the single-phase steady state found is used as starting point for the two-phase simulations. Bubble injection and extraction are modelled as displayed in Figure 5.2a. For what concerns boundary conditions and empirical correlations employed in the modelling of the various phenomena, the same choices made for the 2D model and described in the previous section were followed, both for the thermal-hydraulics and the neutronics of the system.

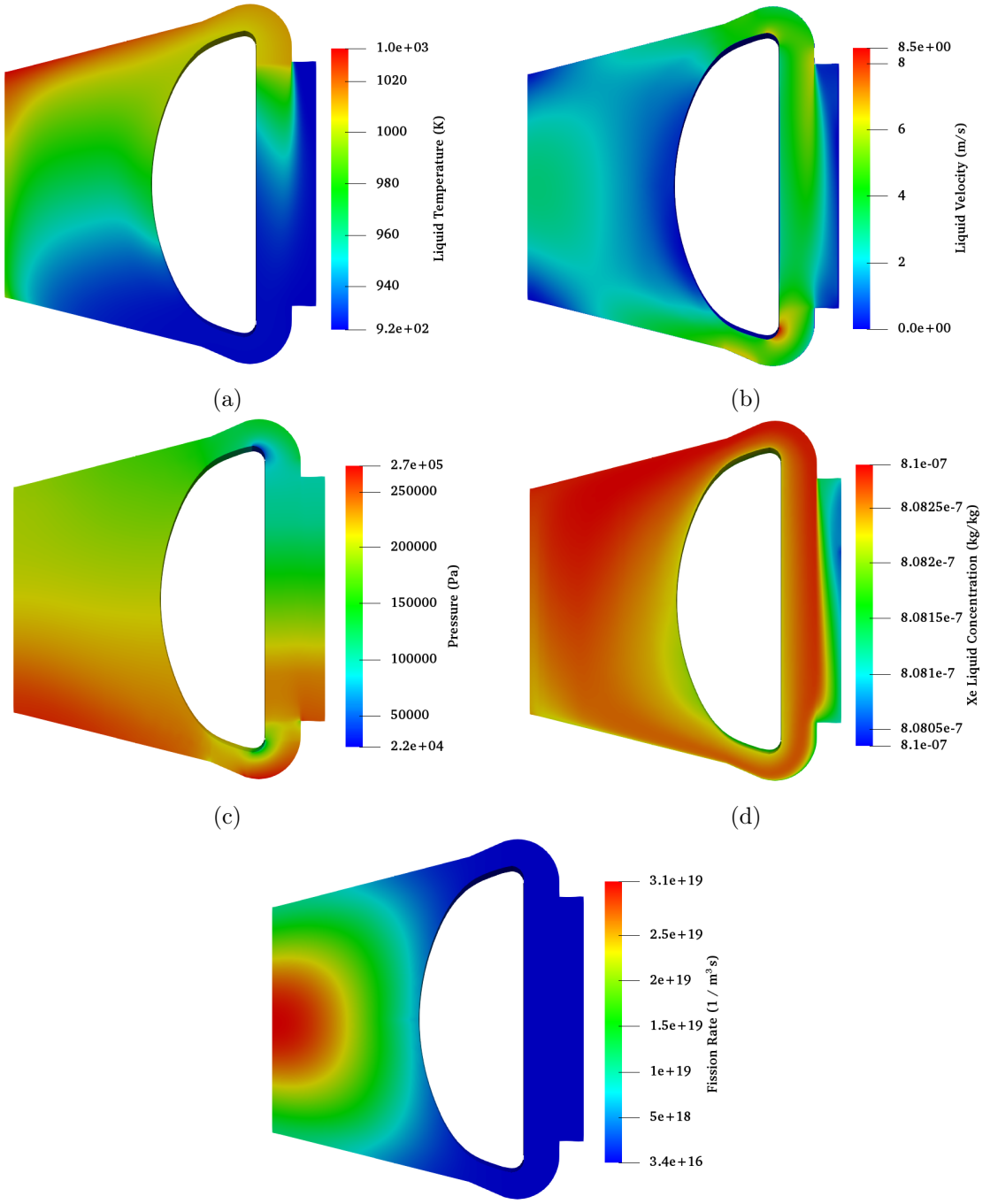

Figure 5.12. Color map plots for the single-phase steady-state conditions found for the 3D model of a quarter of the reactor (vertical sections). (a) Temperature (b) Velocity (c) Pressure (d) Xenon concentration (e) Fission rate

The obtained distribution for the void fraction in the core is displayed in Figure 5.13, both for a vertical section of a single leg, and for a horizontal one, displaying the condition of the whole reactor core.

As for the previous simulations, the main result of this analysis is the calculated

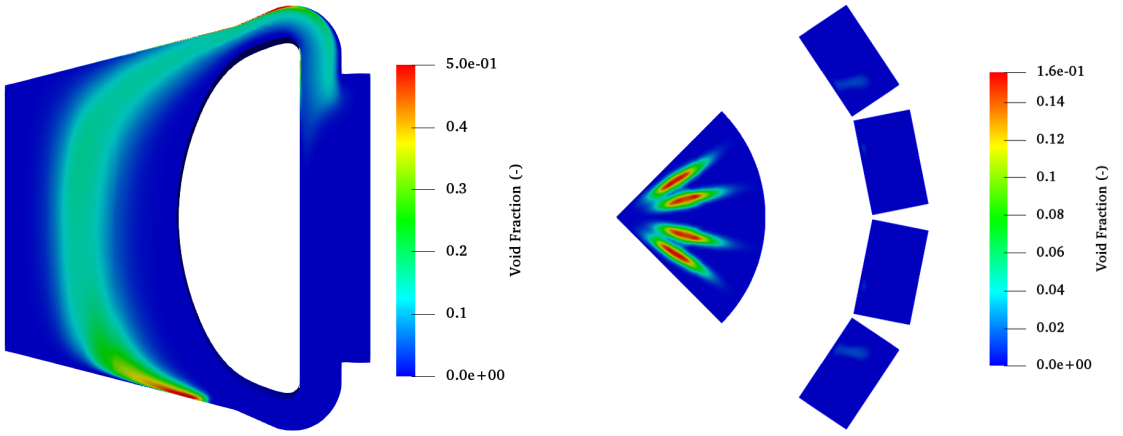

(a) (b)

Figure 5.13. Void fraction profile for the quarter of the reactor. (a) Vertical section (b) Horizontal section

halving time, following Eq. (5.4). The graph in Figure 5.14 displays the trend in time for this quantity, together with information about the inlet flow of helium and the extraction rate of the gaseous phase employed for the simulation. The value obtained for the halving time is in the same order of magnitude of the results of the 2D simulations, helping to confirm the validity of the previous analyses and to verify the up-scaling capabilities of the implemented model.

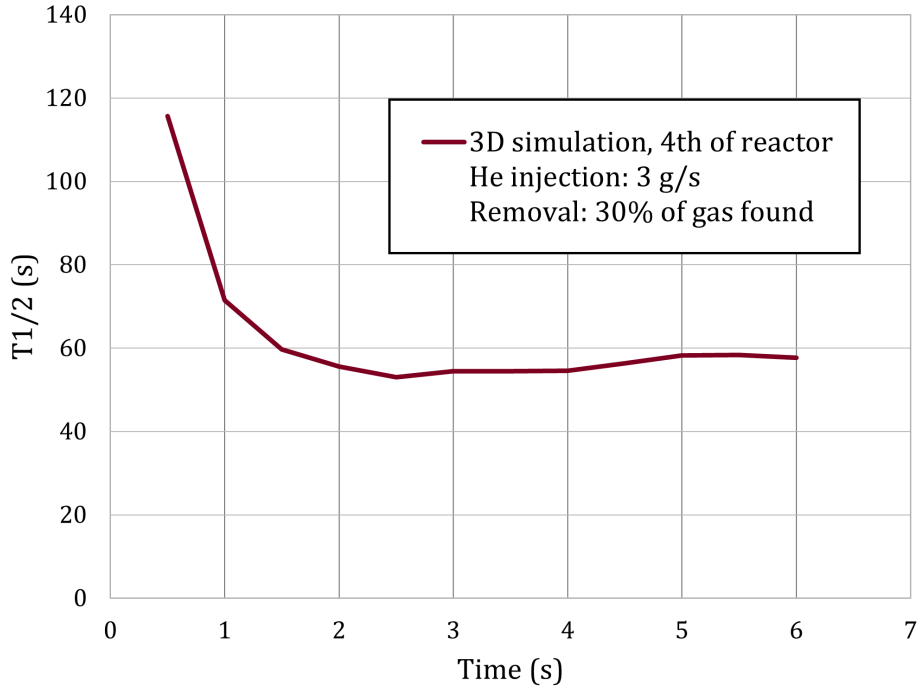

Figure 5.14. $T_{1/2}$ trend in time for the 3D case (quarter of the reactor)

As it can be seen from the graph, the simulated time for the 3D model was not very long, even if the initial transient is much shorter than the 2D case and the $T_{1/2}$ is

seen to reach already a value which remains almost constant in time. The additional features introduced with this thesis, as a matter of fact, had surely an impact in increasing the computational resources needed to perform a complete simulation of the system which, due to the refinement of this particular mesh (counting almost 2 million elements), were already considerably high.

In the matter of 3D computations, as a last task, a new 3D geometry, based on a sixteenth of the full-scale reactor, was tested. This addition of a new model can help for potential future analyses, particularly those focused on the symmetrical aspects of the physics of the reactor system, as opposed to the quarter, which is more useful when non-symmetrical peculiarities are of interest. In order to keep up with the new development of the OpenFOAM toolkit as well, the test was conducted on the newest version released, OpenFOAM 8 (https://openfoam.org/release/8/), modifying the bubbleFoam solver to make it work in this framework.

5.6 Conclusive Remarks

In this chapter, the new functionalities implemented in the bubbleFoam solver are tested on geometries which resemble the MSFR system. At first, extensive analyses are conducted on a 2D simplified model, in order to display the computational capabilities of the environment and to make comparisons among simulations run with different parameters. The main result is the analysis of efficiency of helium bubbling through the computation of the halving time of Xenon in the core, which, for the reference case, resulted to be of approximately 80 seconds. This gives credit to the order of magnitude of the quantity proposed by the SAMOSAFER designers. In addition, various other considerations are made. An analytical verification of the value of Xenon inventory in steady-state conditions is firstly presented. Then, a comparison between the mass transfer coefficient computed by OpenFOAM and the values suggested in the works of Oak Ridge National Laboratories is shown. Additionally, the neutronics part of the problem is considered, showing the void reactivity feedback obtained in the simulations. After all these considerations on the 2D model, the solver is then employed on a more complex 3D computational geometry, to verify the up-scaling capabilities of the tool and to give confirmation of the validity of the analyses proposed for the simplified case. Again, the halving time was calculated for the simulation, and it was found to be of approximately 57 seconds, which is closer, with respect to the 2D case, to the value of 30 seconds that has been used in the past. As mentioned, the computational resources needed to perform the 3D simulations on the chosen mesh were found to be too high to perform extensive analyses in the framework of this thesis, but the few results gathered already represent a solid indication that the solver is capable of performing under those conditions as well. Furthermore, the upgrade to the new version of the OpenFOAM framework, together with the test made on the smaller mesh of a sixteenth of the reactor, help to lay the ground for new simulations in the future.

Conclusions

Nowadays, numerical modelling is an affirmed approach in the progress of research and development of new technological designs. In the field of nuclear system, where the perceived risk can be higher with respect to other areas of energy production, computational simulations represent the main way to proceed in the first steps of analysis. Nuclear reactor concepts need to be tested thoroughly before they can be approved for experimental studies and, after enough confirmations, for commission.

The Molten Salt Fast Reactor is a circulating-fuel nuclear system under development in the framework of the Generation IV International Forum. In this kind of reactors, the fuel motion introduces the need to analyze and control the different material flows, especially for what concerns the fission products, in their transport to the off-gas system or the fuel treatment unit. The treatment of GFPs in particular is of critical importance in the core, since they affect the neutronics through different feedback contributions (e.g. void effect). The knowledge of their concentration and their location is fundamental in order to accurately predict both the operative conditions of the reactor and the accidental scenarios that can occur. Moreover, the control of the composition of the fuel and the treatment of the fission products are features of great interest in the design of circulating-fuel reactors, since they can lead to better resource utilization and other advantages, both on the subjects of economy and safety. A foreseen characteristic of the MSFR design is thus the presence of an helium bubbling system, aiming at an efficient removal of the gaseous and metallic fission products from the core to carry them to the off-gas system. The introduction of this apparatus, however, implies the need to develop new and improved simulation tools, in order to assess its effect on the system.

In this thesis, the capabilities of a state-of-the-art multiphysics OpenFOAM solver are extended, with the introduction of the ability to predict the behavior of gaseous fission products in the core. Rather than a one-fluid formulation, or the introduction of a separate phase in the set-up, the code is modified to allow for the presence of multiple species (components) for each phase. Xenon-135 is chosen as a reference isotope, in view of its importance in a nuclear reactor environment as neutronic poison. The modelling focuses mainly on the production of the nuclide via fission, its consumption through radioactive decay and neutron captures and, most importantly, on its interaction with the helium bubbling system, for what concerns both the transfer between phases and the transport out of the core to the off-gas system. The multi-component modelling is thus implemented in combination with proper simulation of

mass transfer phenomenology (driven by concentration gradients).

The analytical verification performed on the 2D tube, in combination with the analyses carried out on the 2D and 3D models of the reactor core, showed good results overall. The main point of interest gathered from the modelling results can be summarized as follows:

- The implemented feature is able to reproduce the generation of Xenon, and the single-phase simulations reach the correct equilibrium conditions with its consumption in terms of concentration and overall mass inventory.
- The computation of the mass transfer performed by the chosen thermo-hydraulic model is in agreement with analytical calculations, for simple laminar conditions with uniform and constant thermophysical properties.
- The results of the two-phase simulations seem to be reasonable also for turbulent conditions and considering the interactions with the neutronics of the MSFR system.
- A way to calculate a parameter indicating the efficiency of the helium bubbling system in the removal of gaseous fission products is established, in view also of a link with other works in the context of the H2020 SAMOSAFER project.
- The efficiency of the bubbling system is seen to show a linear dependence on the chosen inlet mass flow of helium, meaning that the calculated halving time decreases as the flow increases, through inverse proportionality.
- A direct connection is maintained with the works of Oak Ridge National Laboratory regarding the Molten Salt Reactor Experiment and Molten Salt Breeder Reactor. This is done by employing the same values of Xenon diffusivity in the salt and Henry constant which are suggested in the reports. The link shows also in the fact that the values of the mass transfer coefficient between the fluid and gaseous phases obtained in the simulations are similar to the experimental results registered on the MSRE.

From the point of view of the numerical results of the simulations, the following can be said:

- The effect of the helium bubbling system on the inventory of Xenon in the MSFR core simulated by OpenFOAM was in good agreement with the assumptions made initially, showcasing an exponential time trend analogous to a radioactive decay. Additionally, the calculated value of the removal constant was significantly higher than the ones characterizing other consumption processes, demonstrating that the helium bubbling effect can drive the dynamics of the system.
- It was possible to obtain, raising enough the value of helium inlet flow, an halving time of 30 seconds, which was supposed by the designers of the MSFR. In view of the safety concerns discussed for the neutronics of the system, however, it

should be envisaged to keep the helium injection low enough. Even accounting for this, anyway, an order of magnitude of tens of seconds for the $T_{1/2}$ was demonstrated to be an resonable assumption.

- The values for the Xenon inventory at single-phase steady-state conditions were verified analytically, finding good agreement both for the 2D and the 3D geometries.

- The analogies between the main 2D and 3D results showed the up-scaling capabilities of the OpenFOAM model, demonstrating the possibility to conduct valid studies on both cases, depending on the particular phenomena to be observed, except for the eventual effects of the presence, in the 2D geometry, of the mentioned stagnation zone.

- The inlet helium flow was seen to have a fundamental impact on the calculated halving time, but a significant effect was also found, for the void fraction profile, when changing the configuration to second-order numerical schemes.

In view of the results presented, this work constitutes a step forward in the multiphysics analysis of the MSFR design. Thanks to the flexibility of the OpenFOAM environment, the results obtained for Xe-135 in the demonstration of the simulation capabilities can be easily extended to other relevant species as well, so that the conclusions presented can be valid for the analysis of any gaseous fission product. The upgrade and development of the solver performed in this work help to maintain its identity as one of the most advanced modelling approaches for the MSFR as of today. Additionally, the changes made add up to the long-term objective of obtaining a single computational tool with the ability to reproduce all the physical aspects intervening and interacting in the environment of the nuclear reactor core under analysis.

The analyses carried out in this thesis help to lay the ground for many future possible developments on the matter:

- The Henry model for interface composition was employed here, together with the Higbie correlation for the mass transfer model. Once an experimental setup is constructed to obtain more precise data regarding the MSFR conditions, more accurate models can be adopted and implemented in the code of the solver.

- This work was limited to the study of gaseous fission products in the salt. New features could be implemented in the solver, so that, for example, the production and deposition of metallic particles, together with their interactions with the helium bubbles, can be considered as well.

- In this work, the injection and removal of the helium bubbles were modelled arbitrarily since no detail about their implementation is available at the present. In the future, a sensitivity analysis could be carried out to verify the impact of a change in the bubbling and removal setup on the efficiency of the system.

- The results of the 3D simulation on the quarter of the reactor put in evidence the fact that the implementation of new features in the solver leads to an increase in the computational resources needed to perform the analyses. The development of reduced order models could help in this matter, potentially decreasing runtimes and facilitating the performance of more studies.

Appendix A

OpenFOAM

The Open-source Field Operation And Manipulation (Weller et al., 1998) framework is a C++ library suitable for modelling complex coupled problems. Its design is based on the finite-volume approaches, employing spatial discretization in order to solve partial differential equations (both scalar and vector ones), with differencing and interpolation schemes specified by the user. In addition to various pre-implemented solvers and models for various problems, OpenFOAM presents a particular ease of implementation of new constitutive equations defined by the user. This high level of flexibility and versatility provided by the toolkit motivates its extensive employment for CFD simulations of all kinds. The software is ideal for modelling and solving any continuum mechanics problem, involving phenomena such as turbulence, chemical reactions and heat transfer.

The library has been observed to be especially useful in multiphysics applications and the analysis of strongly coupled systems, just as nuclear reactors, justifying its choice as framework for the analysis conducted in this thesis. A particularly attractive feature of OpenFOAM is the embedded top-level C++ representations of equations, which closely resembles their mathematical descriptions. As an example, the transport equation of a scalar quantity T, which is written in analytical form as

$$\frac{\partial T}{\partial t} + \nabla \cdot (\mathbf{U}\, T) - \nabla^2 (D\, T) = 0 \tag{A.1}$$

is easily implemented in OpenFOAM as

```
    fvm::ddt(T)
  - fvm::div(phi, T)
  + fvm::laplacian(D, T)
==
    0
```

where `phi` represents the volumetric flux associated with **U**.

Appendix B

Precursor Data

In this work, the composition of the fuel salt is assumed to be the ^{233}U-enriched option, with the molar fractions reported in Table B.1.

Table B.1. Fuel composition adopted in the work

Specie	Molar fraction (% mol)
LiF	77.5
ThF_4	20.0
$^{233}UF_4$	2.5

Following the works of (Aufiero, 2014) and (Cervi, 2020), it is chosen to adopt, with this composition, eight groups for the delayed neutron precursors, and three groups for the decay heat precursors, as mentioned in Section 2.5.3. For these groups, fractions and decay constants are reported in Table B.2 and Table B.3. In the case of the decay heat precursors, the fractions refer to the portion of decay power density for each group.

Table B.2. Delayed neutron precursors properties

Group	Fraction β	Decay constant λ (s^{-1})
1	$22.2 \cdot 10^{-5}$	$1.24667 \cdot 10^{-2}$
2	$48.1 \cdot 10^{-5}$	$2.82917 \cdot 10^{-2}$
3	$40.5 \cdot 10^{-5}$	$4.25244 \cdot 10^{-2}$
4	$64.5 \cdot 10^{-5}$	$1.33042 \cdot 10^{-1}$
5	$102.1 \cdot 10^{-5}$	$2.92467 \cdot 10^{-1}$
6	$17.7 \cdot 10^{-5}$	$6.66488 \cdot 10^{-1}$
7	$22.3 \cdot 10^{-5}$	1.63478
8	$5.1 \cdot 10^{-5}$	3.55460

Finally, in Equations (2.23) and (2.24), the laminar Schmidt number Sc is set to 20 and the turbulent Schmidt number Sc_T is set to 0.85. (Cervi, 2020)

Table B.3. Decay heat precursors properties

Group	Fraction β	Decay constant λ (s^{-1})
1	$1.86 \cdot 10^{-2}$	$3.580 \cdot 10^{-4}$
2	$1.29 \cdot 10^{-2}$	$1.680 \cdot 10^{-2}$
3	$1.17 \cdot 10^{-2}$	$1.973 \cdot 10^{-1}$

Appendix C

Xenon Cross Sections

In this work, the behavior of Xenon-135 inside the reactor is modelled by the introduction of appropriate source and sink terms in the equations relative to the species balance inside each phase. The terms relative to the neutronics part of the problem are based on values for the microscopic neutronic cross sections of absorption of the nuclide. These data were collected from a simulation performed on the Serpent-2 Monte Carlo code for burnup analysis (http://montecarlo.vtt.fi/; Leppänen et al., 2015). The values obtained, together with the indication of the energy boundaries for the 6-group subdivision, are reported in Table C.1.

Table C.1. Ranges for energy groups and corresponding Xenon absorption cross sections

Group	Energy Range (MeV)	Cross Section (barns)
1	2.23 - 20.00	$0.003927 \pm 2.2 \cdot 10^{-6}$
2	$4.98 \cdot 10^{-1}$ - 2.23	$0.012113 \pm 6.5 \cdot 10^{-6}$
3	$2.48 \cdot 10^{-2}$ - $4.98 \cdot 10^{-1}$	$0.35825 \pm 3.7 \cdot 10^{-5}$
4	$5.53 \cdot 10^{-3}$ - $2.48 \cdot 10^{-2}$	$0.1162 \pm 1.4 \cdot 10^{-4}$
5	$7.49 \cdot 10^{-4}$ - $5.53 \cdot 10^{-3}$	$0.3342 \pm 5.1 \cdot 10^{-4}$
6	0 - $7.49 \cdot 10^{-4}$	$1.0438 \pm 4.2 \cdot 10^{-3}$

To obtain these results, the simulation was performed on a geometry representing the full-scale reactor, which is shown in Figure C.1.

The simulation was conducted considering 1 million neutron histories (100 cycles with a population of 10000 neutrons per cycle). The predictor-corrector routine was enabled, with Linear Extrapolation for the predictor part and Linear Interpolation for the correctors (LELI option). For more details about these simulations, in the specific framework of the MSFR design, the reader is referred to (Aufiero, 2014; Cervi, 2020), and similar works.

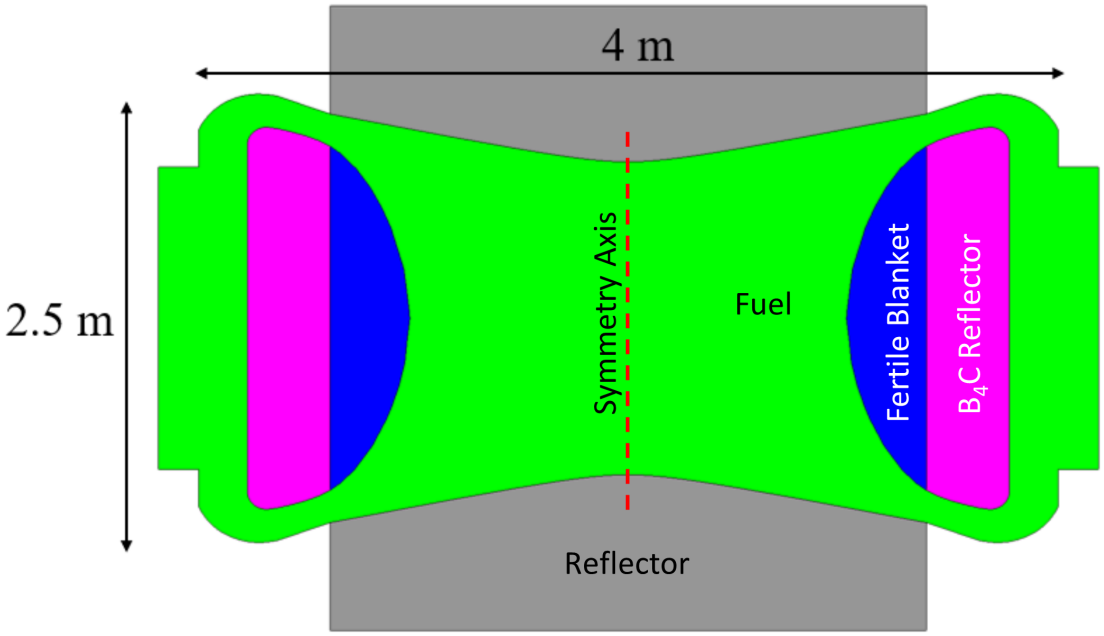

Figure C.1. Vertical section of the reactor geometry employed in Serpent simulations

Acronyms

CFD	Computational Fluid Dynamics
CNRS	Centre Nationale de la Recherche Scientifique
GFPs	Gaseous Fission Products
GIF-IV	Generation IV International Forum
LMFR	Liquid Metal Fast Reactor
MOSART	MOlten Salt Actinide Recycler and Transmuter
MSBR	Molten Salt Breeder Reactor
MSFR	Molten Salt Fast Reactor
MSRs	Molten Salt Reactors
MSRE	Molten Salt Reactor Experiment
ODE	Ordinary Differential Equation
ORNL	Oak Ridge National Laboratory
TRUs	Trans-Uranic Elements
VOF	Volume-Of-Fluid

Nomenclature

Greek Symbols

α	Phase fraction, -
$\bar{\nu}$	Mean neutrons per fission, -
β	Delayed neutron precursor fraction, -
β_i	Albedo coefficient for the i-th neutron energy group, -
β_h	Decay heat energy fraction, -
χ	Neutron yield, -
γ_{bub}	Bubbling system constant, s^{-1}
λ	Decay constant, s^{-1}
λ_h	Decay heat precursor decay constant, s^{-1}
λ_k	Delayed neutron precursor decay constant, s^{-1}
μ	Dynamic viscosity, Pa s
ν	Kinematic viscosity, $\mathrm{m}^{-2}\ \mathrm{s}^{-1}$
ρ	Density, kg m^{-3}
Σ	Macroscopic cross section, m^{-1}
σ	Microscopic cross section, m^2
φ	Neutron flux (diffusion equation), $\mathrm{m}^{-2}\ \mathrm{s}^{-1}$
φ_0	Neutron flux (SP_3 equation), $\mathrm{m}^{-2}\ \mathrm{s}^{-1}$
φ_2	Neutron flux second moment (SP_3 equation), $\mathrm{m}^{-2}\ \mathrm{s}^{-1}$

Latin Symbols

$\mathbf{g}$	Gravitational acceleration, m s^{-2}
$\mathbf{u}$	Velocity, m s^{-1}

A	Interfacial area for mass transfer, m^2
a	Interfacial area for mass transfer per unit volume, m^{-1}
B	Cross section temperature coefficient, m
C	Species concentration, kg m^{-3}
c	Delayed neutron precursor density, kg^{-1}
C_p	Constant pressure specific heat, W kg^{-1} K^{-1}
D	Diffusivity, m^2 s
d	Decay heat precursor density, W kg^{-1}
d_0	Reference bubble diameter, m
d_b	Bubble diameter, m
D_H	Hydraulic diameter, m
D_n	Neutron diffusion coefficient, m
E_f	Fission energy, J
fR	Fission rate, m^{-3} s^{-1}
H	Henry coefficient, -
h	Specific enthalpy, J kg^{-1}
K	Mass transfer coefficient, m s^{-1}
k	Specific kinetic energy, J kg^{-1}
k_{eff}	Effective multiplication factor, -
K_{th}	Modified thermal diffusivity, J m^{-1} s^{-1} K^{-1}
L	Inter-phase heat transfer coefficient, W m^{-3} K
M	Inter-phase momentum transfer, kg m^{-2} s^{-2}
m	Mass, kg
N_{Av}	Avogadro number, mol^{-1}
Nu	Nusselt number, -
p	Pressure, Pa
p_0	Reference pressure, Pa
pcm	per cent mille ($=10^{-5}$)

Pr	Prandtl number, -
Q	Power source density, W m^{-3}
Re	Reynolds number, -
S	Mass source, kg m^{-3} s^{-1}
Sc	Schmidt number, -
Sh	Sherwood number, -
T	Temperature, K
t	Time, s
$T_{1/2}$	Halving time, s
V	Volume, m^3
v	Neutron velocity, m s^{-1}
Y	Dimensionless species concentration, -
y	Fission yield, -

Subscripts and Superscripts

b	Bubble
d	Delayed
f	Fission
g	Gas
h	Decay heat
l	Liquid
p	Prompt
r	Removal
s	Scattering
$s2$	Second order inelastic scattering
$s3$	Third order inelastic scattering
T	Turbulent
t	Total
tr	Transport
Xe	Xenon

Bibliography

Allibert, M., Aufiero, M., Brovchenko, M., Delpech, S., Ghetta, V., Heuer, D., Laureau, A., & Merle-Lucotte, E. (2016). Molten salt fast reactors. In I. L. Pioro (Ed.), *Handbook of generation iv nuclear reactors* (pp. 157–188). Elsevier.

Aufiero, M., Cammi, A., Fiorina, C., Leppänen, J., Luzzi, L., & Ricotti, M. E. (2013). An extended version of the SERPENT-2 code to investigate fuel burn-up and core material evolution of the Molten Salt Fast Reactor. *Journal of Nuclear Materials*, *441*(1-3), 473–486.

Aufiero, M. (2014). *Development of Advanced Simulation Tools for Circulating-fuel Nuclear Reactors* (Doctoral dissertation). Politecnico di Milano.

Aufiero, M., Brovchenko, M., Cammi, A., Clifford, I., Geoffroy, O., Heuer, D., Laureau, A., Losa, M., Luzzi, L., Merle-Lucotte, E., Ricotti, M. E., & Rouch, H. (2014a). Calculating the effective delayed neutron fraction in the Molten Salt Fast Reactor: Analytical, deterministic and Monte Carlo approaches. *Annals of Nuclear Energy*, *65*, 78–90.

Aufiero, M., Cammi, A., Geoffroy, O., Losa, M., Luzzi, L., Ricotti, M. E., & Rouch, H. (2014b). Development of an OpenFOAM model for the Molten Salt Fast Reactor transient analysis. *Chemical Engineering Science*, *111*, 390–401.

Avramova, M. N., & Ivanov, K. N. (2010). Verification, validation and uncertainty quantification in multi-physics modeling for nuclear reactor design and safety analysis. *Progress in Nuclear Energy*, *52*(7), 601–614.

Baraldi, A., Dodd, M., & Ferrante, A. (2014). A mass-conserving volume-of-fluid method: Volume tracking and droplet surface-tension in incompressible isotropic turbulence. *Computers & Fluids*, *96*, 322–337.

Bell, G. I., & Glasstone, S. (1970). *Nuclear Reactor Theory*.

Bhusare, V. H., Dhiman, M. K., Kalaga, D. V., Roy, S., & Joshi, J. B. (2017). CFD simulations of a bubble column with and without internals by using OpenFOAM. *Chemical Engineering Journal*, *317*, 157–174.

Blander, M., Grimes, W. R., Smith, N. V., & Watson, G. M. (1959). Solubility of noble gases in molten fluorides. II. In the LiF-NaF-KF eutectic mixture. *Journal of Physical Chemistry*, *63*(7), 1164–1167.

Brantley, P. S., & Larsen, E. W. (2000). Simplified P3 approximation. *Nuclear Science and Engineering*, *134*(1), 1–21.

Brovchenko, M., Merle Lucotte, E., Rouch, H., Alcaro, F., Allibert, M., Aufiero, M., Cammi, A., Dulla, S., Feynberg, O., Frima, L., Geoffroy, O., Ghetta, V., Heuer, D., Ignatiev, V., Kloosterman, J. L., Lathouwers, D., Laureau, A., Luzzi, L.,

Merk, B., ... Yamaji, B. (2013). Optimization of the pre-conceptual design of the MSFR. *Deliverable*, *2*, 1–69.

Cammi, A., Di Marcello, V., Guerrieri, C., & Luzzi, L. (2011). Transfer Function Modeling of Zero-Power Dynamics of Circulating Fuel Reactors. *Journal of Engineering for Gas Turbines and Power*, *133*(5).

Cervi, E., Cammi, A., & Di Ronco, A. (2018). Stability analysis of the Generation-IV nuclear reactors by means of the root locus criterion. *Progress in Nuclear Energy*, *106*, 316–334.

Cervi, E., Lorenzi, S., Cammi, A., & Luzzi, L. (2019a). Analysis of the Effect of Fuel Compressibility on Super-Prompt-Critical Dynamics of the Molten Salt Fast Reactor, 3485–3496.

Cervi, E., Lorenzi, S., Cammi, A., & Luzzi, L. (2019b). Development of a multiphysics model for the study of fuel compressibility effects in the Molten Salt Fast Reactor. *Chemical Engineering Science*, *193*, 379–393.

Cervi, E., Lorenzi, S., Cammi, A., & Luzzi, L. (2019c). Development of an SP3 neutron transport solver for the analysis of the Molten Salt Fast Reactor. *Nuclear Engineering and Design*, *346*, 209–219.

Cervi, E., Lorenzi, S., Luzzi, L., & Cammi, A. (2019d). Analysis of the Void Reactivity Effect in the Molten Salt Fast Reactor: Impact of the Helium Bubbling System, 463–474.

Cervi, E. (2020). *An Innovative Multiphysics Modelling Approach for the Analysis and the Development of the Generation IV Molten Salt Fast Reactor* (Doctoral dissertation). Politecnico di Milano.

Cervi, E., Lorenzi, S., Cammi, A., & Luzzi, L. (2017). An Euler-Euler Multiphysics Solver for the Analysis of the Helium Bubbling System in the MSFR.

Cervi, E., Lorenzi, S., Luzzi, L., & Cammi, A. (2019e). Multiphysics analysis of the MSFR helium bubbling system: A comparison between neutron diffusion, SP3 neutron transport and Monte Carlo approaches. *Annals of Nuclear Energy*, *132*, 227–235.

Delpech, S., Merle-Lucotte, E., Heuer, D., Allibert, M., Ghetta, V., Le-Brun, C., Doligez, X., & Picard, G. (2009). Reactor physic and reprocessing scheme for innovative molten salt reactor system. *Journal of Fluorine Chemistry*, *130*(1), 11–17.

Engel, J., & Steffy, R. (1971). *Xenon Behavior in the Molten Salt Reactor Experiment* (tech. rep.). Oak Ridge National Laboratory (ORNL). Oak Ridge, TN (United States).

Fiorina, C., Hursin, M., & Pautz, A. (2017). Extension of the GeN-Foam neutronic solver to SP3 analysis and application to the CROCUS experimental reactor. *Annals of Nuclear Energy*, *101*, 419–428.

Fiorina, C., Lathouwers, D., Aufiero, M., Cammi, A., Guerrieri, C., Kloosterman, J. L., Luzzi, L., & Ricotti, M. E. (2014). Modelling and analysis of the MSFR transient behaviour. *Annals of Nuclear Energy*, *64*, 485–498.

Gelbard, E. M. (1962). Applications of the Simplified Spherical Harmonics equations in spherical geometry. *Bettis Atomic Power Laboratory*, ii, 7 leaves.

Gerardin, D., Allibert, M., Heuer, D., Laureau, A., Merle-Lucotte, E., & Seuvre, C. (2017). Design evolutions of Molten Salt Fast Reactor.

Grimes, W. R., Smith, N. V., & Watson, G. M. (1958). Solubility of Noble Gases in Molten Fluorides. I. In Mixtures of NaF–ZrF 4 (53–47 Mole %) and NaF–ZrF 4 –UF 4 (50–46–4 Mole %). *The Journal of Physical Chemistry*, *62*(7), 862–866.

Guerrieri, C., Aufiero, M., Cammi, A., Fiorina, C., & Luzzi, L. (2012). A Preliminary Study of the MSFR Dynamics. *Volume 5: Fusion Engineering; Student Paper Competition; Design Basis and Beyond Design Basis Events; Simple and Combined Cycles*, *5*(1), 229–238.

Haroun, Y., Legendre, D., & Raynal, L. (2010). Volume of fluid method for interfacial reactive mass transfer: Application to stable liquid film. *Chemical Engineering Science*, *65*(10), 2896–2909.

Haroun, Y., Raynal, L., & Legendre, D. (2012). Mass transfer and liquid hold-up determination in structured packing by CFD. *Chemical Engineering Science*, *75*, 342–348.

Higbie, R. (1935). The rate of absorption of a pure gas into still liquid during short periods of exposure. *Institution of Chemical Engineers*, *35*, 36–60.

Hyman, J. M. (1984). Numerical methods for tracking interfaces. *Physica D: Nonlinear Phenomena*, *12*(1-3), 396–407.

Ishii, M., Hibiki, T., Ishii, M., & Hibiki, T. (2011). Two-fluid Model. *Thermo-fluid dynamics of two-phase flow* (pp. 155–216). Springer New York.

Kedl, R. J. (1967). *A Model for Computing the Migration of Very Short-lived Nobel Gases into MSRE Graphite* (tech. rep.). Oak Ridge National Laboratory (ORNL). Oak Ridge, TN (United States).

Kedl, R. J. (1972). *Migration of a class of fission products (noble metals) in the Molten-Salt Reactor Experiment* (tech. rep.). Oak Ridge National Laboratory (ORNL). Oak Ridge, TN (United States).

Kedl, R., & Houtzeel, A. (1967). *Development of a Model for Computing 135Xe Migration in the MSRE* (tech. rep.). Oak Ridge National Laboratory (ORNL). Oak Ridge, TN (United States).

Lathouwers, D. (1999). *Modelling and Simulation of Turbulent Bubbly Flow* (Doctoral dissertation). Technische Universiteit Delft.

Leppänen, J., Pusa, M., Viitanen, T., Valtavirta, V., & Kaltiaisenaho, T. (2015). The Serpent Monte Carlo code: Status, development and applications in 2013. *Annals of Nuclear Energy*, *82*, 142–150.

Luzzi, L., Di Marcello, V., & Cammi, A. (2012). *Multi-Physics Approach to the Modeling and Analysis of Molten Salt Reactors*. Nova Science Publishers, Inc., New York, NY.

Marschall, H. (2011). Towards the Numerical Simulation of Multi-Scale Two-Phase Flows. *undefined*, 322.

Nieves-Remacha, M. J., Yang, L., & Jensen, K. F. (2015). OpenFOAM Computational Fluid Dynamic Simulations of Two-Phase Flow and Mass Transfer in an Advanced-Flow Reactor. *Industrial and Engineering Chemistry Research*, *54*(26), 6649–6659.

Panda, S. K., Singh, K. K., Shenoy, K. T., & Buwa, V. V. (2017). Numerical simulations of liquid-liquid flow in a continuous gravity settler using OpenFOAM and experimental verification. *Chemical Engineering Journal*, *310*, 120–133.

Peebles, F. N. (1968). *Removal of Xe-135 from Circulating Fuel Salt of the MSBR by Mass Transfer to Helium Bubbles* (tech. rep.). Oak Ridge National Laboratory (ORNL). Oak Ridge, TN (United States).

Ranz, W. E., & Marshall, W. R. (1952). Evaporation from drops. Parts I & II. *Chem. Eng. Progr*, *48*(22), 141–173.

Reinhardt, Y., Meinen, N., & Meyer, D. W. (2013). Modeling anisotropic Reynolds-stress dissipation in particle- or droplet-laden flows. *International Journal of Multiphase Flow*, *56*, 1–3.

Rhodes, M. (2008). *Introduction to Particle Technology: Second Edition*. John Wiley & Sons, Ltd.

Rusche, H. (2002). *Computational Fluid Dynamics of Dispersed Two-Phase Flows at High Phase Fractions* (Doctoral dissertation *December*). Imperial College of Science, Technology and Medicine.

Santamarina, A., Bernard, D., Rugama, Y., & OECD Nuclear Energy Agency. (2009). The JEFF-3.1.1 nuclear data library : JEFF report 22, validation results from JEF-2.2 to JEFF-3.1.1. *OECD 2009 NEA No. 6807, ISBN 978-92-64-99074-6*, 61.

Schiller, L., & Naumann, A. (1933). Über die grundlegenden Berechnungen bei der Schwerkraftaufbereitung. *Verein Deutscher Ingenieure*, *44*, 318–320.

Tano, M., Rubiolo, P., & Doche, O. (2017). Progress in modeling solidification in molten salt coolants. *Modelling and Simulation in Materials Science and Engineering*, *25*(7), 074001.

Thummala, P. P., Un, U. T., & Celik, A. O. (2020). Investigating the advantages and limitations of modeling physical mass transfer of CO2 on flat plate by one fluid formulation in openfoam. *Periodica Polytechnica Chemical Engineering*, *64*(1), 124–134.

Watson, G. M., Evans, R. B., Grimes, W. R., & Smith, N. V. (1962). Solubility of Noble Gases in Molten Fluorides. In LiF-BeF2. *Journal of Chemical and Engineering Data*, *7*(2), 285–287.

Weller, H. G., Tabor, G., Jasak, H., & Fureby, C. (1998). A tensorial approach to computational continuum mechanics using object-oriented techniques. *Computers in Physics*, *12*(6), 620.